# Development of high-water-permeance polyketone (PK) membrane via thermally induced phase separation

顶, 上

(Degree)
博士（学術）

(Date of Degree)
2024-03-25

(Date of Publication)
2025-03-01

(Resource Type)
doctoral thesis

(Report Number)
甲第8937号

(URL)
https://hdl.handle.net/20.500.14094/0100490162

# Doctoral Dissertation

Development of high-water-permeance polyketone (PK) membrane via thermally induced phase separation

(熱誘起相分離法による高水透過性ポリケトン膜の開発)

**January 2024**

Graduate School of Engineering,
Kobe University

**XIANG SHANG**
**项 上**

## Acknowledgment

First of all, I am sincerely grateful to my supervisor, professor Hideto Matsuyama, who provided me with a valuable opportunity to study at the Research Center for Membrane and Film Technology at Kobe University. Based on the encouragement, support, and guidance of Prof. Matsuyama, I quickly adapted to life in Japan and carried out my experiments smoothly. Finally, I satisfactorily completed my doctoral course. In addition, I have deep admiration the Prof. Matsuyama, due to his profound knowledge and dedicated attitude, which profoundly influenced my future in my learning and life. I hope to learn and follow his passion for life and dedication to research in the future.

I would like to express my gratitude to Dr. Pengfei Zhang and Dr. Saeid, who continuously encouraged and assisted me throughout my doctoral research. Many of my ideas were developed through discussions with them. I thoroughly enjoyed our conversations, whether they pertained to learning, experimental guidance, writing papers, responding to comments from reviewers, or various interesting experiences in life. I learned many good qualities and habits from them. I sincerely appreciate their help.

I am deeply thankful to the members of the research group, especially Prof. Ryosuke Takagi, and Dr. Rulph, who provided valuable advice and assistance in advancing my research and revising papers.

I also want to thank Professors Tomohisa Yoshioka, Keizo Nakagawa, Hideyuki Kamio, and others, who provided valuable insights during Saturday seminars.

I appreciate the company and assistance of everyone in this laboratory. To me, it’s like a big family, made up of all of us together, recording our efforts, hardships, and joys, which made my doctoral life enjoyable.

Finally, I want to thank my family numbers and friends for their unwavering support, as they have been a great source of motivation throughout my doctoral process.

**XIANG SHANG**

Graduate School of Engineering

Kobe University, Japan

November 2023

Table of contents

# Chapter 1

## General introduction

### *1.1 Membrane separation technology*

#### *1.1.1 Overview*

Membrane separation technology refers to the method of separating, grading, purifying, and enriching solutes and solvents in a mixture by utilizing the selective permeation properties of membranes, with the membrane playing a decisive role. Membranes are widely found in the natural world and originally existed in the form of natural membranes, closely related to the origin of life and all life activities. As early as 1748, Abbe Nollet observed the phenomenon of water spontaneously diffusing into an alcohol-water solution through a pig bladder and named it “osmosis” [1]. In 1861, Graham found that sugar and salt could quickly pass through parchment paper into water, while gelatin and gum arabic could not pass through parchment paper into water [2]. Since then, membrane separation technology has embarked on a long journey of exploration and development. Today, membrane separation technology has gradually matured, industrialized, and is applied in various fields, including water treatment (desalination, industrial wastewater treatment, urban sewage treatment) [2-4], the food industry (dairy, wine, and juice clarification) [5, 6], the pharmaceutical industry (artificial lungs, hemodialysis) [7, 8], etc. Because it exhibits minimal pollution, lower energy consumption, higher separation efficiency, and lower operational costs than traditional water treatment processes. With the rapid development of the global economy, some regions face severe water pollution, posing significant health risks to humans. Furthermore, the distribution of freshwater resources is highly uneven globally, with water scarcity being a significant hindrance to urban development in some areas.

The rapid development of membrane separation technology will bring significant environmental benefits, social benefits, and economic benefits.

### *1.1.2 Definition of "Membrane"*

A membrane is a thin barrier that permits selective mass transport. Membranes can be fabricated from a wide variety of organic (e.g. polymers, liquids) or inorganic (e.g. carbons, zeolites etc.) materials [9]. In 1996, the International Union of Pure and Applied Chemistry (IUPAC) defined a membrane as a three-dimensional structure in which one dimension is significantly smaller than the other two dimensions, and mass transfer can occur through various driving forces. This definition emphasizes the relative size of dimensions and functionality compared to the original definition.

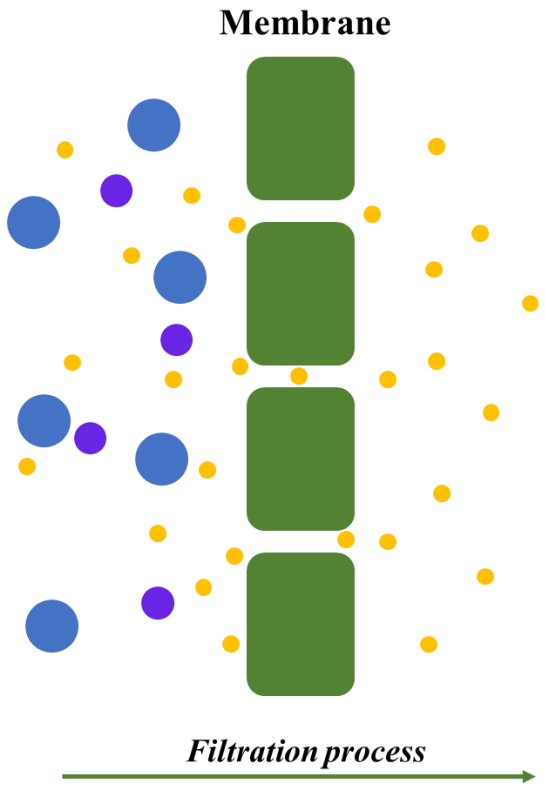


**Fig. 1-1** Schematic representation of a filtration process by a membrane.

### *1.1.3 Membrane processes*

Membrane processes are based on the differential rates of mass transfer of chemical substances across the membrane interface, which are determined by factors such as driving forces, component mobility within the membrane, and component concentrations at the phase interface. Mobility is primarily influenced by the molecular size and the material structure of the solute at the phase interface, while the concentration at the phase interface is influenced by factors like the affinity between the solute and the phase interface material, solute size, and membrane structure. The magnitude of flux provided by a given driving force is determined by the size of these migration rates and affinities.

Currently, various types of membrane processes are reported in the literature, typically categorized based on separation size and principles into microfiltration (MF), ultrafiltration (UF), nanofiltration (NF), reverse osmosis (RO), electrodialysis (ED), gas separation (GS), and pervaporation (PV). Microfiltration has pore sizes ranging from approximately 50 nm to 10 μm, operating at pressures of 0.5-5 bar, and functions primarily through size exclusion. It is commonly used to remove contaminants like bacteria from water and serves as a pre-treatment step for nanofiltration and reverse osmosis. Ultrafiltration, with pore sizes in the range of 2-50 nm and operating pressures of 1-7 bar, also relies on size exclusion. It is typically used to retain viruses, proteins, and colloids. Nanofiltration, with pore sizes around 0.5-2 nm and operating pressures of 3-30 bar, employs both electrostatic and size-based effects. It is often applied for dye separation and removal of divalent salts. Reverse osmosis features pore sizes between 0.3-0.6 nm and operates at pressures of 7-55 bar, relying on the principle of solute diffusion. It can be used for the removal of monovalent salts and low-molecular-weight organic compounds. Electrodialysis is a process for the removal or enrichment of ions in a solution, and its separation mechanism involves ion migration through ion-exchange membranes. Gas separation involves the separation and concentration of gas mixtures, with a separation mechanism based on the dissolution-diffusion molecular

sieve effect. Pervaporation is employed for the separation of volatile liquid mixtures, and its separation mechanism is based on the dissolution-diffusion process.

### *1.1.4 Membrane materials*

As earlier mentioned, membranes can be fabricated from a wide variety of organic (e.g. polymers) or inorganic materials.

Inorganic membranes are primarily categorized into ceramic membranes [10], metal membranes [11], molecular sieve composite membranes [12], metal-organic hybrid membranes [13], and more. Among these, ceramic membranes are the most widely applied due to their high-temperature resistance, corrosion resistance, mechanical strength, and good permeation performance. However, ceramic membranes are relatively expensive to manufacture, and their brittleness limits their application to some extent.

Compared with inorganic membranes, polymeric membranes are widely chosen resulting in a simple fabrication process, low cost, and excellent performance. Polymers possess a wide variety with significantly different properties, making them suitable for various usage requirements. Many polymer materials have been developed and utilized to produce commercial membranes, as shown in Table 1-1.

**Table 1-1** Polymer materials used for the preparation of commercial membranes [14].

| Membrane material | Membrane process |
|---|---|
| Cellulose regenerated | D, UF, MF |
| Cellulose nitrate | MF |
| Cellulose acetate | GS, RO, D, UF, MF |
| Polyamide | RO, NF, D, UF, M |
| Polysulfone | GS, UF, MF |
| Poly(ether sulfone) | UF, MF |
| Polycarbonate | GS, D, UF, MF |
| Poly(ether imide) | UF, MF |

| | |
|---|---|
| Poly(2,6-dimethyl-1,4-phenylene oxide) | GS |
| Polyimide | GS |
| Poly(vinylidene fluoride) | UF, MF |
| Polytetrafluoroethylene | MF |
| Polypropylene | MF |
| Polyacrylonitrile | D, UF, MF |
| Poly(methyl methacrylate) | D, UF, |
| Poly(vinyl alcohol) | PV |
| Polydimethylsiloxane | PV, GS |

MF = microfiltration; UF = ultrafiltration; NF = nanofiltration; D = dialysis; PV = pervaporation; GS = gas separation

Polymeric membranes, especially microporous membranes, have found widespread applications in various fields such as organic solvent separation, membrane distillation, industrial and municipal wastewater treatment, and drinking water purification due to their excellent performance. This exceptional performance stems from their material properties and the various membrane preparation methods and processes, which allow for the synthesis of numerous new polymer materials to meet specific separation requirements. However, the superior performance of membranes depends not only on the characteristics of the polymer membrane materials but is also influenced by membrane structure and fabrication methods, with these factors collectively playing a crucial role.

### *1.2 Formation of the polymeric porous membrane*

Polymeric porous membranes, based same polymer materials, can exhibit significant structural and performance differences due to variations in membrane preparation methods and processes. Therefore, the development of a high-performance and advanced membrane fabrication process with optimal process parameters is the primary factor in producing high-performance separation membranes. The main methods for

preparing polymeric porous membranes include the melt-spinning stretching method, non-solvent-induced phase separation (NIPS), and thermal-induced phase separation (TIPS), which are detailed below.

### *1.2.1 Melt-spinning and cold-stretching (MSCS) method*

This method involves the extrusion or sheeting of partially crystalline polymer materials, followed by stretching the material perpendicular to the extrusion direction to align the crystallites in the direction of stretching [15, 16]. Under mechanical stress, small fractures occur, resulting in a porous structure. This method is commonly known as the "Celgard method" The process typically involves several steps. Initially, the polymer, heated to near its melting point, is extruded and rapidly cooled to form a highly oriented crystalline membrane. Then, the membrane is stretched several times in the mechanical force direction, disrupting its crystalline structure and creating crack-like pores.

In this approach, commercial polypropylene is often used as the membrane material, and the stretching rate is much higher than the extrusion rate [17]. The polypropylene molecules transform into a microfiber form aligned with the direction of mechanical force. These microfibers act as nucleation sites for the formation of a thin, folded chain of crystals oriented parallel to the mechanical force. Subsequently, stretching is performed at temperatures lower than the polymer's melting temperature but higher than the initial annealing temperature, causing the deformation of the amorphous regions between the thin sheets into microfibers. This results in the formation of a porous interconnected network oriented along the direction of mechanical force. The pore size depends on the microfibers formed after stretching. Using this method, the membrane pore size typically ranges from approximately 0.1 μm to a maximum of about 3 μm. Only crystalline or partially crystalline materials can be processed using this method. The porosity of membranes produced by this method can be significantly higher compared to sintering methods, with porosity reaching up to 90%.

### *1.2.2 Non-solvent induced phase separation (NIPS) method*

Non-solvent induced phase separation (NIPS) method is widely employed to prepare the polymer porous membranes, based on the mass transfer or double diffusion between solvent and non-solvent to induce phase separation [18].

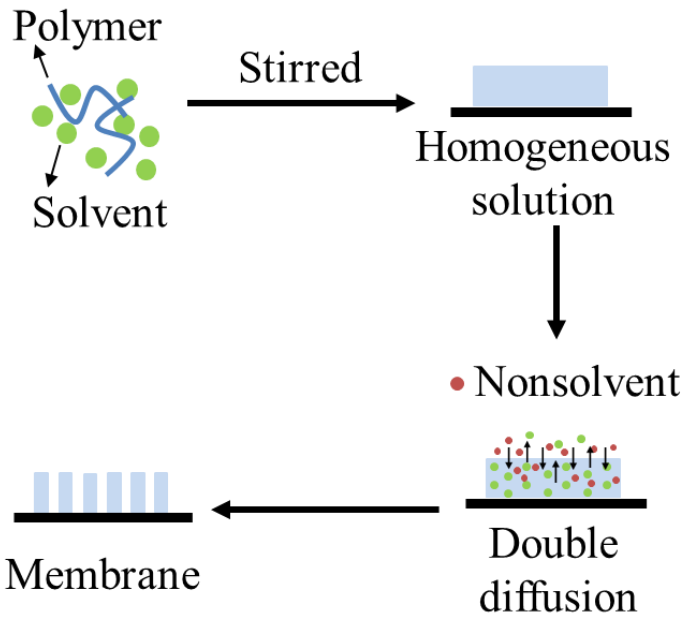


**Fig. 1-2** Schematic diagram of the polymeric membrane preparation process via the NIPS process

The detailed membrane preparation process：

1. The polymer is mixed and stirred with the solvent and heated at relatively low-temperature conditions or room temperature so that the polymer will be dissolved by the solvent to form a homogeneous solution (polymer solution).

2. The prepared polymer solution needs to be allowed to stand for some time to remove air bubbles.

3. The polymer solution is immersed in a coagulation bath after being cast or extruded by spinneret. Mass transfer occurs between the non-solvent from the coagulation bath and the solvent from the polymer solution. The introduction of the non-solvent destabilizes the polymer solution, causing phase separation, resulting in a polymer-rich

phase and a polymer-lean phase. As double diffusion continues, the polymer-rich phase begins to solidify, forming a membrane.

4. The prepared primary membrane is immersed in the extraction solution to extract the solvent. After the solvent is completely extracted, the membrane is stored in the deionized water or air environment.

**Advantages**:

1. Simple requirements for membrane preparation equipment, without high-temperature operating conditions.

2. The prepared membrane exhibits good permeance resulting from the high porosity and porous surface structure.

**Disadvantages:**

1. The preparation process is complex, the multitude of polymer solution components and process parameters leads to decreased stability in the process, making it difficult to precisely control the structure and performance of the membrane; the use of solvents is typically toxic, which induces a challenging post-treatment processing.

2. The mechanical strength of the prepared membrane is low resulting from the low polymer concentration.

4. The variety of polymers is limited because it is hard to screen the suitable solvent to dissolve some polymers at low-temperature conditions, which possess great resistance to organic solvents.

### *1.2.3 Thermally induced phase separation (TIPS) method*

The membrane formation mechanism of the TIPS method, based on heat transfer, involves dissolving the polymer at high temperatures to induce polymer solution, subsequently, inducing phase separation to form a membrane during the cooling process.

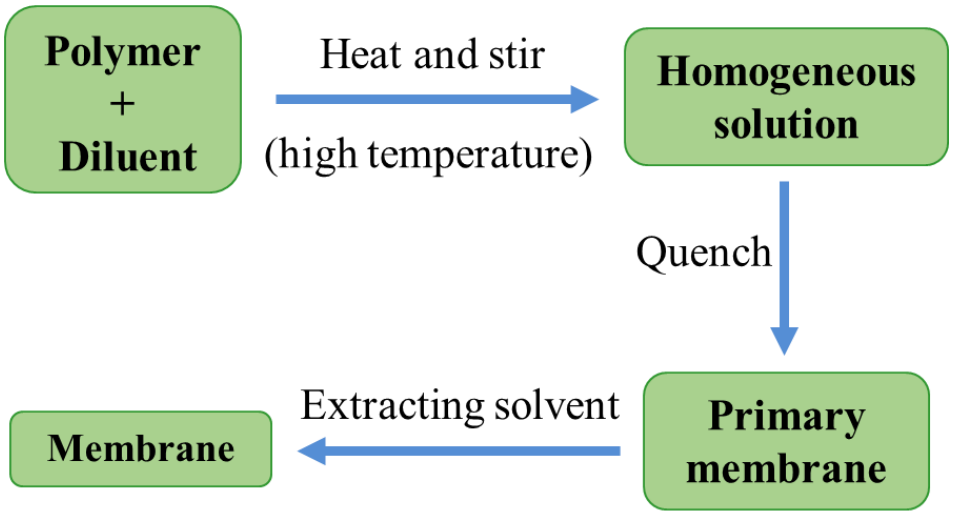


**Fig. 1-3** Schematic diagram of the polymeric membrane preparation process via the TIPS process [19, 20]

The detailed membrane preparation process：

1. Mixed the diluent (high boiling point, low molecular weight) and polymer to form a homogeneous solution at elevated temperatures.

2. The polymer solution is cast or extruded into the desired shape, for example, flat sheet, or hollow fiber, and phase separation, including solid-liquid or liquid-liquid phase separation, will occur to form the primary membrane resulting from the decreased temperature of the polymer solution.

3. Subsequently, the primary membrane was immersed in the quenching bath (i.e., water) to remove the diluent.

4. The prepared primary membrane is immersed in the extraction solution to extract the solvent. After the solvent is completely extracted, store it in a deionized water or air environment.

**Advantages:**

1. Excellent mechanical strength and self-supporting for hollow fiber membranes. The prepared membrane via the TIPS method exhibits excellent mechanical strength resulting from the interconnected membrane structure and a high polymer concentration.

2. The wide range of polymer types. Especially some polymers, for example, polyetheretherketone (PEEK), polyphenylene sulfide (PPS), polyimide (PI), and polyamide (PA), that are difficult to dissolve at room temperature.

3. The regulation of membrane bulk structure is simple and mainly depends on the interaction between polymer and diluent.

4. There are some potential low-toxic or non-toxic solvents for membrane formation. With increasing awareness of environmental and health concerns, low-toxic or non-toxic membrane fabrication processes are becoming a future focus.

**Disadvantages:**

1. The spinning equipment needs to withstand high-temperature conditions.

2. Membranes prepared typically have a low surface porosity (dense skin layer) due to the evaporation of the diluent based on the high-temperature conditions, and fast cooling rate, resulting in a low water permeance.

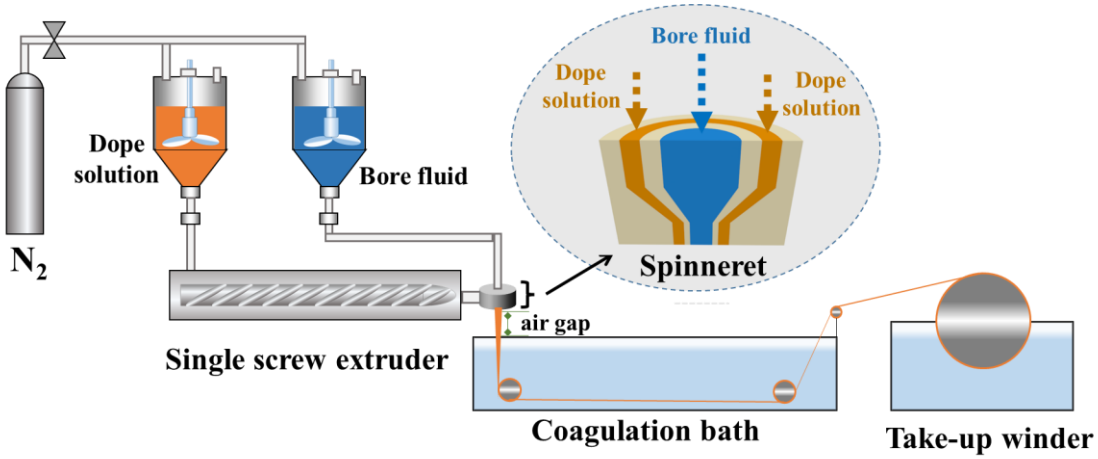


**Fig. 1-4** Schematic diagram of hollow fiber membrane spinning equipment and process [21].

The configurations of porous polymer membranes mainly include flat sheet membranes and hollow fiber membranes. Compared to flat sheet membranes, hollow fiber membranes present clear advantages, such as high packing density and ease of backwashing. Particularly, hollow fiber membranes prepared using the TIPS method

exhibit high strength. Hollow fiber membranes can achieve self-support and are widely used in commercial membrane applications.

During the TIPS process, the diluent exhibits a crucial role in the membrane microstructure, characteristics, and performance. When using a semi-crystalline polymer, TIPS can proceed either via solid-liquid phase separation or liquid-liquid (L-L) phase separation, mainly depending on the interaction with the polymer and diluent.

1.2.3.1. Soild-liquid phase separation process

The solid-liquid phase separation system of a semi-crystalline polymer is a crystallization process of the polymer from the polymeric solution during the cooling process. The addition of diluent results in a decrease in the melting point of the polymer and the relationship between the polymer melting point and the mixed components and $\chi$ is represented by the melting point depression curve, which reflects its crystallization kinetics [19]:

$$\frac{1}{T_m} - \frac{1}{T_m^0} = \frac{RV_u}{\Delta H_u V_d}(\varphi_d - \chi\varphi_d^2) \quad (1\text{-}1)$$

where $T^0_m$ and $T_m$ are the melting point of the pure polymer and the polymer in the polymer solution, respectively. $\varphi_d$ is the volume fraction of the diluent. $V_d$ and $V_u$ are the molar volume of the diluent and polymer solution, respectively. $\Delta H_u$ is the standard enthalpy of formation of the polymer solution. $\chi$ is the Flory-Huggins interaction parameter.

Plotting with $\varphi_p = 1-\varphi_d$ as the x-axis and $T_m$ as the y-axis, as shown in Fig. 1-5. The region above the curve is the single-phase region, while below is the two-phase region. As the $\chi$ increases, indicating weaker polymer-solvent interactions, the temperature at which phase separation occurs increases. When $\chi < 0$, the curve exhibits a convex shape; when $\chi = 0$, the curve takes on a linear form; and when $\chi > 0$, it appears concave. If $\chi$ is very large and the initial polymer concentration is low, the curve gradually levels off, indicating that the system is prone to liquid-liquid phase separation. Under other constant conditions, the decreased $\Delta H_u$ and increased $V_u/V_d$ ratio leads to a lower $T_m$.

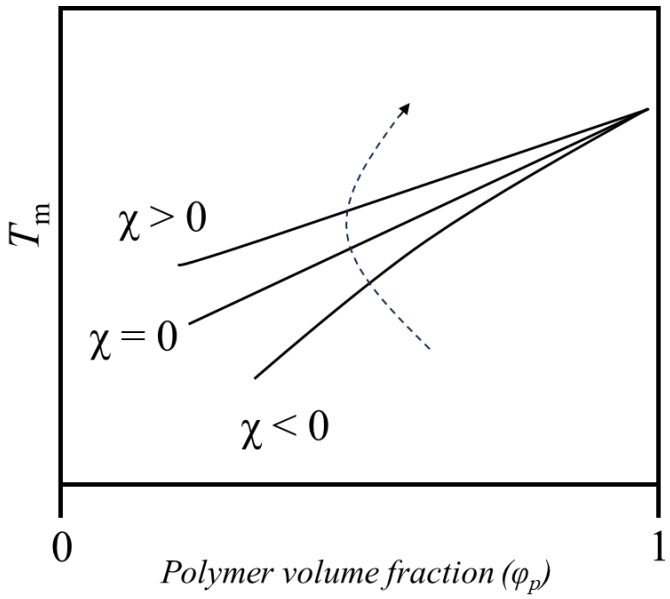


**Fig. 1-5** Relationship of polymer melting temperature and polymer volume fraction for a semi-crystalline polymer-diluent system [19].

The occurrence of S-L phase separation in the polymer solution resulted from strong interactions between the polymer and the solvent. Therefore, polymers are usually dissolved at temperatures below the polymer melting temperature to form homogeneous solutions. As the temperature decreases, only the polymer crystallizes to form spherical particle structures in the membrane bulk structure. However, due to the evaporation of solvent and rapid crystallization, the outer or upper surface of the membrane tends to form a dense layer, significantly reducing the membrane's permeability. Additionally, the accumulation of spherical particle structures leads to poor mechanical properties of the membrane, based on the same polymer concentrations.

1.2.3.2. Liquid-liquid phase separation

The extent of mixing between a polymer and a solvent can be represented by the Gibbs free energy ($\Delta G_m$) of the mixture and the second partial derivative of $\Delta G_m$ to the polymer volume fraction ($\varphi$) at a fixed temperature ($T$) and pressure ($P$) [20].

$$\Delta G_m < 0 \tag{1-2}$$

$$\left(\frac{\partial^2 \Delta G_m}{\partial \varphi^2}\right)_{T,P} > 0 \quad (1\text{-}3)$$

The miscibility of the polymer and solvent depends on these conditions. When either of the conditions in the above two equations is not met, phase separation occurs. The relationship between $\Delta G_m$ and composition exhibits three different types of curves at different temperatures, as shown in Fig. 1-6. Curve a has $\Delta G_m > 0$ across the entire composition range, indicating immiscibility. Curve B satisfies Eq. 1-2 but not Eq. l-3, making it a partially miscible system. In the composition range where $((\partial^2 \Delta G_m)/(\partial \varphi^2))_{T,P} < 0$, phase separation occurs to reach the equilibrium state with the lowest free energy. Curve c satisfies both conditions, representing a completely miscible system.

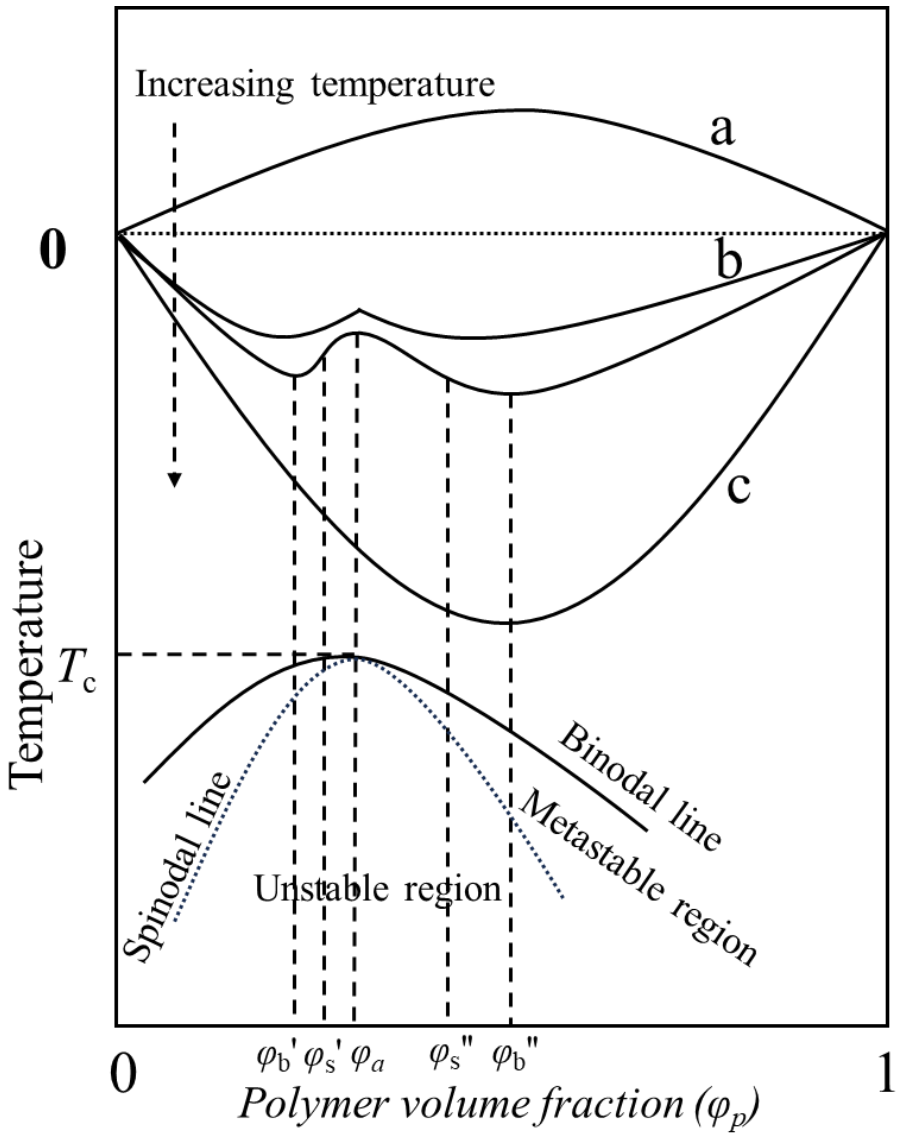


**Fig. 1-6** Relationship between the Gibbs free energy and temperature to the polymer volume fraction, based on partially miscible systems with a high critical miscibility temperature ($T_c$). $\varphi_b'$ and $\varphi_b''$ are the minimum values of the tangent line, respectively. $\varphi_s'$, and $\varphi_s''$ are the inflection points, and $\varphi_a$ is the critical point [20].

For curve B in Fig. 1-6, the system has the highest critical miscibility temperature (UCST). The lowest point on curve b, which changes with temperature, is called the binodal, and the inflection point that changes with temperature is called the spinodal, as shown in Fig. 1-6. When the composition is between $\varphi_b'$ and $\varphi_b''$, the $\Delta G_m$ of the homogeneous solution is higher than that of the two-phase system at $\varphi_b'$ and $\varphi_b''$, so the

system undergoes phase separation in this composition range to reach the equilibrium state with the lowest free energy.

When the temperature drops into the region between the binodal and spinodal or when the composition is between $\varphi_b'$ and $\varphi_s'$, $\varphi_s''$ and $\varphi_b''$, the system enters a metastable region. In this region, the system is stable, based on the small concentration fluctuations. However, when concentration fluctuations become significant, non-spontaneous liquid-liquid phase separation occurs, and the phase-separated domains grow as the solvent diffuses along the concentration gradient. The mechanism of phase separation in this region is nucleation and growth. When the temperature is further reduced into the region below the spinodal or when the composition is between $\varphi_s'$ and $\varphi_s''$, it becomes unstable, and spontaneous phase separation occurs, resulting in a polymer-poor phase and a polymer-rich phase, following the spinodal phase separation mechanism. If the temperature is lowered further, the polymer-rich phase solidifies, leading to solid-liquid phase separation, as described earlier.

Another crucial factor that affects the phase equilibrium in polymer-solvent systems is the Flory-Huggins interaction parameter χ [20]. Typically, the $\Delta G_m$ for a polymer-solvent binary system can be represented as Eq.1-4.

$$\Delta G_m = RT[\frac{\varphi_d \ln \varphi_d}{X_d} + \frac{\varphi_p \ln \varphi_p}{X_p} + \chi \varphi_d \varphi_p] \quad (1\text{-}4)$$

where $\varphi_d$ and $\varphi_p$ represent the volume fractions of the diluent and polymer, respectively. $X_d$ and $X_p$ represent the number of lattice sites occupied by solvent molecules and polymer chain segments, respectively.

The first two terms in the equation reflect the contribution of entropy and are always negative. The last term reflects the contribution of enthalpy, which can be positive or negative and mainly depends on the magnitude of χ. When χ is positive and sufficiently large, $\Delta G_m$ is positive, leading to phase separation. The impact of χ on the position and shape of the binodal is illustrated in Fig. 1-7. As χ increases, the polymer and solvent exhibit a weak interaction. This results in the phase separation being more likely to occur, and it occurs at higher temperatures.

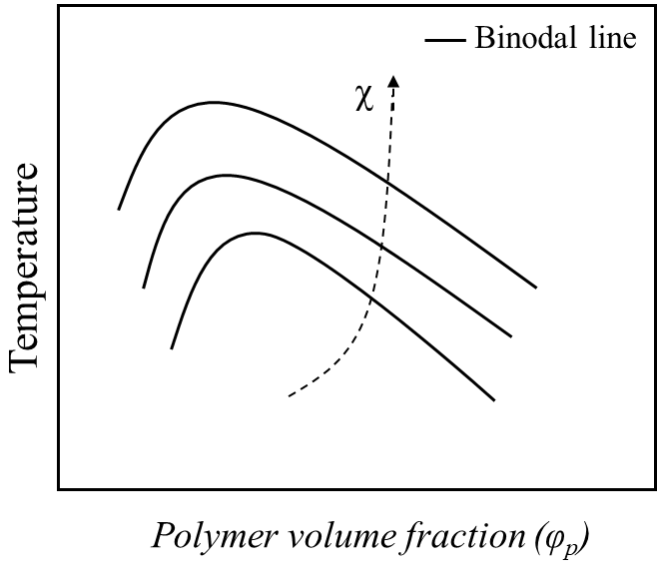


**Fig. 1-7** The effect of the interaction parameter on the binodal line [20].

Thermodynamics of phase equilibrium is used to study the types of phase transitions that occur, but the final structure of membranes depends on the kinetics of the phase separation process.

As the temperature decreases in a polymer solution, the appearance of a cloud point signifies the occurrence of liquid-liquid phase separation. Under the influence of surface tension, liquid droplets tend to minimize their surface energy. This increases the diameter of the liquid droplets while reducing their number. This process is known as coarsening. Coarsening is influenced by the crystallization or glass transition of the polymer and eventually terminates. Therefore, the cooling rate is a critical dynamic factor in determining the coarsening process. In other words, changing the cooling rate can control the size of the liquid droplets, i.e., the pore size. Additionally, factors such as polymer concentration and molecular weight have a significant impact on pore size.

The mechanisms involved in the coarsening process include: Ostwald ripening: This theory suggests that due to differing sizes of droplets leading to different surface curvatures, the smaller droplets possess higher solubility. Consequently, the smaller droplets eventually dissolve and disappear, while the larger droplets gradually grow.
Coalescence theory: This theory proposes that the aggregation of droplets occurs due to mutual collisions induced by Brownian motion. Hydrodynamic flow mechanism:

This theory suggests the presence of nucleation processes in the fluid, creating surfaces with irregular curvature. This phenomenon triggers dynamics, causing fluid flow, thereby accelerating droplet growth.

The occurrence of L-L phase separation in the polymer solution results from weak interactions between the polymer and the solvent. Therefore, polymers are typically dissolved at temperatures above polymer melting temperature to prepare homogeneous solutions. As the temperature decreases, the polymer solution undergoes droplets coarsening, forming polymer-lean phases and polymer-rich phases. When the temperature reaches the crystallization point of the polymer, the polymer crystallizes, fixing the membrane structure. The interconnected membrane structure formed by L-L phase separation is beneficial for both the filtration process of the membrane and its mechanical properties. Hence, compared to S-L phase separation systems, L-L phase separation systems attract more attention.

## *1.3 Factors affecting polymeric porous membrane structure and performance in the TIPS process*

### *1.3.1 Polymer*

Polymer is an important part of the polymer solution. Hence, the type, concentration, and molecular weight of the polymer exhibit a significant effect on the membrane structure and performance [22]. At first, the types of polymers can be roughly classified into hydrophobic polymers, such as polyvinylidene fluoride (PVDF), polyethylene (PE), polypropylene (PP), and hydrophilic polymers, for example, poly (vinyl butyral) (PVB), poly (ethylene-co-vinyl alcohol) (EVOH), polyamide (PA), and polymethyl methacrylate (PMMA). Typically, compared to hydrophobic membranes, membranes prepared from hydrophilic materials exhibit better permeance and resistance to organic fouling, which is advantageous for the filtration process [23]. Secondly, aside from the properties of the prepared membrane, including the overall porosity, water permeance, and mechanical strength, polymer concentrations also exhibit a significant influence on the phase separation mechanism of the polymer solution. Specifically, when the

polymer concentration is below the monotectic point, L-L phase separation occurs in the polymer solution to form the cellular structure during the cooling process. Conversely, when the polymer concentration is above the monotectic point, the S-L phase separation occurs in the polymer solution to prepare the spherulite structure during the cooling process. In detail, Matsuyama et al [24] conducted a study on the ethylene-propylene acrylic acid copolymer/diphenyl ether system. When the polymer concentration is in the range of 10 wt% to 40 wt%, L-L phase separation precedes S-L phase separation, resulting in the formation of a connected spherical pore structure within the system. However, when the polymer concentration exceeds 60 wt%, polymer crystallization (S-L phase separation) occurs before L-L phase separation, leading to the appearance of isolated closed pores. Kim et al [25] investigated the phase diagram and pore structure of the fatty amine/polypropylene system, which suggested that only when the polymer component concentration is lower than the concentration corresponding to the cloud point in the phase diagram, it is possible to obtain an interconnected structure during the L-L phase separation process by adjusting the component concentrations and cooling rate. Zhang et al investigated in detail the effects of PVDF concentration and molecular weight on membrane structure and properties [26]. Firstly, when the PVDF molecular weight and the polymer solution concentration in the membrane preparation decreased, the cloud point temperature and crystallization temperature slightly decreased owing to the higher stability of the dope solution caused by the entropy effect. Secondly, the reduction in polymer molecular weight led to decreased viscosity, allowing the penetration of the extrusion solvent (propylene carbonate, PC) to influence the membrane structure. As a result, the membrane structure transitioned from a continuous cellular structure to a spherical particle structure and a porous outer surface. Finally, the resultant membranes exhibited higher water permeability, larger pore size, and reduced mechanical properties.

### *1.3.2 Secondary polymer*

Secondary polymers essentially function as polymer modifiers, typically serving to enhance hydrophilic properties or mechanical strength. The most common application is the blending modification of PVDF, due to the low water permeance and poor fouling resistance resulting from the hydrophobicity of the polymer. For example, Cui et al [27] used the TIPS method to prepare PVDF/polyvinyl butaral (PVB) hollow fiber membranes. With the addition of the amphiphilic copolymer PVB, a significant amount of fiber structures formed within the membrane, leading to a substantial improvement in the tensile strength of the membrane to 17.08 MPa. The water flux also increased from 20 L $m^{-2}h^{-1}$ to 929 L $m^{-2}h^{-1}$, due to increased pore size and hydrophilicity of the blend membrane. Based on the TIPS method, a PVDF/polyamide 6 (PA6) blend membrane was prepared in another work [23]. The addition of PA6 did not alter the S-L phase separation process of PVDF, but the hydrophilic PA6 introduced water molecules for pore formation, ultimately resulting in the formation of a continuous cellular structure. Additionally, the addition of PA6 significantly reduced the water contact angle and increased the water permeance from 12.8 L $m^{-2}h^{-1}$ to 298.3 L $m^{-2}h^{-1}$. Meanwhile, the tensile strength of the prepared blend membrane significantly increased from 1.91 to 5.85 MPa resulting from the different morphology of PA6 in membrane bulk structure. Wu et al [28] used the TIPS method to prepare a PVDF/styrene maleic anhydride (SMA) blend membrane, where PVDF and SMA formed a partially compatible system. The results indicated that when the SMA content was low (less than 3 wt%), the compatibility between SMA and PVDF was poor. Additionally, SMA acted as a nucleating agent for PVDF, which led to an increase in the crystallization temperature of PVDF. On the other hand, when the SMA content was higher than 3 wt%, the compatibility between SMA and PVDF improved, but the aggregation of SMA hindered PVDF crystallization. With different levels of SMA added, PVDF exhibited a solid-liquid phase separation. However, as the SMA content increased, the hindering effect of SMA on PVDF crystallization became more pronounced, and the cross-sectional morphology of the membrane changed from spherical particles to a

interconnected structure. Furthermore, during the extraction process, SMA underwent a diffusion effect and precipitated on the surface of the already solidified PVDF matrix and skin layer. The presence of the SMA deposition layer and the change in membrane structure significantly enhanced the hydrophilicity of the membrane surface and improved its permeability.

### *1.3.3 Diluent*

Diluents play a crucial role in determining the structure of the membrane matrix. In common cases, a spherical structure is formed in a S-L phase separation system, due to the strength interaction between the polymer and the diluent. Conversely, a cellular structure is prepared by the L-L phase separation process, resulting from the weak interaction between the polymer and the diluent. In addition, the selection and use of low-toxic or non-toxic solvents (green solvents) have attracted increasing attention, due to the increased environmental awareness. The solvent systems with low-toxic or non-toxic properties are used in the preparation of porous polymer membranes and are summarized in Table 1-2.

**Table 1-2** Porous polymer membranes prepared via TIPS using low-toxic or non-toxic solvent systems.

| Polymer | Diluent | |
|---|---|---|
| Polyvinylidene fluoride | Triethylene glycol diacetate | [29] |
| Poly (ethylene chlorotrifluoroethylene) | Toctyl trimellitate | [30] |
| Polyvinylidene fluoride | PolarClean | [31] |
| Polyvinylidene fluoride | Acetyl tributyl citrate | [32] |
| Polyvinylidene fluoride | Acetyl tributyl citrate | [22] |
| Polyvinylidene fluoride/Polysulfone | PolarClean | [33] |

| | | |
|---|---|---|
| Poly (ethylene chlorotrifluoroethylene) | triglyceride diacetate /trioctyl trimellitate | [34] |
| Polypropylene | Castor oil/soybean oil | [35] |
| Polypropylene | Carnauba wax/soybean oil | [36] |
| Poly (ethylene chlorotrifluoroethylene) | Acetyl tributyl citrate | [37] |
| Polyvinylidene fluoride/polyvinyl butyral | Propylene carbonate | [27] |
| Low-density polyethylene | Butyl acetate/liquid paraffin | [38] |
| Poly(4-methyl-1-pentene) | Myristic acid | [39] |

### *1.3.4 Secondary solvent*

Typically, a pure diluent and polymer system tends to form an S-L phase separation system and is less likely to form an L-L phase separation in the TIPS method [40]. Hence, a common method is to introduce a secondary diluent to decrease the interaction between the polymer and the mixed diluent system by altering the proportions of the mixed diluents. This modification helps in controlling the phase separation process of the polymer solution and membrane structure[41].

While membranes prepared using an L-L phase separation system often exhibit a continuous and superior structure with excellent performance. However, the membrane preparation temperature for L-L phase separation is higher than the melting point of the polymer. Hence, prolonged exposure to high temperatures and solvent environments can potentially lead to polymer degradation. To lower the membrane fabrication temperature in the TIPS process, triethyl phosphate (TEP) and PC can lower the cloud point temperatures ($T_{cloud}$) in various PVDF/diluent systems, showing promise in reducing membrane preparation temperatures. Interestingly, TEP and PC also serve as diluents for PVDF in the TIPS process, inducing S-L phase separation because they

exhibit stronger interactions with PVDF than dimethyl phthalate (DMP) and diphenyl carbonate (DPC) [26, 42]. In addition, in a PVDF/DPC/PC system, increasing the PC concentration sharply reduces the $T_{cloud}$ temperature and the membrane preparation temperature. These findings indicate that membrane preparation temperature can be decreased by simply introducing a secondary diluent that interacts effectively with the polymer while preserving the desired network structure resulting from L-L phase separation.

The secondary solvent, belonging to the diluent (in the TIPS process) [43] or solvent (in the NIPS process) [44], was added to prepare the homogenous solution (polymer solution) at a temperature below the melting temperature of the polymer, which was named as low-temperature thermally induced phase separation (L-TIPS) in previous report work.

### *1.3.5 Additives in polymeric solution*

Many additives, including nucleating agents, templates, and modifiers, are introduced into the polymer solution to control membrane structure and performance. During the polymer crystallization phase, the amount of nucleating agent added can regulate the rate of nucleation, and the number of nuclei, and ultimately influence the shape and size of the crystalline grains, thus affecting the shape and size of membrane pores. For example, Lim et al [28] studied the crystallization kinetics of a system using benzoic acid as a nucleating agent. The results showed that the addition of the nucleating agent increased the crystallization temperature, accelerated the crystallization rate, and reduced the size of spherical crystals. Guo et al [45] investigated the effect of a template, poly(vinylpyrrolidone) (PVP), on membrane structure and performance. The curing of PVP from the diluent not only hindered the crystallization of PVDF but also led to the formation of a porous surface, eliminating the thick and dense skin layer, resulting in an interconnected structure and a higher porosity (maximum porosity of 88.9%). The maximum pure water flux reached 3420 L $m^{-2}h^{-1}bar^{-1}$. Cui et al [46] used the TIPS method to prepare PVDF/$SiO_2$ blend

membranes. The results showed that at $SiO_2$ concentration below 5%, the pure water flux gradually increased due to the presence of $SiO_2$, which increased the membrane pore size. Furthermore, with increasing $SiO_2$ concentration the system tended to undergo L-L phase separation, and the cross-sectional structure changed from spherical particles to a cellular structure. However, when $SiO_2$ concentration exceeded 5%, the pure water flux gradually decreased. This was attributed to the increase in $SiO_2$ particles, which hindered the growth and aggregation of polymer microcrystals, leading to increased nucleation density, reduced membrane porosity, decreased permeability, and increased permeation resistance. Jiang et al [47] used the TIPS method to prepare PA6/$CaCO_3$ hollow fiber membranes. The addition of $CaCO_3$ increased the porosity pore size, and water permeability of the membrane. However, the aggregation of $CaCO_3$ particles was observed in the cross-sectional structure of the membrane, leading to a significant reduction in the mechanical properties of the membrane.

### *1.3.6 Cooling rate*

The increase in cooling rate results in an increase in the driving force for phase separation, leading to a simultaneous increase in the chances of the L-L phase separation and crystallization. Because smaller crystalline particles have a diminishing effect on phase separation, generally, increasing the cooling rate is beneficial for obtaining a connected microporous structure. Furthermore, a fast cooling rate can lower the crystallization temperature of the polymer, thus affecting the membrane structure. For example, Matsuyama [48] studied the influence of the cooling rate on the phase diagram shape of the PP-TA system and found that the cooling rate has an insignificant impact on the positions of the double spinodal lines. At higher cooling rates, lower crystallization temperature values are obtained, at the same time, the monotectic point moves to the right (high polymer concentration). When the polymer concentration is near the monotectic point, the phase separation behavior of the polymer concentration can be determined by different cooling rates, resulting from the changed crystallization temperature. Berghmans [49] conducted a comprehensive study on the effect of cooling

rate on the final pore structure in the poly(2,6-dimethyl-1,4-phenylene ether)/cyclohexanol system. When the cooling rate is sufficiently slow, the resulting membrane exhibits large spherulites, resulting from the higher crystallization temperature, compared with the $T_{cloud}$ of the polymer solution. Increasing the cooling rate reduces spherulite size, while both the number and size of cellular structure in the L-L phase separation structure were increased. As the cooling rate increases to a certain value, spherulites disappear entirely, leaving only the cellular structure of the L-L phase separation. Further increasing the cooling rate leads to an increase in the number of micro-pores and a decrease in pore size in the L-L phase separation. Additionally, in the S-L phase separation systems, a faster cooling rate results in smaller spherulite sizes because higher cooling rates favor nucleation in the early stages of crystallization. Under the same polymer concentration conditions, the number and size of the spherulite structure increases.

### *1.3.7 Air gap distance*

Fang et al [50] prepared a PVDF hollow fiber membrane via the TIPS method using a triple-orifice spinneret to extrude solvent (propylene carbonate (PC)) on the outside of the PVDF solution. In addition, the effect of air gap distance (0.5 cm, 5 cm, 10 cm, 15 cm, 20 cm) on membrane structure and performance was detailed investigated. At first, the diphenyl carbonate (DPC) was used as a diluent in the PVDF solution to form an interconnected membrane structure resulting from L-L phase separation, and the extruded solvent (PC) exhibited a better interaction with PVDF to induce S-L phase separation. Hence, for the morphology of the cross-section structure near the outer surface of the membrane, the extruded PC penetrated the polymer solution from the contact interface, which resulted in a change in the compatibility between PVDF and diluent (DPC). Thus, the phase separation mechanism changed from L-L to S-L. As the air gap distance increased, a higher PC amount penetrated the polymer solution, thus forming clear spherulites. The combination of spherulites with the bi-continuous network (composite-like structure) near the outer surface is an interesting structure with

outstanding properties. Furthermore, the spherulitic thickness generally increased in the radial direction with increased air gap distances. For the outer surface of the membrane, when PC was extruded, the DPC moved towards the surface to decrease the PVDF surface concentration, and the PVDF moving towards the interface possibly occurred to increase the polymer surface concentration, due to the good interaction among them. Notably, the molecular weight of DPC is much lower than that of PVDF, in which a higher rate of DPC movement is expected. Hence, the DPC rapid moving towards the interface at a short contact time (short air gap distance) decreases the PVDF surface concentration. Contrary to the short air gap, when the contact time increased by increasing the air gap distance, the PVDF molecular chains began moving towards the interface, enhancing the PVDF surface concentration. As a result, the pore size and porosity of the membrane surface are reduced by increasing the air gap distance. Hence, air gap distances play a significant role in the segregations of polymer and/or diluent to tailor the membrane surface pore structure when the extruded solvent has high compatibilities to both the polymer and diluent.

### *1.3.8 Composition of coagulation bath*

The phase separation of the TIPS method is achieved by the cooling process. Polymer solutions primarily rely on coagulation baths to induce phase separation and solidify into shape, and the polymer solution direct contact with the coagulation bath. Hence, the composition of the coagulation bath shows an important role in membrane structure and properties. Due to its advantages of safety, convenience, and cost-effectiveness, water is frequently used as a coagulation bath in the TIPS process. Zhang et al [51] prepared a PVDF/Pluronic F127 blend membrane and added NaCl to the water bath. NaCl interacted with PVDF during the phase transition process, causing PVDF to transform from the common $\alpha$-crystalline form to the $\beta$-crystalline form (fully trans structure). This change in crystalline structure imparted improved hydrophilicity to the membrane, enhancing its resistance to organic fouling. In detail, when the NaCl concentration in the coagulation bath was higher than 50 g $L^{-1}$, X-ray diffraction (XRD) indicated that PVDF was nearly in the β-crystalline form. The pure water flux for

sample MF0 (NaCl concentration in the coagulation bath is 0 g $L^{-1}$) was 492 L $m^{-2}h^{-1}bar^{-1}$, while sample MF35 (NaCl concentration in the coagulation bath is 350 g $L^{-1}$) exhibited an increased permeation flux of 887 L $m^{-2}h^{-1}bar^{-1}$, corresponding to different permeation performance. The rejection rate for Suwannee River Natural Organic Matter (SRNOM) increased from 78% to 98%. Through fouling flux testing, MF35 maintained 66% of its initial flux, while MF0 maintained 59%. After simple cleaning, the permeation flux of MF35 recovered to 80%, significantly higher than MF0, revealing the impact of salt addition in the coagulation bath on the PVDF crystalline structure and its relationship with membrane fouling resistance. Matsuyama et al. [52] investigated the effect of NIPS (non-solvent induced phase separation) on membrane structure in the PMMA system using a coagulation bath possessing different interactions for the diluent (cyclohexanol). The results indicate that when water, which has weaker interactions with cyclohexanol, was used as the coagulation bath, the membrane pore structure close to the epidermis formed immediately due to cooling, with mass transfer occurring subsequently. After prolonged mass transfer, non-solvent permeation led to the formation of larger pores near the epidermis, and the effects of TIPS and NIPS occurred sequentially. When methanol, which has stronger interactions with cyclohexanol, was used as the coagulation bath, the mass transfer between methanol and cyclohexanol was rapid. As a result, the membrane structure was rapidly determined, with NIPS producing large pores near the upper surface and TIPS leading to small pores near the upper surface.

### *1.3.9 Temperature of coagulation bath*

When the coagulation bath temperature is relatively high, the cooling rate on the outer surface of the membrane is lower, which results in a slower crystallization rate for the polymer and an extended time for droplet coarsening. This condition is beneficial for the formation of a porous skin layer in the polymer membrane. Zhang et al [53] used a mixed diluent of triethyl phosphate (TEP) and polyethylene glycol 400 (PEG400) to investigate the unidirectional adjustment of the cross-sectional radius of

hollow fiber membranes made of PVDF based on the coagulation bath temperature. The results show that at lower coagulation bath temperatures, the TIPS process plays a dominant role because PEG400 has weaker interactions with the coagulation bath. As the temperature increases, the interaction between PEG400 and the coagulation bath leads to a roughening of the outer surface of the membrane. The finger-like pore structures near the outer skin layer increase, while the region near the inner skin layer adopts a cellular structure. Different microstructures form at varying distances from the outer skin layer within the cross-section of the hollow fiber membrane. Additionally, PEG400 acts as a pore-forming agent and structure regulator during the membrane formation process, enhancing the permeability and mechanical properties of the membrane.

### *1.4 Challenge in polymeric porous membrane preparation via TIPS method.*

Numerous polymer membrane materials have been developed using the TIPS method, including polyvinylidene fluoride (PVDF) [54-56], polypropylene (PP) [57-59], poly (vinyl butyral) (PVB) [60], polyamide (PA) [61-63], polyethylene (PE) [64-66], poly (ethylene-co-vinyl alcohol) (EVOH) [67, 68], poly (ethylene chlorotrifluoroethylene) (ECTFE) [69], polystyrene (PS) [70], polysulfone (PSF) [71, 72], polyphenylene sulfide (PPS) [73], and polymethyl methacrylate (PMMA) [52]. Among the abovementioned polymer materials, poly (vinylidene fluoride) (PVDF) is widely used to manufacture porous membranes for microfiltration (MF), membrane bioreactor (MBR), and ultrafiltration (UF) treatment systems due to its excellent inherent properties such as good processability, high thermal stability, and great chemical resistance, which occupies approximately two-thirds of the nowadays membrane filtration market for potable water. But, unfortunately, PVDF belongs to the fluoropolymer and is made from a fluorinated monomer [74]. It was confirmed that PVDF is included as a PFAS (Per- and poly-fluoroalkyl substances (PFAS) – ECHA (Europa. eu)). The European Union has opted for the elimination of all potential sources of contamination by fluorinated organics as the most effective approach to combat

environmental pollution caused by them. Although the current leaching tests indicated no leaching of monomers or molecular fragments injurious to health, the synthesis of PVDF polymer involves fluorinated monomer, and the potential harm of PVDF to the environment and human beings remains challenge in terms of the PVDF production process and the potential for leakage or degradation during use. Therefore, in response to increasing concerns from regulatory authorities about their environmental consequences, the importance of developing more secure porous membranes to replace or reduce the usage of PVDF membranes has grown significantly.

### *1.5 Polyketone*

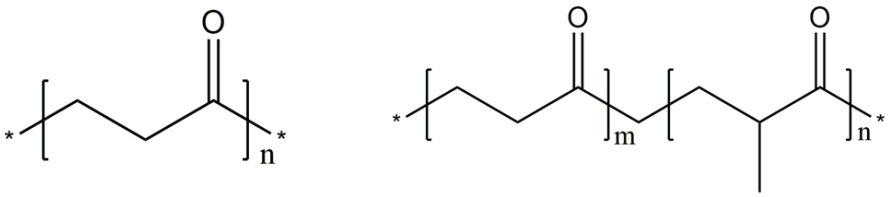


**Fig. 1-8** Polyketone molecular structure of homopolymer (HPK) (a) and copolymer (CPK) including 6 mol % of propylene (b) [75].

The semi-crystalline polymer polyketone (HPK), as shown in Fig. 1-8, has a high melting point (257°C) and considerable crystallinity degree (50-80%), consisting of ethylene and carbon monoxide. However, the high melting point temperature makes processing difficult. In addition, the polymer may decompose under long-term high-temperature conditions. To mitigate this challenge, a third monomer, propylene, was introduced into the polymerization process, resulting in a PK copolymer (CPK) with a lower melting temperature of approximately 220°C. The feedstock of synthesis of the PK polymer is cheap. It has been of extensive interest to the chemical industry because of its good mechanical properties, and high thermal and chemical resistance.

Compared with PVDF, PK shows more hydrophilic and excellent solvent resistance properties due to the ketone groups and the high crystallinity with a strongly packed structure. Consequently, in recent years, PK polymer has frequently been used as a new membrane material to prepare a high-performance microporous membrane for water treatment or as a base membrane for nanofiltration (NF) and reverse osmosis (RO) processes [76, 77]. However, PK membrane prepared by the current NIPS method involves highly toxic solvents that have negative effects on the environment and human health, such as hexafluoroisopropyl alcohol (HFIP) or m-cresol. Owing to excellent solvent resistance, PK is soluble only in powerful hydrogen bonding solvents so it is difficult to seek a new kind of harmless solvent used for the NIPS process. Thus, given the escalating stringency of environmental protection regulations, it is both intriguing and practical to explore environmentally friendly solvents for PK membrane fabrication through experimental and industrial means.

Apart from the NIPS method, TIPS is another useful technique for fabricating polymeric membranes. Compared with NIPS, TIPS, based on heat transfer, offers numerous advantages for membrane fabrication, including a straightforward preparation process, and resulting membranes with narrow pore size distribution and strong mechanical properties. Furthermore, the TIPS method can be applied to a wide range of polymeric materials, including polymers for which porous membranes cannot be prepared by the conventional NIPS method. Therefore, the preparation of PK membranes by TIPS to replace the highly toxic and complicated NIPS process is very promising.

### *1.6 Purpose of this dissertation*

This dissertation aims to develop high-water-permeance PK hollow fiber membranes using the TIPS method. PK, as a crystalline polymer, possesses excellent hydrophilicity, mechanical properties, and chemical stability, demonstrating significant potential and cost-effectiveness in the field of polymer porous membranes. This is particularly due to its low-cost synthetic materials, including ethylene, carbon monoxide, and propylene.

At present, the polyketone membrane was prepared via the NIPS process, and the prepared PK membrane exhibits excellent performance in oil-water separation or as a support layer for organic solvent nanofiltration and reverse osmosis processes, due to its outstanding solvent resistance [78-79]. However, these PK membrane preparation techniques involve toxic solvents, as well as complicated and multistep membrane-forming processes using the NIPS method [80]. Therefore, the development of a facile and environment-friendly method for PK membrane preparation is necessary. Compared to the NIPS method, the TIPS method may be more suitable due to its simple membrane formation process and the potential use of low-toxic or non-toxic solvents. However, there is less reported on the preparation of PK membranes using the TIPS process. Therefore, the study initially screened solvents for preparing PK membranes based on the TIPS process. Subsequently, based on the selected solvents, low-toxic or non-toxic solvent systems were chosen to develop porous PK fiber membranes and investigate the influence of membrane formation parameters on membrane structure and performance. During the experimental process, it was found that traditional spinning equipment (double orifice spinnerets) had difficulty effectively controlling the outer surface structure of PK hollow fiber membranes. Therefore, a triple orifice spinneret was used to extrude solvent on the outside of the polymer solution to control membrane structure and produce high-throughput PK hollow fiber membranes.

### *1.7 Overview of this dissertation*

This dissertation included five chapters, as follows:

Chapter 1, the background and purpose of this research are generally introduced.

Chapter 2, PK membranes were developed via TIPS methods. The diluent applicable to PK polymer in the TIPS process may be selected by comparing the Hanson solubility parameters of the solvent tried. In this work, more attention has been paid to the diluents that induced an L-L phase separation regarding the phase diagrams and membrane structure with different preparation conditions including a change of quenching bath temperature and cooling rate. For the copolymer PK (CPK), polyethylene 300 (PEG300)

and di-n-propyl phthalaate (DPrP) can induce an L-L phase separation meaning a weak interaction with CPK, while only polyethylene 200 (PEG200) can induce an L-L phase separation for homopolymer PK (HPK). Meanwhile, mixed diluents of the PEG series were also investigated in the case of HPK and found that increasing the amount of non-diluent PEG or the molecular weight can weaken the interaction between the diluent and PK. Finally, comparisons including structure, water permeance, and mechanical properties in membranes prepared by NIPS and TIPS processes respectively have been implemented. Even at higher PK concentrations, the prepared membranes via TIPS have a relatively high pure water permeance.

Chapter 3, the PK hollow fiber membrane was prepared via the TIPS method using the low-toxic PEG300/TEG system. The effects of TEG ratio in the diluent, PK concentration, and bore liquid composition on the phase diagram, membrane structure, and performance have been extensively investigated. Interestingly, due to the addition of TEG, an S-L phase separation system diluent for PK, in the dope solution, the spinning temperature of PK/diluents significantly decreased from 245°C to 200°C, meanwhile, the interconnected membrane with negligible changes in performances was formed, based on the L-L phase separation process. The increased PK concentration significantly enhanced the tensile strength from 3.3 MPa to 8.4 MPa. With the increased PC ratio in bore liquid, a high surface porosity is formed on the inner surface, leading to a significant enhancement in pure water permeability. Finally, the prepared PK hollow fiber membrane exhibits excellent stability for organic solvents, including methanol (MeOH), toluene, acetone, dimethylformamide (DMF), dimethyl sulfoxide (DMSO), hexane, chloroform, isopropanol (IPA), and tetrahydrofuran (THF).

Chapter 4, PK hollow fiber membranes were prepared via the TIPS method using the triple orifice spinneret. The interconnected bulk structure was formed during the L-L phase separation in the TIPS process and the porous inner surface resulted from the penetration of bore liquid propylene carbonate (PC). In order to prepare the porous outer surface to improve the water permeance, a triple orifice spinneret was employed to extrude the solvent on the outside of the PK solution by the third channel. Based on

the fixed air gap of 5 cm, different types of extrusion solvents, including PC, sulfolane (SFL), dimethyl phthalate (DMP), diethyl phthalate (DEP), triethylene glycol (TEG), PEG300, and polyethylene 600 (PEG600), were used to prepare PK hollow fiber membranes. when the extrusion solvent, including TEG, PEG300, and PEG600, exhibits high interaction with the diluent, and the diluent aggregation on the outside of the PK solution induces a porous outer surface. When PC, SFL, DMP, and DEP were used as the extrusion solvent, the penetration of the extrusion solvent induced the porous outer surface, even the extrusion solvent possessed a better interaction with PK than diluent. Finally, the prepared PK hollow fiber membrane exhibits high water permeance by extruded solvent on the outside of the PK solution, while having a slight decrease in mechanical strength. The effects of preparation parameters on membrane structure and performance were investigated. SFL was extruded on the outside of the PK solution, when the air distance increased from 1 to 5 cm, the water permeance increased significantly increased significantly from 179 to 1892 L $m^{-2}h^{-2}bar^{-1}$. When PK solution contracts air (without extrusion solvent), the water permeance rapidly decreased to 27 L $m^{-2}h^{-2}bar^{-1}$, despective the air gap was fixed at 5 cm.

Chapter 5, all chapters were summarized as the conclusion for the whole dissertation.

***References***

[1] J.A.A. Nollet, Investigations on the causes for the ebullition of liquids, J. Membr. Sci., 100 (1995) 1-3.

[2] J. Wisniak, Thomas Graham. II. Contributions to diffusion of gases and liquids, colloids, dialysis, and osmosis, Educación Química, 24 (2013) 506-515.

[3] X. Tan, D. Rodrigue, A review on porous polymeric membrane preparation. part I: production techniques with polysulfone and poly (vinylidene fluoride), Polymers (Basel), 11 (2019) 1160.

[4] Y. Tang, Y. Lin, W. Ma, X. Wang, A review on microporous polyvinylidene fluoride membranes fabricated via thermally induced phase separation for MF/UF application, J. Membr. Sci., 639 (2021) 119759.

[5] D. Yadav, S. Karki, P.G. Ingole, Nanofiltration (NF) membrane processing in the food industry, Food Eng. Rev., 14 (2022) 579-595.

[6] C. Charcosset, Classical and recent applications of membrane processes in the food industry, Food Eng. Rev., 13 (2020) 322-343.

[7] E.R. Radu, S.I. Voicu, V.K. Thakur, Polymeric membranes for biomedical applications, Polymers (Basel), 15 (2023) 619.

[8] A. Sueoka, K. Takakura, Hollow fiber membrane application for blood treatment, Polym J, 23 (1991) 561-571.

[9] Cabasso, I. In encyclopedia of polymer science and engineering Vol. 9, John Wiley & Sons, New York, 1987, pp 509-579.

[10] C. Li, W. Sun, Z. Lu, X. Ao, S. Li, Ceramic nanocomposite membranes and membrane fouling: A review, Water Res, 175 (2020) 115674.

[11] B. Zhu, M. Duke, L.F. Dumee, A. Merenda, E. des Ligneris, L. Kong, P.D. Hodgson, S. Gray, Short review on porous metal membranes-fabrication, commercial products, and applications, Membranes (Basel), 8 (2018) 83.

[12] H. Li, Y. Liu, A review of polymer-derived carbon molecular sieve membranes for gas separation, NEW CARBON MATER, 37 (2022) 484-507.

[13] B. Liang, B. Li, Z. Li, B. Chen, Progress in multifunctional metal-organic frameworks/polymer hybrid membranes, Chemistry, 27 (2021) 12940-12952.

[14] I. Pinnau, B.D. Freeman, Membrane Formation and Modification, Copyright, Advisory Board, Foreword, (1999).

[15] J. Kima, T. Jang, Youngdon Kwon, U. Kim, S. Kimb, Structural- study of microporous polypropylene hollow fiber membranes made by the melt-spinning and cold-stretching method, J. Membr. Sci., 93 (1994) 209-215.

[16] C. Du, Y. Xu, B. Zhu, Structure formation and characterization of PVDF hollow fiber membranes by melt-spinning and stretching method, J. Appl. Polym. Sci., 106 (2007) 1793-1799.

[17] K. Gerlach, E. Kessler and W. Henne, Hollow fiber membrane for plasma separation, U.S. Pat. 4,708,799 (1987).

[18] X. Dong, D. Lu, T.A.L. Harris, I.C. Escobar, Polymers and solvents used in membrane fabrication: A review focusing on sustainable membrane Development, Membranes (Basel), 11 (2021) 309.

[19] D.R. Lloyd, Microporous membrane formation via thermally induced phase separation. I. solid-liquid phase separation, J. Membr. Sci., 52 (1990) 239-261.

[20] D.R. Lloyd, S.S. Kim, K.E. Kinzer, Microporous membrane formation via thermally induced phase separation. II. Liquid-liquid phase separation, J. Membr. Sci., 64 (1991) 1-11.

[21] S. Xiang, X. Tang, S. Rajabzadeh, P. Zhang, Z. Cui, H. Matsuyama, Fabrication of PVDF/EVOH blend hollow fiber membranes with hydrophilic property via thermally induced phase process, Sep. Purif. Technol., 301 (2022) 122031.

[22] N.T. Hassankiadeh, Z. Cui, J.H. Kim, D.W. Shin, A. Sanguineti, V. Arcella, Y.M. Lee, E. Drioli, PVDF hollow fiber membranes prepared from green diluent via thermally induced phase separation: Effect of PVDF molecular weight, J. Membr. Sci., 471 (2014) 237-246.

[23] S. Xiang, Z. Guo, Y. Wang, H. Liu, J. Zhang, Z. Cui, H. Wang, J. Li, The microstructure regulation, strengthening, toughening and hydrophilicity of polyamide6 in fabricating poly (vinylidene fluoride)-based flat membrane via the thermally induced phase separation technique, Eur. Polym. J., 126 (2020) 109568.

[24] H. Matsuyama, Y. Takida, T. Maki, M. Teramoto, Preparation of porous membrane by combined use of thermally induced phase separation and immersion precipitation, Polymer 43 (2002) 5243-5248.

[25] J. Kim, J. Hwang, U. Kim, S. Kim, Operation parameters of melt spinning of polypropylene hollow fiber membranes, J. Membr. Sci., 108 (1995) 25-36.

[26] P. Zhang, C. Fang, S. Rajabzadeh, W. Liu, Y. Jia, Q. Shen, L. Zhang, S. Wang, N. Kato, H. Matsuyama, Effect of polymer molecular weight on structure and performance of PVDF hollow fiber membranes prepared via TIPS process with co-extrusion of solvent using triple orifice spinneret, J. Membr. Sci., 620 (2021) 118854.

[27] Z. Cui, W. Li, H. Zeng, X. Tang, J. Zhang, S. Qin, N. Han, J. Li, Fabricating PVDF

hollow fiber microfiltration membrane with a tenon-connection structure via the thermally induced phase separation process to enhance strength and permeability, Eur. Polym. J., 111 (2019) 49-62.

[28] Z. Wu, Z. Cui, T. Li, S. Qin, B. He, N. Han, J. Li, Fabrication of PVDF-based blend membrane with a thin hydrophilic deposition layer and a network structure supporting layer via the thermally induced phase separation followed by non-solvent induced phase separation process, Appl. Surf. Sci., 419 (2017) 429-438.

[29] Z. Cui, N.T. Hassankiadeh, S.Y. Lee, K.T. Woo, J.M. Lee, A. Sanguineti, V. Arcella, Y.M. Lee, E. Drioli, Tailoring novel fibrillar morphologies in poly(vinylidene fluoride) membranes using a low toxic triethylene glycol diacetate (TEGDA) diluent, J. Membr. Sci., 473 (2015) 128-136.

[30] G. Liu, J. Pan, X. Xu, Z. Wang, Z. Cui, Preparation of ECTFE porous membrane with a green diluent TOTM and performance in VMD process, J. Membr. Sci., 612 (2020) 118375.

[31] N.T. Hassankiadeh, Z. Cui, J.H. Kim, D.W. Shin, S.Y. Lee, A. Sanguineti, V. Arcella, Y.M. Lee, E. Drioli, Microporous poly(vinylidene fluoride) hollow fiber membranes fabricated with PolarClean as water-soluble green diluent and additives, J. Membr. Sci., 479 (2015) 204-212.

[32] Z. Cui, N.T. Hassankiadeh, S.Y. Lee, J.M. Lee, K.T. Woo, A. Sanguineti, V. Arcella, Y.M. Lee, E. Drioli, Poly(vinylidene fluoride) membrane preparation with an environmental diluent via thermally induced phase separation, J. Membr. Sci., 444 (2013) 223-236.

[33] D. Zou, H.W. Kim, S.M. Jeon, Y.M. Lee, Fabrication and modification of PVDF/PSF hollow-fiber membranes for ginseng extract and saline water separations via direct contact membrane distillation, J. Membr. Sci., 644 (2022) 120101.

[34] S. Yu, Y. Huang, L. Zhang, Q. Wang, Z. Wang, Z. Cui, E. Drioli, ECTFE membrane fabrication using green binary diluents TEGDA/TOTM and its performance in membrane condenser, Membranes (Basel), 12 (2022) 757.

[35] Y. Wang, Y. Liu, X. Wei, L. Ding, Y. Feng, Z. Zhao, Polypropylene hollow fiber

membrane prepared with green binary diluents via TIPS: Effects of spinning process parameters and VMD desalination performance, Desalination, 541 (2022) 116026.

[36] S. Yan, Y. Wang, W. Wang, Z. Zhao, Effect of extrusion temperature on PP hollow fiber membrane properties and its $CO_2$ degassing performance, IOP Conf. Ser.: Earth Environ. Sci., 330 (2019) 032108.

[37] K. Xu, Y. Cai, N.T. Hassankiadeh, Y. Cheng, X. Li, X. Wang, Z. Wang, E. Drioli, Z. Cui, ECTFE membrane fabrication via TIPS method using ATBC diluent for vacuum membrane distillation, Desalination, 456 (2019) 13-22.

[38] H. Ajari, B. Chaouachi, F. Galiano, T. Marino, F. Russo, A. Figoli, A novel approach for dissolving crystalline LDPE using non-toxic solvents for membranes preparation, Environ. Sci. Technol., 16 (2018) 5375-5386.

[39] A. Borchers, T. Pieler, Programming pluripotent precursor cells derived from Xenopus embryos to generate specific tissues and organs, Genes (Basel), 1 (2010) 413-426.

[40] Y. Tang, Y. He, X. Wang, Effect of adding a second diluent on the membrane formation of polymer/diluent system via thermally induced phase separation: Dissipative particle dynamics simulation and its experimental verification, J. Membr. Sci., 409-410 (2012) 164-172.

[41] Z. Yang, P. Li, L. Xie, Z. Wang, S. Wang, Preparation of iPP hollow-fiber microporous membranes via thermally induced phase separation with co-solvents of DBP and DOP, Desalination, 192 (2006) 168-181.

[42] G. Ji, C. Du, B. Zhu, Y. Xu, Preparation of porous PVDF membrane via thermally induced phase separation with diluent mixture of DBP and DEHP, J. Appl. Polym. Sci., 105 (2007) 1496-1502.

[43] H. Zhang, X. Lu, Z. Liu, Z. Ma, S. Wu, Z. Li, X. Kong, J. Liu, C. Wu, The unidirectional regulatory role of coagulation bath temperature on cross-section radius of the PVDF hollow-fiber membrane, J. Membr. Sci., 550 (2018) 9-17.

[44] J. Liu, X. Lu, J. Li, C. Wu, Preparation and properties of poly (vinylidene fluoride) membranes via the low temperature thermally induced phase separation method, J.

Polym. Res., 21 (2014) 2-16.

[45] Z. Guo, Y. Yang, S. Xiang, X. Du, Z. Cui, B. He, H. Wang, J. Li, T. Jiang, Preparation of PVDF membrane based on “In-situ Template-TIPS” technology and the investigation on membrane formation mechanism, microstructure regulation and permeability, J. Membr. Sci., 620 (2021) 118839.

[46] A. Cui, Z. Liu, C. Xiao, Y. Zhang, Effect of micro-sized $SiO_2$-particle on the performance of PVDF blend membranes via TIPS, J. Membr. Sci., 360 (2010) 259-264.

[47] Z. Jiang, C. Xiao, X. Hu, Preparation and characterization of polyamide-6/$CaCO_3$ hybrid hollow fiber membranes, e-Polymers, 13 (2013) 1-10.

[48] Hideto Matsuyama, Stephane Berghmans, D.R. Lloyd, Formation of hydrophilic microporous membranes via thermally induced phase separation, J. Membr. Sci., 142 (1998) 213-224.

[49] S. Berghmans, H. Berghmans, H.E.H. Meijer, Spinning of hollow porous fibers via the TIPS mechanism, J. Membr. Sci., 116 (1996) 171-189.

[50] C. Fang, S. Rajabzadeh, H. Wu, X. Yu, N. Kato, M. Kunimatsu, T. Yoshioka, H. Matsuyama, Effect of mass transfer at the interface of the polymer solution and extruded solvent during the air gap on membrane structures and performances in TIPS process using triple-orifice spinneret, J. Membr. Sci., 595 (2020) 117513.

[51] Y. Zhang, L. Ye, B. Zhang, Y. Chen, W. Zhao, G. Yang, J. Wang, H. Zhang, Characteristics and performance of PVDF membrane prepared by using NaCl coagulation bath: Relationship between membrane polymorphous structure and organic fouling, J. Membr. Sci., 579 (2019) 22-32.

[52] H. Matsuyama, Y. Takida, T. Maki, M. Teramoto, Preparation of porous membrane by combined use of thermally induced phase separation and immersion precipitation, Polymer, 43 (2002) 5243-5248.

[53] H. Zhang, X. Lu, Z. Liu, Z. Ma, S. Wu, Z. Li, X. Kong, C. Wu, Study of the dual role mechanism of water-soluble additive in low temperature thermally-induced phase separation, J. Membr. Sci., 543 (2017) 1-9.

[54] G. Ji, L. Zhu, B. Zhu, C. Zhang, Y. Xu, Structure formation and characterization

of PVDF hollow fiber membrane prepared via TIPS with diluent mixture, J. Membr. Sci., 319 (2008) 264-270.

[55] M. Gu, J. Zhang, X. Wang, H. Tao, L. Ge, Formation of poly(vinylidene fluoride) (PVDF) membranes via thermally induced phase separation, Desalination, 192 (2006) 160-167.

[56] P. Zhang, S. Rajabzadeh, Q. Song, R.R. Gonzales, Y. Jia, S. Xiang, Z. Li, H. Matsuyama, Development of loose nanofiltration PVDF hollow fiber membrane for dye/salt separation, Desalination, 549 (2023) 116315.

[57] W. Yave, R. Quijada, D. Serafini, D. Lloyd, Effect of the polypropylene type on polymer–diluent phase diagrams and membrane structure in membranes formed via the TIPS process Part II. Syndiotactic and isotactic polypropylenes produced using metallocene catalysts, J. Membr. Sci., 263 (2005) 154-159.

[58] W. Yave, R. Quijada, M. Ulbricht, R. Benavente, Syndiotactic polypropylene as potential material for the preparation of porous membranes via thermally induced phase separation (TIPS) process, Polymer, 46 (2005) 11582-11590.

[59] Y.J. Wang, Z.P. Zhao, Z.Y. Xi, S.Y. Yan, Microporous polypropylene membrane prepared via TIPS using environment-friendly binary diluents and its VMD performance, J. Membr. Sci., 548 (2018) 332-344.

[60] Y.R. Qiu, H. Matsuyama, G.Y. Gao, Y.W. Ou, C. Miao, Effects of diluent molecular weight on the performance of hydrophilic poly(vinyl butyral)/Pluronic F127 blend hollow fiber membrane via thermally induced phase separation, J. Membr. Sci., 338 (2009) 128-134.

[61] S. Jeon, H. Karkhanechi, L. Fang, L. Cheng, T. Ono, R. Nakamura, H. Matsuyama, Novel preparation and fundamental characterization of polyamide 6 self-supporting hollow fiber membranes via thermally induced phase separation (TIPS), J. Membr. Sci., 546 (2018) 1-14.

[62] N. Kato, R.R. Gonzales, A. Nishitani, Y. Negi, T. Ono, H. Matsuyama, Single-step preparation of nanocomposite polyamide 6 hollow fiber membrane with integrally skinned asymmetric structure for organic solvent nanofiltration, Colloids Surf. A

Physicochem. Eng. Asp., 620 (2021) 126538.

[63] K. Umakoshi, R.R. Gonzales, N. Kato, P. Zhang, T. Ono, H. Matsuyama, Effect of polymer-solvent compatibility on polyamide hollow fiber membranes prepared via thermally induced phase separation, Colloids Surf. A Physicochem. Eng. Asp., 642 (2022) 128704.

[64] M.A. Kivi, H. Alinia, Y. Jafarzadeh, R. Yegani, High-density polyethylene membranes embedded with carboxylated and polyethylene glycol-grafted nanodiamond to be used in membrane bioreactors, J. Appl. Polym. Sci., 136 (2019) 47914.

[65] Y. Jafarzadeh, R. Yegani, S.B. Tantekin-Ersolmaz, Effect of $TiO_2$ nanoparticles on structure and properties of high density polyethylene membranes prepared by thermally induced phase separation method, Polym. Adv. Technol., 26 (2015) 392-398.

[66] Y. Jafarzadeh, R. Yegani, M. Sedaghat, Preparation, characterization and fouling analysis of ZnO/polyethylene hybrid membranes for collagen separation, Chem. Eng. Res. Des., 94 (2015) 417-427.

[67] M. Shang, H. Matsuyama, M. Teramoto, J. Okuno, D.R. Lloyd, N. Kubota, Effect of diluent on poly(ethylene-co-vinyl alcohol) hollow-fiber membrane formation via thermally induced phase separation, J. Appl. Polym. Sci., 95 (2005) 219-225.

[68] M. Shang, H. Matsuyama, M. Teramoto, D.R. Lloyd, N. Kubota, Preparation and membrane performance of poly(ethylene-co-vinyl alcohol) hollow fiber membrane via thermally induced phase separation, Polymer, 44 (2003) 7441-7447.

[69] J. Pan, W. Ma, L. Huang, R. Li, Q. Huang, C. Xiao, Z. Jiang, Fabrication and characterization of ECTFE hollow fiber membranes via low-temperature thermally induced phase separation (L-TIPS), J. Membr. Sci., 634 (2021) 119429.

[70] G.C. You, L. An, F.L. Xian, Y.X. Su, S.J. Cong, Factors controlling surface morphology of porous polystyrene membranes prepared by thermally induced phase separation, Polym. Int., 49 (2000) 323-328.

[71] H.Q. Liang, H.N. Li, H.H. Yu, Y.T. Zhou, Z.K. Xu, Polysulfone membranes via thermally induced phase separation, Chin. J. Chem. Eng., 35 (2017) 846-856.

[72] H. Matsuyama, T. Maki, M. Teramoto, K. Kobayashi, Effect of PVP additive on porous polysulfone membrane formation by immersion precipitation method, Sep Sci Technol, 38 (2003) 3449-3458.

[73] T. Fan, Z. Li, B. Cheng, J. Li, Preparation, characterization of PPS micro-porous membranes and their excellent performance in vacuum membrane distillation, J. Membr. Sci., 556 (2018) 107-117.

[74] F. Faiz, G. Baxter, S. Collins, F. Sidiroglou, M. Cran, Polyvinylidene fluoride coated optical fibre for detecting perfluorinated chemicals, Sens. Actuators B Chem., 312 (2020) 128006.

[75] S. Xiang, P. Zhang, S. Rajabzadeh, R.R. Gonzales, Z. Li, Y. Shi, S. Zhou, M. Hu, K. Guan, H. Matsuyama, Development of porous polyketone membrane via liquid–liquid thermally induced phase separation, J. Membr. Sci., 677 (2023) 121639.

[76] C. Wang, M.J. Park, D.H. Seo, S. Phuntsho, R.R. Gonzales, H. Matsuyama, E. Drioli, H.K. Shon, Inkjet printed polyelectrolyte multilayer membrane using a polyketone support for organic solvent nanofiltration, J. Membr. Sci., 642 (2022) 119943.

[77] C. Liu, R. Takagi, D. Saeki, L. Cheng, T. Shintani, T. Yasui, H. Matsuyama, Highly improved organic solvent reverse osmosis (OSRO) membrane for organic liquid mixture separation by simple heat treatment, J. Membr. Sci., 618 (2021) 118710.

[78] K. Guan, L. Zhang, S. Wang, R. Takagi, H. Matsuyama, Controlling the formation of porous polyketone membranes via a cross-linkable alginate additive for oil-in-water emulsion separations, J. Membr. Sci., 611 (2020) 118362.

[79] Y. Jia, K. Guan, L. Zhang, Y. Lin, Q. Shen, P. Zhang, H. Matsuyama, Enabling polyketone membrane with underwater superoleophobicity via a hydrogel-based modification for high-efficiency oil-in-water emulsion separation, J. Membr. Sci., 618 (2021) 118705.

[80] Y. Jia, K. Guan, P. Zhang, Q. Shen, T. Istirokhatun, Y. Lin, H. Matsuyama, Nanostructural manipulation of polyphenol coatings for superwetting membrane surfaces, ACS Sustain. Chem. Eng., 9 (2021) 14525-14536.

# Chapter 2

## Development of porous polyketone membrane via liquid–liquid thermally induced phase separation

### *2.1 Introduction*

Semicrystalline aliphatic polyketone (PK) is one of the most attractive polymeric materials in a broad range of chemical industries because of its useful combination of excellent mechanical properties and high thermal and chemical resistance, as well as its low-cost precursor monomers [1-4]. The homopolymer of PK is considered a regular structure (Fig. 2-1(a)) consisting of perfectly alternating ethylene and carbon monoxide and featuring a high melting temperature of approximately 257 °C [2, 5]. However, the application of this type of PK is limited because of its rapid decomposition at high processing temperatures [2]. To avoid this problem, an appropriate proportion of a third monomer, propylene, was introduced during the polymerization process to obtain a random copolymer with a melting temperature of 220 °C, as illustrated in Fig. 2-1(b), which also exhibits many desirable characteristics [2, 4, 6, 7]. Notably, the PK copolymer has lower hydrophilicity than the PK homopolymer because of the introduction of methyl groups from propylene.

In recent years, PK has attracted increasing attention as a material for membrane separation technologies owing to its intrinsic hydrophilicity and excellent resistance to organic solvents [5, 8-12]. For example, a PK membrane with a fibril-like porous structure features superwetting/antiwetting states in oil–water emulsion systems [5]. Using a PK membrane as the support layer for thin film composite (TFC) membranes,

organic solvent reverse osmosis (OSRO) membranes were prepared, and good separation of several solvent mixtures was obtained [13, 14]. However, these PK membrane preparation techniques involve toxic solvents, as well as complicated and multistep membrane-forming processes using the nonsolvent induced phase separation (NIPS) method [10, 15, 16]. For example, in the NIPS method, an aqueous resorcinol solution, which may also contain mixed salts, is usually used as the solvent to obtain a homogeneous PK solution; this poses a serious threat to human health and the environment [12, 17]. Then, a methanol/water solution is employed to induce phase separation and form a primary membrane, which is immersed successively in hexane and acetone for a certain time [12]. In addition, owing to its excellent solvent resistance, finding other suitable solvents for dissolving PK for the NIPS method is difficult. Therefore, the development of a facile and environment-friendly method for PK membrane preparation is in high demand.

Apart from the NIPS method, the thermally induced phase separation (TIPS) method is another common technology for preparing porous membranes based on the removal of thermal energy from a polymeric solution system [18]. Normally, during the TIPS method, the polymer and diluent are first mixed at high temperature to form a homogeneous solution, which is then extruded or cast into a primary membrane with a desired shape. The membrane is then quenched into a cooling medium to induce phase separation. After extraction of the diluent, a microporous membrane is obtained [19]. Notably, the diluent used in the TIPS method requires a high boiling point [18-20]. Compared to the NIPS method, the TIPS method can be applied to a broad range of polymers, including polymers for which porous membranes cannot be prepared by the conventional NIPS method. TIPS has been frequently employed to prepare polymeric membranes including polypropylene (PP) [21-23], polyvinylidene fluoride (PVDF) [24, 25], polyamide (PA) [20, 26], poly (ethylene chlorotrifluoroethylene) (ECTFE) [27, 28], poly(ethylene-co-vinyl alcohol) (EVOH) [29], polystyrene (PS) [30], polyacrylonitrile (PAN) [31], and polysulfone (PSF) [32-34]. Although PK porous membranes have

already been prepared using the TIPS method [35], a detailed investigation of the phase separation mechanism has not been carried out.

In the TIPS technique, the diluent plays a crucial role in the membrane structure, properties, and filtration performance. For a semi-crystalline polymer, TIPS can proceed via solid–liquid (S-L, polymer crystallization) phase separation or liquid–liquid (L-L) phase separation, depending on the compatibility between the polymer and diluent [18, 19]. If the polymer/diluent compatibility is high, the polymer/diluent system undergoes S-L phase separation, leading to a spherulitic structure of the resultant membrane. Conversely, L-L phase separation occurs in polymer/diluent system with low compatibility, forming an interconnected or cellular structure [36]. Membranes with spherulitic structures have been reported to have poor mechanical properties because of the low interconnection between the spherulites [37, 38], whereas a porous membrane with an interconnected structure usually possesses a relatively high mechanical strength. In addition, membrane preparation conditions such as polymer concentration [39], additives in the polymer dope solution [40, 41], quenching bath temperature [42, 43], composition of the quenching bath [44], and post-treatment [45] could also influence the membrane formation process, as well as the final membrane structure and performance.

In this study, porous PK membranes with interconnected structures were prepared via the TIPS method for two types of PKs of copolymer PK (CPK) and homopolymer PK (HPK). First, diluents suitable for inducing the L-L phase separation were screened. The effects of cooling conditions and polymer concentration on the membrane structure were comprehensively investigated for different PK/diluent systems. Finally, porous structure, water permeability and mechanical properties of the membranes prepared using the NIPS and TIPS methods were compared.

## *2.2 Experiment*

### *2.2.1 Materials*

Two types of polyketone (homopolymer and copolymer, Fig. 2-1) were studied in this work. The PK homopolymer (HPK) was supplied by Asahi Kasei Co., Ltd. (Japan). The PK copolymer (CPK, grade M630A) was purchased from Hyosung Corporation Co., Ltd. (South Korea). Polyethylene glycol (PEG200, PEG300, PEG400, and PEG600), di-*n*-propyl phthalate (DPrP), lithium chloride (LiCl), calcium chloride ($CaCl_2$), zinc chloride ($ZnCl_2$), ethanol and 1-Butanol were purchased from Tokyo Chemical Industry Co., Ltd. (Japan). Resorcinol, sulfolane (SFL), propylene carbonate (PC), caprolactam (CPL), dimethyl sulfone ($DMSO_2$), diphenyl carbonate (DPC), dimethyl phthalate (DMP), diethyl phthalate (DEP), triethylene glycol (TEG), glycerol, propylene glycol 400 (PPG400), diethylene glycol (DEG), glycerol triacetate (GTA), triethyl citrate (TEC), acetyl tributyl citrate (ATBC), acetyl triethyl citrate (ATEC), dibutyl sebacate (DBS), diphenylmethane (DPM), diisobutyl adipate (DIBA) and ethylene glycol (EG), were purchased from Wako Pure Chemical Corp. (Japan). Pure water was obtained using a Milli-Q IQ 7000 ultrapure water system (Millipore SAS, France). None of the reagents were purified before use.

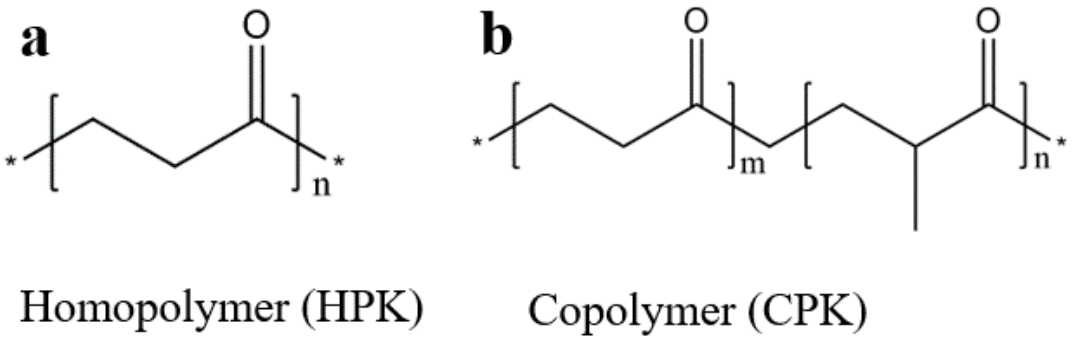


**Fig. 2-1** Polyketone molecular structure of homopolymer (HPK) (a) and copolymer (CPK) including 6 mol % of propylene (b).

### *2.2.2 Screening of diluent for PK membrane preparation*

To prepare the polyketone membrane, a large number of diluents were used to dissolve the PKs. In detail, the weighed PK and diluent were mixed in a test tube and heated in an oil bath at a maximum temperature of 250 °C. If a homogeneous solution formed, the PK solution was quenched in liquid nitrogen to induce solidification. The solid was then cut into small pieces and placed between a pair of microscope coverslips with a square opening Teflon film of 100 μm thickness. The sample was heated by LK-600 PH hot stage (Linkam, Surrey, UK) to form a homogenous transparent solution and cooled to 25 °C at a controlled rate of 10 °C $min^{-1}$. Upon cooling, an Olympus BX50 optical microscope (Tokyo, Japan) was used to observe the appearance of cloud points or crystallization to confirm whether the system underwent S-L or L-L phase separation.

### *2.2.3. Phase diagram of cloud point and crystallization temperature of the selected polymeric solutions*

The cloud point temperature ($T_{cloud}$) for the PK/diluent system was measured using a hot stage and an optical microscope, as described above. $T_{cloud}$ is the temperature at which droplets appear during the cooling process.

Differential scanning calorimetry (DSC; DSC-8500, Perkin Elmer, USA) was used to measure the crystallization temperature ($T_{cry}$) of samples at a cooling rate of 10 °C $min^{-1}$. The initial temperature of the exothermic peak during cooling process was selected as $T_{cry}$.

### *2.2.4 Preparation of small size membrane*

Small-size membranes were prepared using a hot stage to evaluate the porous membrane structures. After the polymeric sample was heated on the hot stage to form a homogeneous solution, the polymer solution with coverslip was cooled to prepare a primary membrane by different cooling procedures, which included water bath (10 °C and 50 °C) quenching and controlled cooling (50 °C $min^{-1}$ and 10 °C $min^{-1}$ cooling rates)

by hot stage. After extracting the diluent with ethanol, a primary membrane was obtained.

### *2.2.5 Preparation of flat sheet membranes*

For the TIPS method, after dissolving PK into the diluent and degassing at the preparation temperatures, the homogeneous PK/diluent solution was cast onto a preheated stainless-steel plate (15 × 15 cm) with a square opening Teflon film of 200 μm thickness. Then, it was covered with another preheated stainless-steel plate and immersed in a water quenching bath (10 °C) to induce phase separation. Finally, a flat sheet membrane was prepared and stored in pure water after extraction with ethanol. The diluents used for HPK and CPK membranes were PEG200 and PEG300, respectively.

For the NIPS method, HPK and CPK flat sheet membranes were prepared by referring to previously published works [15, 46]. In brief, as for the HPK membrane, the pre-weighed HPK polymer was dissolved into mixed solvent including resorcinol (65 wt%) and water (35 wt%) at 80 °C with stirring to form a homogeneous solution. After removing the bubbles in an oven for 12 h at 60 °C, the dope solution was cast onto a glass plate of thickness 200 μm and immersed in a methanol/water (35:65 w/w) mixed solution for 20 min to form the primary membrane. After washing the primary membrane with acetone and hexane for 20 min each, the HPK flat sheet membrane was dried in air and stored.

In the case of CPK membrane, the pre-weighed CPK polymer was dissolved in a mixed salt solution, containing lithium chloride (10 wt%), calcium chloride (10 wt%), zinc chloride (40 wt%), and water (40 wt%), at 80 °C overnight. Resorcinol (2 wt%) was then added to the polymer solution to obtain a homogenous dope solution. After removing the bubbles in an oven for 24 h at 60 °C, the dope solution was cast on a glass plate of thickness 200 μm and immediately dipped into a water bath for approximately 10 min to form the primary membrane. After washing the primary membrane with

hydrochloric acid (0.05%), acetone, and hexane for 10 min each, the CPK flat sheet membrane was dried in air and stored.

The prepared membranes were named according to the preparation method and PK concentration. For example, T-25 means that the membrane was prepared with a PK concentration of 25 wt% via the TIPS method and N-15 indicates that the membrane was prepared by the NIPS method with a PK concentration of 15 wt%.

### *2.2.6 Membrane Characterization*

Field-emission scanning electron microscopy (FE-SEM, JEOL, JSF-7500F) was used to observe the membrane morphology. Prior to observation, the membrane samples were dipped in liquid nitrogen and subsequently fractured. After vacuum drying for 12 h, the cross-section and surface were sprayed with cesium tetroxide before FESEM observation. A liquid–liquid porometer (LLP-1100A, Porous Material Inc., Ithaca, USA) was used to measure the pore diameter of the flat sheet membranes.

Self-designed cross-flow filtration equipment [47] was used to evaluate the pure water permeability (*PWP*). After running at 1.5 bar for 30 min, the operation pressure was decreased to 1 bar to test the water permeability, and the volume of permeate was recorded. *PWP* (L $m^{-2}h^{-1}bar^{-1}$) was calculated using Eq. (2-1).

$$PWP = \frac{V}{A \times \Delta t \times P} \tag{2-1}$$

where $V$ is the permeate volume (L). $A$, $\Delta t$ and $P$ represent the effective membrane area ($m^2$), operation time (h), and operation pressure (bar), respectively.

A precision tensile tester (AGS-X, Shimadzu, Japan) was used to measure the mechanical properties of flat sheet membranes. The tensile strength (MPa) and elongation at break (%) of the membranes were measured using a 50 mm measurement length and 10 mm $min^{-1}$ strain rate.

### *2.3 Results and discussion*

#### *2.3.1 Diluent screening*

According to the Hansen solubility parameter theory, the interaction parameter *R*a between the polymer and diluent can be estimated using Eq. (2-2) [48].

$$Ra = \sqrt{4(\delta_{D2} - \delta_{D1})^2 + (\delta_{P2} - \delta_{P1})^2 + (\delta_{H2} - \delta_{H1})^2} \quad (2\text{-}2)$$

where $\delta_D$, $\delta_P$ and $\delta_H$ represent the dispersion, polar and hydrogen bonding, respectively; and 1 and 2 represent components 1 and 2, respectively. A low *R*a value indicates high compatibility. The diluents tested in this study are listed in Table S2-1, from those with low *R*a to those with high *R*a. The phase separation conditions are also included in this table. Basically, in the cases of diluents with low *R*a (approximately less than 15 $(MPa)^{0.5}$), the compatibility between PK and diluents was good, and S-L phase separation occurred. Conversely, when *R*a is as high as 15 $(MPa)^{0.5}$, PK cannot dissolve in the diluents owing to the low compatibility. L-L phase separation occurred when diluents with *R*a of 12-17 $(MPa)^{0.5}$ were used (HPK/PEG200, CPK/PEG300, and CPK/DPrP cases). This is reasonable because the L-L phase separation occurred in the case of moderate compatibility between PK and diluents. Because *R*a values are not completely precise, some exceptions to the above description exist. However, rough diluent screening was found to be possible based on *R*a values.

The phase separation conditions of the mixed diluent systems are summarized in Table S2-2. *R*a values were not significantly different.

#### *2.3.2 PK copolymer (CPK) membrane*

2.3.2.1 Phase diagram of CPK/diluent system

As shown in Table S2-1, two types of diluents, water-soluble PEG300 and water-insoluble DPrP, were found to be suitable for L-L phase separation. Fig. 2-2 shows the phase diagrams of CPK/PEG300 and CPK/DPrP binary systems. The monotectic point, that is, the intersection of the cloud point line and the crystallization line, is an important parameter associated with the phase separation method. If the polymer concentration is

below this point, L-L phase separation will occur prior to polymer crystallization because $T_{cloud}$ is higher than $T_{cry}$, whereas S-L phase separation will occur above the monotectic point. As presented in Fig. 2-2(a), for the CPK/PEG300 system, a monotectic point appeared at approximately 53 wt% of CPK. The L-L phase separation region was observed below this concentration, which consequently induced the formation of an interconnected or cellular structure. Conversely, the monotectic point for the CPK/DPrP system was located at approximately 27 wt% CPK, as shown in Fig. 2-2(b). This is much lower than that of the CPK/PEG300 system, suggesting that the CPK/DPrP system has a narrower range, inducing an L-L phase separation. Simultaneously, the $T_{cloud}$ of the CPK/DPrP system was significantly lower than that of the CPK/PEG300 system at the same polymer concentration. This could be attributed to the relatively better compatibility between CPK and DPrP (Ra value of approximately 12.2, Table S2-1) than that between CPK and PEG300 (*R*a value of approximately 16.9, Table S2-1) because the cloud point shifts to a higher temperature at a fixed polymer concentration with a less compatible diluent [19].

In addition, the cooling rate has a notable influence on $T_{cry}$ for these two systems, as shown in Fig. S2-1. Higher cooling rate (50 °C $min^{-1}$ vs. 10 °C $min^{-1}$) results in a depressed apparent crystallization temperature, much lower than its corresponding equilibrium crystallization [49]. The shift of $T_{cry}$ to a lower temperature owing to the high cooling rate results in a longer time for L-L phase separation because the cooling rate has a relatively minor effect on $T_{cloud}$ [19]. The phase diagrams shown in Fig. 2-2 indicate that the porous structure of the CPK membrane can be controlled by the type of diluent and the polymer concentration.

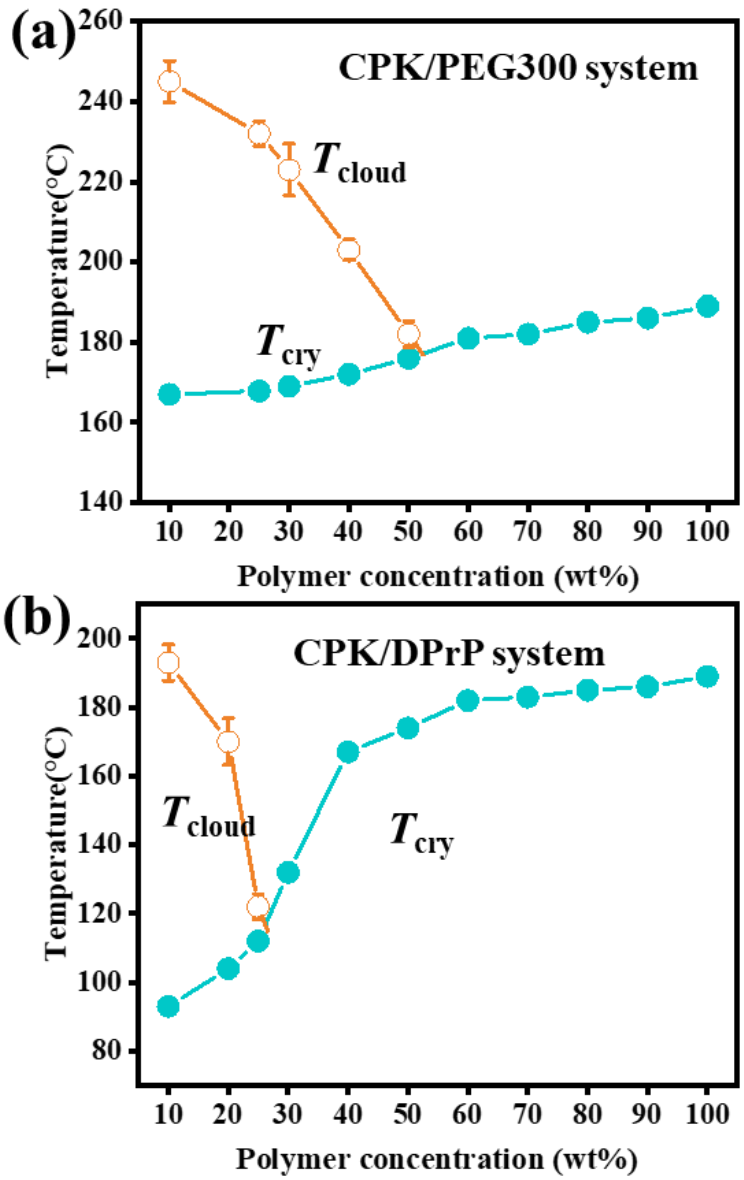


**Fig. 2-2** Cloud point and crystallization temperature of CPK/diluent systems: CPK/PEG300 system (a) and CPK/DPrP system (b).

2.3.2.2 CPK membrane structures

When a homogeneous polymer solution is cooled to a temperature below $T_{cloud}$, the system forms a large number of droplets of diluent-rich phase in the matrix of polymer-rich phases during the L-L phase separation. By coarsening, the droplets grow to large sizes until the temperature reaches $T_{cry}$, minimizing of the interfacial free energy by reducing the interfacial area [50]. Thus, the cooling rate during the coarsening process

has a significant effect on the final size of cellular structure.

Fig. 2-3 shows a series of cross-sectional structures of the membranes prepared under different cooling conditions in both the CPK/PEG300 and CPK/DPrP systems. Membranes were prepared by heating using a hot stage. The CPK concentration of all the samples was 25 wt%. An interconnected cellular structure was observed for all prepared membranes owing to the occurrence of L-L phase separation because 25 wt% was lower than the monotectic point (53%), as confirmed in the phase diagram results shown in Fig. 2-2. For the CPK/PEG300 system, the average size of the cellular structure progressively increased in the order of case 1 (quenching in 10 °C bath), case 2 (quenching in 50 °C bath), case 3 (controlled cooling at 50 °C $min^{-1}$), and case 4 (controlled cooling at 10 °C $min^{-1}$), indicating that the lower cooling rate resulted in a larger size of cellular structure. Small and interconnected cellular structures were formed in the membranes shown in Figs. 2-3(a-1) and (a-2), which were prepared by quenching in water bath at temperatures of 10 °C and 50 °C, respectively. A lower quenching bath temperature indicates a higher degree of supercooling, and the diluent-rich phase (pore) does not have sufficient time to grow before crystallization. Thus, the membrane shown in Fig. 2-3(a-1) had a smaller size of cellular structure, as shown in Fig. 2-3(a-2). On the contrary, for the membranes prepared at a controlled cooling rate of 50 °C $min^{-1}$ and 10 °C $min^{-1}$, large cellular pores were observed, as shown in Figs. 2-3(a-3) and (a-4). A slow cooling rate provided sufficient time for the diluent-rich phase to grow into large droplets, and finally, large cellular structures were formed. In the case of the lowest cooling rate of 10 °C $min^{-1}$, the largest pore of approximately 3 μm was formed.

For the CPK/DPrP system, the prepared membrane structure is different from that prepared in the CPK/PEG300 system, although they are both formed by the L-L phase separation process. The coexistence of cellular pores (L-L liquid phase separation) and spherulitic structures (polymer crystallization, S-L phase separation) was clearly observed in the CPK/DPrP system. From the phase diagram of CPK/DPrP system

shown in Fig. 2-2(b), the $T_{cloud}$ (122 °C) was observed to be very close to the $T_{cry}$ (112 °C) at a CPK concentration of 25 wt%, because the monotectic point was 27 wt%. Thus, the L-L phase separation was impeded at the earlier stage of droplet growth by crystallization, and pores existed in the pores in the spherulites.

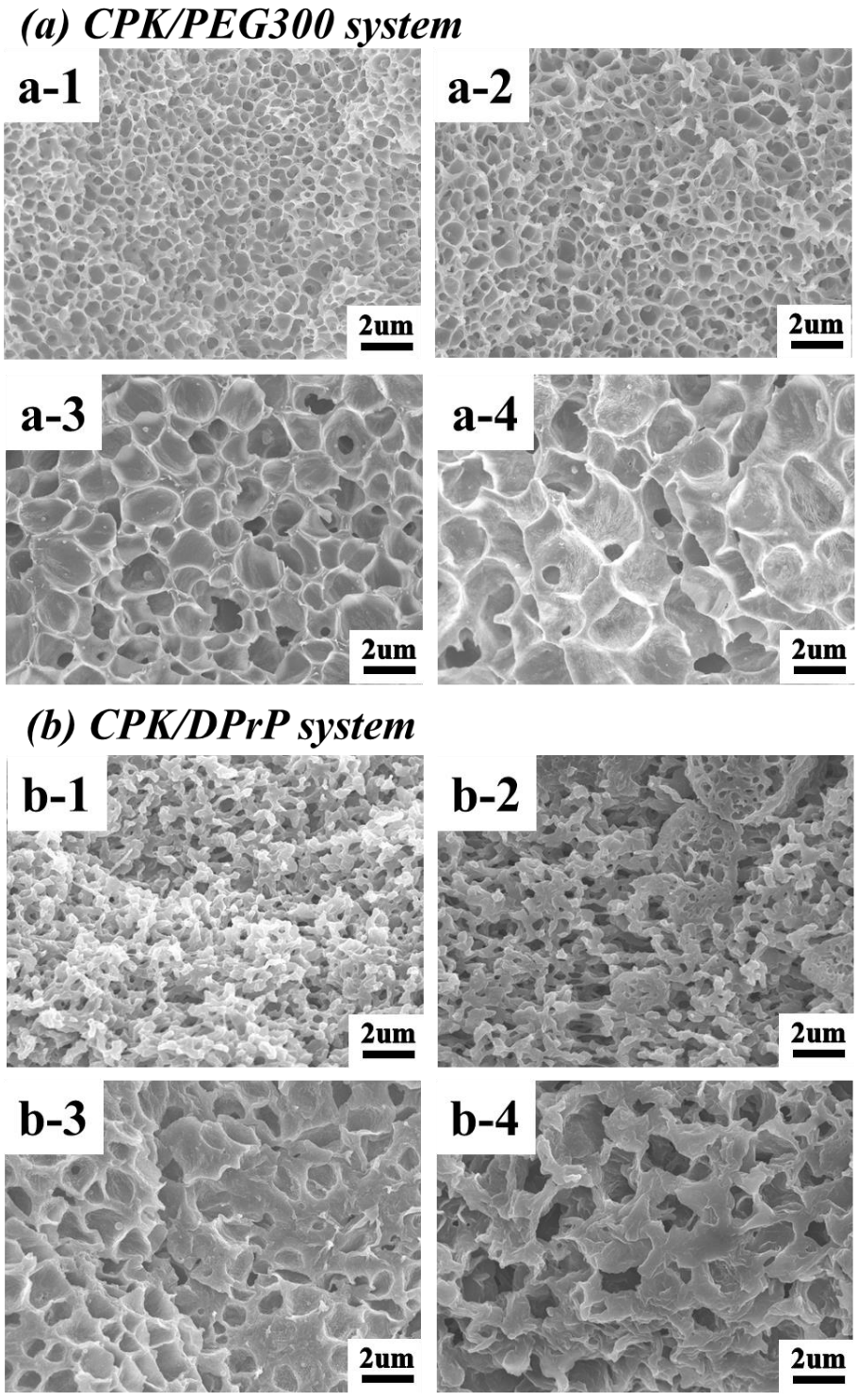

**Fig. 2-3** Cross-section morphology of CPK membranes prepared by the different cooling conditions. a and b represent the CPK/PEG300 system and CPK/DPrP system. 1 and 2 represent the quenching in 10 °C and 50 °C bath, respectively. 3 and 4 represent the controlled cooling of 50 °C $min^{-1}$ and 10 °C $min^{-1}$, respectively. The polymer concentration was 25 wt%.

Fig. 2-4 shows the cross-sectional structure of the membranes prepared with different polymer concentrations in the CPK/PEG300 system. The polymer dope solutions were heated using a hot stage and cooled in water quenching bath at a temperature of 10 °C. With an increase in polymer concentration, the membrane structure varied from an interconnected cellular structure (25 wt%) to a small and closed cellular structure (50 wt%). This can be explained using the phase diagram shown in Fig. 2-2(a). Because the monotectic point is 53 wt%, the fraction of the diluent-rich phase after phase separation in the 50 wt% case is relatively low, resulting in an isolated closed cellular structure.

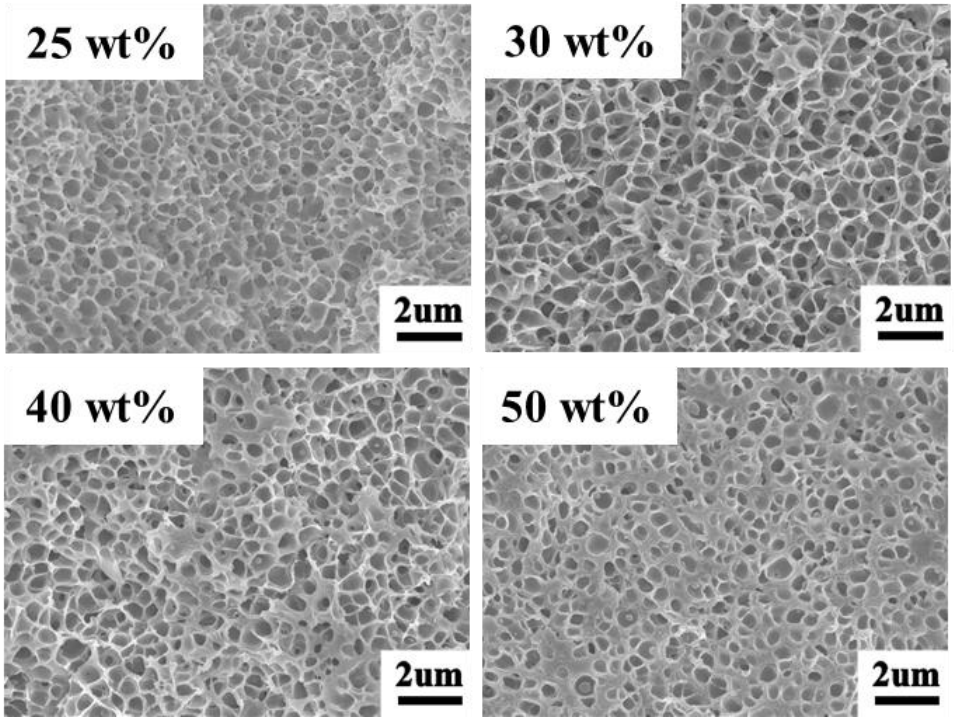


**Fig. 2-4** Cross-section morphology of CPK membranes prepared with different polymer concentrations. The diluent was PEG300 and the cooling condition was the quenching

in the 10 °C bath.

### *2.3.3 PK homopolymer (HPK) membrane*

2.3.3.1 Phase diagram of HPK/diluent system

For the PK homopolymer (HPK), we found only one diluent, PEG200, for the L-L phase separation, as shown in Table S2-1. The phase diagram obtained is shown in Fig. 2-5. The monotectic point of the HPK/PEG200 binary system is approximately 30 wt%. This suggests that the L-L phase separation region between $T_{cloud}$ and $T_{cry}$ was relatively narrow because the polymer concentration in the membrane preparation adopted in the TIPS method was generally higher than 20 wt% to provide a higher mechanical strength. Therefore, PEG300, PEG400, and PEG600 were added to PEG200 as nonsolvents to weaken the interaction between HPK and PEG200 and widen the L-L phase separation region. PEG300, PEG400, and PEG600 cannot dissolve HPK even at a high temperature of 250 °C, as shown in Table S2-1; therefore, these diluents are nonsolvents. The phase diagrams of HPK/PEG200/PEG300, HPK/PEG200/PEG400, and HPK/PEG200/PEG600 are shown in Fig. 2-5. The weight ratio of PEG200 to the nonsolvents was fixed at 9:1. When PEG300 was added to the dope solution, $T_{cloud}$ (blue curve) shifted to a higher temperature and the monotectic point was located at a concentration of approximately 32 wt%. This indicated that the L-L phase separation regions were enlarged because the addition of PEG300 reduced the compatibility between HPK and the diluent. When the nonsolvent was changed to PEG400 or PEG600, $T_{cloud}$ shifted to higher temperatures. Simultaneously, the monotectic points also shifted to 34 wt% and 40 wt% following the addition of PEG400 and PEG600, respectively. As shown in Table S2-1, δh was found to increase in the order of PEG300, PEG400 and PEG600 because of the reduced number of hydroxyl groups. That may be the main reason that induces the nonsolvent ability of the diluent increases in this order. Thus, $T_{cloud}$ and the monotectic points increased in the following order: PEG300, PEG400, and PEG600.

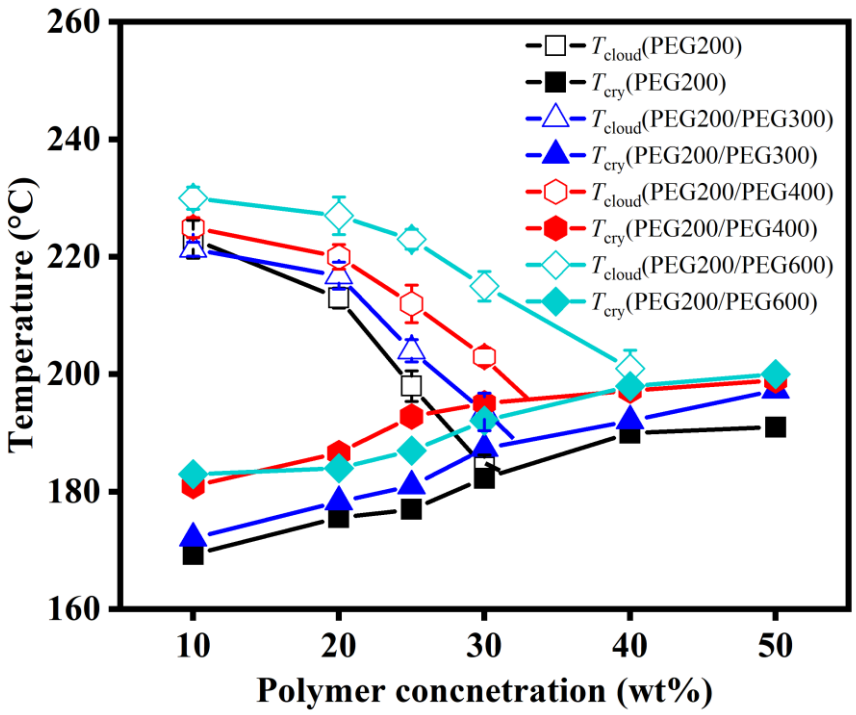


**Fig. 2-5** Cloud points and crystallization temperatures of the HPK/PEG200, HPK/PEG200/PEG300, HPK/PEG200/PEG400 and HPK/PEG200/PEG600 systems. The weight ratio of PEG200 to PEG300, PEG400 and PEG 600 was fixed at 9:1.

The effect of nonsolvent (PEG300) concentration in the polymer dope solution on the phase diagrams is shown in Fig. 2-6. The HPK concentration was fixed at 25 wt%. For the HPK/PEG200 binary system, the $T_{cry}$ and $T_{cloud}$ were 177 °C and 198 °C, respectively. However, it is clearly observed that $T_{cloud}$ significantly increased with the increase in PEG300 concentration, while the increase in $T_{cry}$ was not as obvious. For example, the $T_{cloud}$ was 226 °C in the case of PEG200 and PEG300 ratio of 6/4, while $T_{cry}$ increased only to 181 °C, suggesting that the L-L phase separation region substantially increased. This means that more time was provided for the droplets to coarsen during the cooling process. Thus, altering the concentration of the nonsolvent in the polymer dope solution is an effective way to regulate the membrane formation

process.

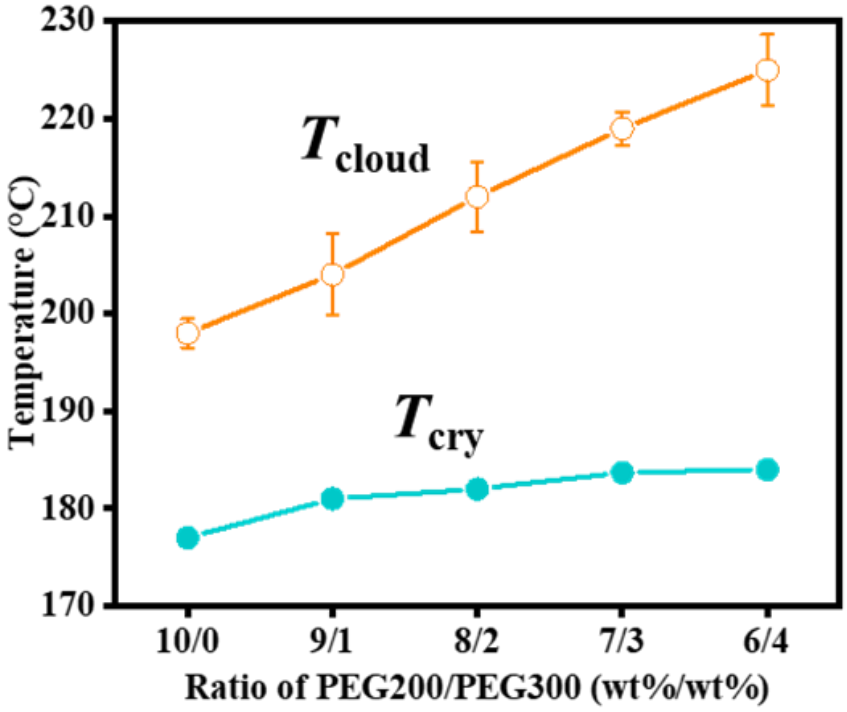


**Fig. 2-6** Cloud point and crystallization temperatures of HPK/PEGE200 binary and HPK/PEG200/PEG300 trinary systems with different ratios of PEG200/PEG300. The HPK concentration was fixed at 25 wt%.

### *3.3.2 HPK homopolymer membrane structures*

Fig. 2-7 shows the cross-sectional structures of the HPK membranes prepared by heating using the hot stage. The HPK concentration of all the samples was 25 wt%, and the weight ratios of PEG200 to PEG300, 400, and 600 in the dope solution were fixed at 9:1. The membrane prepared using the HPK/PEG200 binary system exhibited a cellular structure with clear spherulites. As shown in Fig. 2-5, the monotectic point in this system was 30 wt%, thus, $T_{cloud}$ was close to $T_{cry}$ at a polymer concentration of 25 wt%. Therefore, L-L phase separation occurred together with S-L phase separation. The size of cellular structure increased with a decrease in the cooling rate.

In the case of the addition of nonsolvents (PEG300, PEG400, and PEG600) to the dope solution, no clear spherulites were observed. This was because the difference between $T_{cloud}$ and $T_{cry}$ increased owing to the increase in $T_{cloud}$. Under the same cooling conditions, the size of cellular structure increased in the following order: HPK/PEG200, PEG200/300, PEG200/400, PEG200/600. This order agrees with that of $T_{cloud}$ shown in Fig. 2-5.

The results shown in Fig. 2-7 clearly indicate that the addition of a nonsolvent to the dope solution is a useful way to control the size of cellular structure in membrane preparation based on the L-L phase separation mechanism.

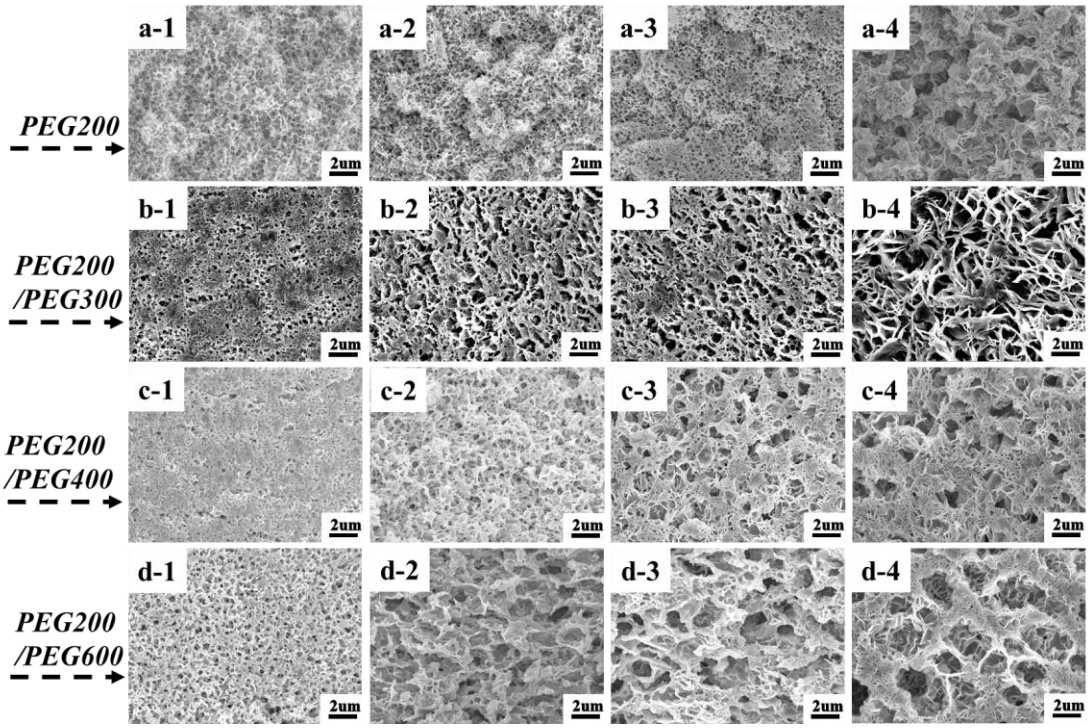


**Fig. 2-7** Cross-section morphology of HPK membranes prepared by the different cooling conditions. a, b, c, and d represent HPK/PEG200, HPK/PEG200/PEG300, HPK/PEG200/PEG400, and HPK/PEG200/PEG600 systems, respectively. 1 and 2 represent the quenching in 10 °C and 50 °C baths, respectively. 3 and 4 represent the controlled cooling of 50 °C $min^{-1}$ and 10 °C $min^{-1}$, respectively. The polymer concentration was 25 wt%. The weight ratio of PEG200 to PEG300, PEG400, and PEG600 was fixed at 9:1.

Fig. 2-8 shows the effect of the nonsolvent (PEG300) concentration on the membrane cross-section structures. The cellular pore size due to L-L phase separation increased as the PEG300 concentration in the dope solution increased because of the increased $T_{cloud}$, as shown in Fig. 2-6. Thus, the size of cellular structure based on L-L phase separation could also be controlled by changing the nonsolvent concentration in the dope solution.

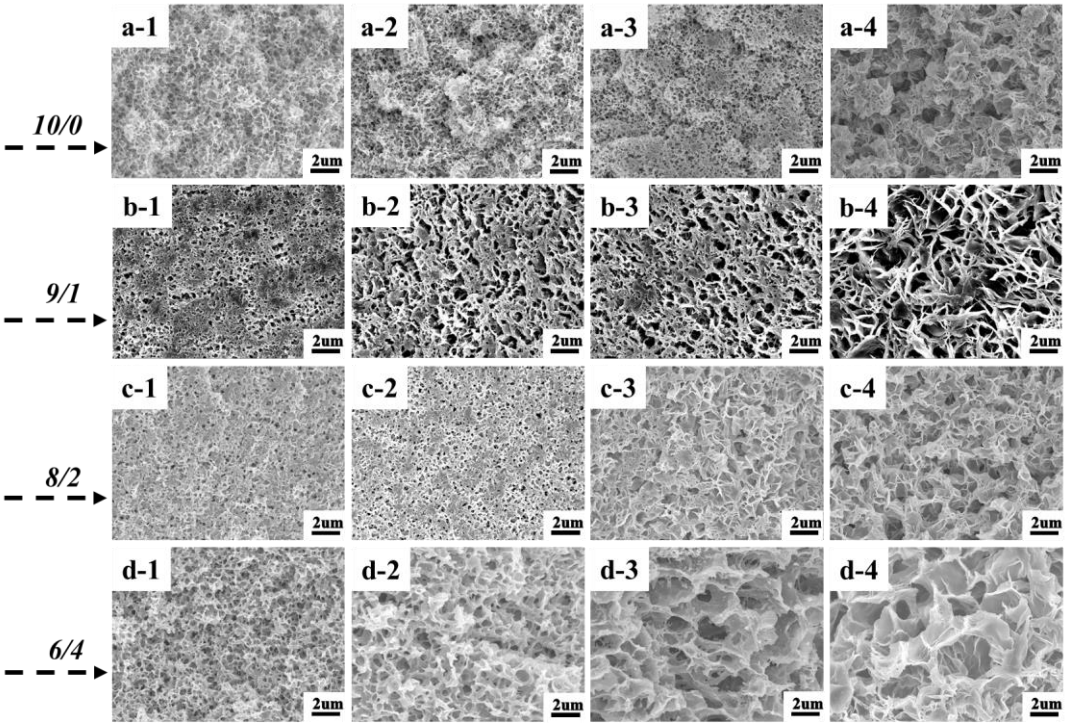


**Fig. 2-8** Cross-section morphology of HPK membranes prepared in HPK/PEG200/PEG300 systems with the different PEG300 concentrations in the dope solution. a, b, c, and d represent the ratio of PEG200/PEG300 in the dope solution are 10/0, 9/1, 8/2, and 6/4, respectively. 1 and 2 represent the quenching in 10 °C and 50 °C bath, respectively. 3 and 4 represent the controlled cooling of 50 °C $min^{-1}$ and 10 °C $min^{-1}$, respectively. The polymer concentration was 25 wt%.

Fig. 2-9 shows the cross-sectional structure of the membranes prepared with different polymer concentrations in the HPK/PEG200 systems. A cellular structure with spherulites was observed in the membrane with 25 wt% polymer concentration.

However, fuzzy spherulites with dense structures were observed as the polymer concentration increased from 30 to 50 wt%. This is because 25 wt% HPK is lower than the monotectic point (approximately 30 wt%), as shown in Fig. 2-6, so L-L phase separation was induced upon the cooling process at this polymer concentration. When the HPK concentration exceeded 30 wt%, S-L phase separation occurred, leading to fuzzy spherulites with dense structures. This means that the change in the dope polymer concentration brought about a change in the phase separation mechanism from the L-L type to the S-L type.

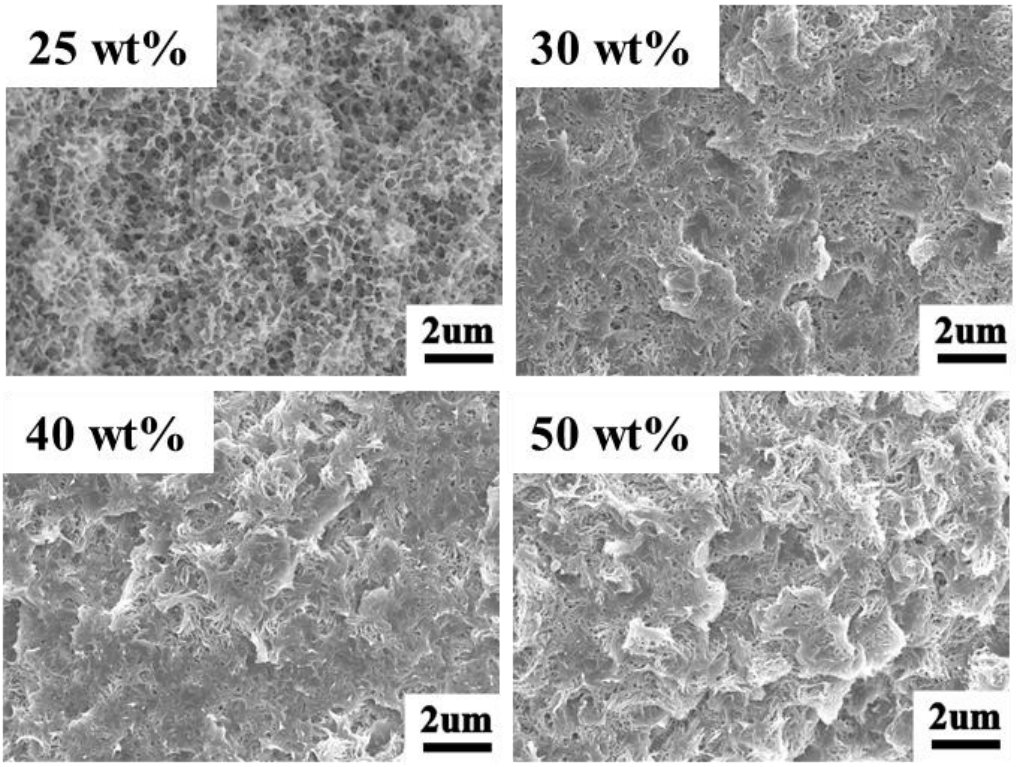


**Fig. 2-9** Cross-section morphology of HPK membranes prepared with different polymer concentrations. The diluent was PEG200 and the cooling condition quenching in the 10 °C bath.

### *2.3.4 Comparison of structures and performances of membranes prepared by TIPS and NIPS methods*

2.3.4.1 Structures of membranes prepared by TIPS and NIPS methods

In the NIPS method, for both CPK and HPK membranes, the polymer concentration was limited to 25 wt% because a higher polymer concentration could lead to a much higher viscosity of the dope solution, preventing membrane formation. In contrast, the membrane could be prepared from a 30 wt% polymer dope solution by the TIPS method, which indicated that the TIPS method is advantageous for the preparation of membranes from high concentration polymer solutions. The structures of the membranes prepared using the TIPS and NIPS methods are compared below.

Fig. 2-10 shows the cross-section, upper and bottom surfaces of the CPK membranes prepared by the TIPS and NIPS methods. These membranes were prepared on a large scale, as described in Section 2.5. For the membranes prepared by the NIPS method, as shown in Figs. 2-10(a) and (b), typical finger-like macrovoid structures (a-1 and b-1) and dense upper surfaces (a-2 and b-2) were formed in both cases with CPK concentrations of 15 wt% and 25 wt%. This typical asymmetric structure suggests that the membrane formation was dominated by instantaneous liquid-liquid demixing at the upper surface due to contact with the nonsolvent solution. Compared with the membrane with low CPK concentration (15 wt%), the membrane with 25 wt% CPK possessed a smaller finger-like structure because of the higher viscosity of the CPK dope solution. In addition, the cellular structures (Figs. S2-2(a-1) and S2-2(b-1)) can be seen in the membrane cross-section area except for the macrovoid, indicating an L-L phase separation. At the bottom surface, porous structures (a-3 and b-3) were formed because of the contact with the glass plate.

In contrast, the CPK membrane prepared via the TIPS method exhibited a perfectly interconnected cellular structure induced by the L-L phase separation without macrovoids (Figs. 2-10(c-1 and d-1) and Figs. S2-2(c-1 and d-1)), because macrovoid formation is usually prevented by the TIPS method [51]. A porous structure was formed on the upper surface of the membrane prepared by the TIPS method, in contrast with the dense upper surface of the membrane prepared by the NIPS method.

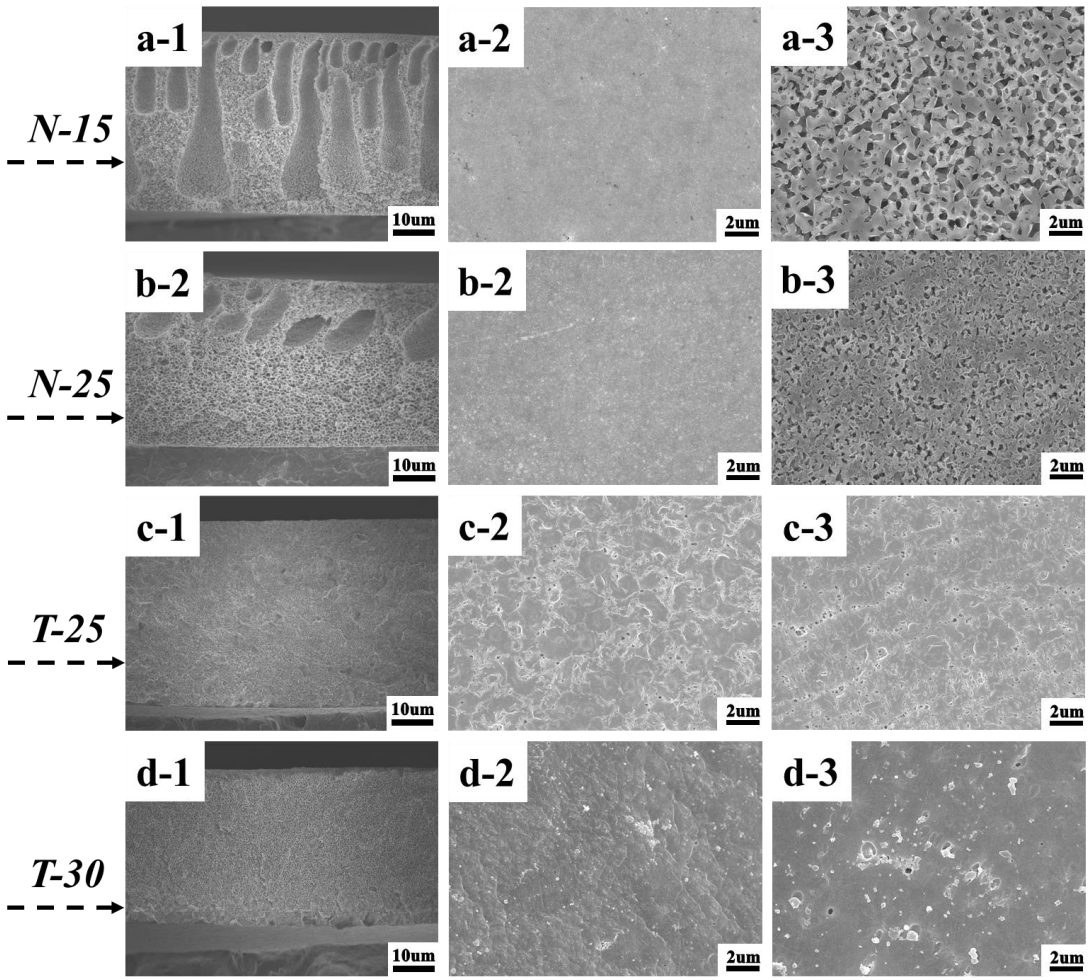


**Fig. 2-10** SEM image of CPK membranes prepared by NIPS and TIPS methods. 1, 2 and 3 represent cross section, upper surface, and bottom surface, respectively. The diluent used in the TIPS method was PEG300.

The cross-section and surface morphologies of the HPK homopolymer membranes prepared by the NIPS and TIPS methods are shown in Fig. 2-11. For the membrane prepared by the NIPS method, a sponge-like structure and porous upper and bottom surfaces were observed in the HPK N-15 membrane, as shown in Fig. 2-11(a). This symmetric and homogeneous structure is not typical for membranes prepared using the NIPS method. This is a characteristic structure of the HPK membrane, particularly when prepared using the diluent and bath components described in Section 2.2.5 [34]. With an increase in the polymer concentration to 25 wt%, denser upper and bottom surfaces of the NIPS membrane were formed, and small pores were still observed on

both surfaces. In this system, a membrane could not be prepared from the 30 wt% polymer dope solution because of the extremely high solution viscosity.

For HPK membranes prepared by the TIPS method using 25 wt% and 30 wt% concentrations, cellular structures with indistinct spherulites resulting from the L-L phase separation with subsequent S-L phase separation were formed in the cross-section (Figs. S2-2(c-1) and (d-1)). A porous structure can be seen from the upper and bottom surfaces of the T-25 membrane (c-2 and c-3), and the pores became denser for the T-30 membrane (d-2 and d-3).

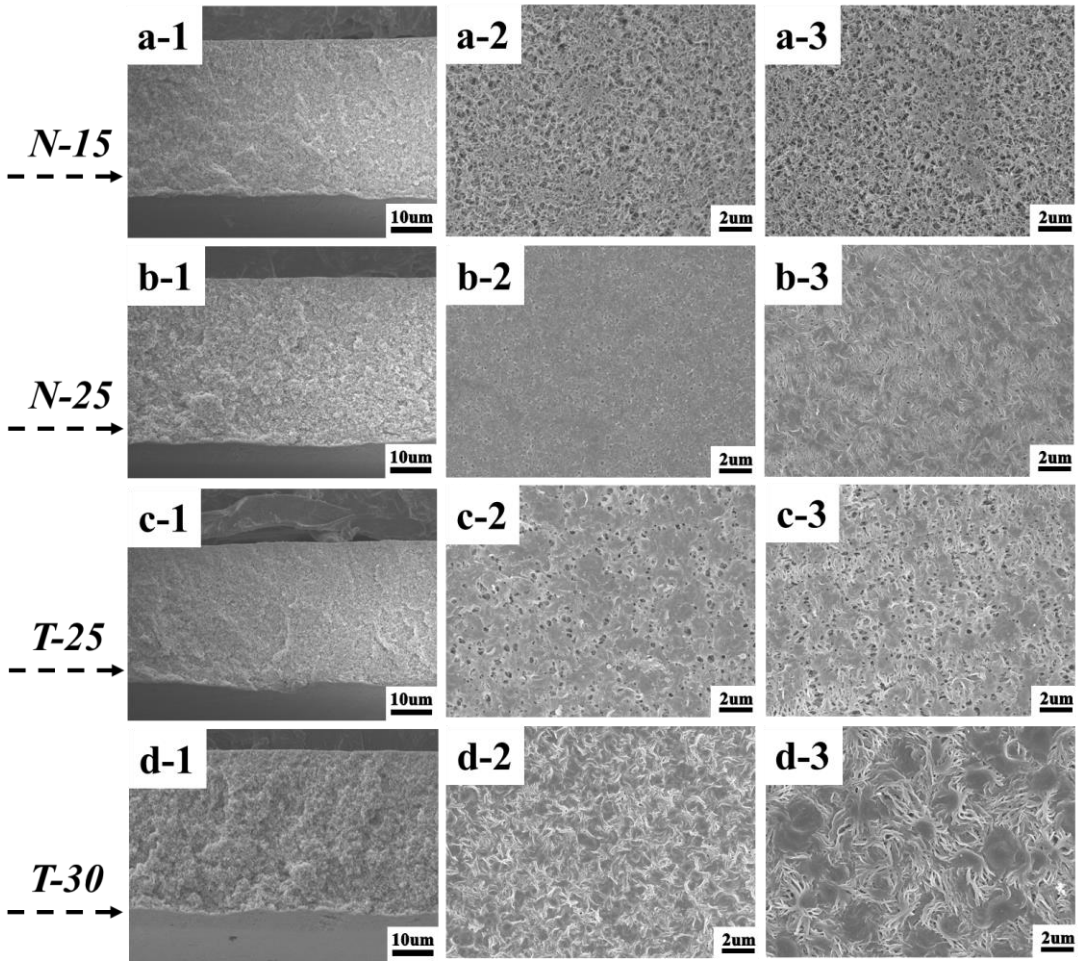


**Fig. 2-11** SEM image of HPK membranes prepared by NIPS and TIPS methods. 1, 2, and 3 represent cross section, upper surface, and bottom surface, respectively. The diluent used in TIPS method was PEG200.

2.3.4.2 Water permeabilities and mechanical properties of membranes prepared by NIPS and TIPS methods

Fig. 2-12 and Fig. 2-13 show the water permeability, mean pore size and mechanical strength of the CPK and HPK membranes prepared using the NIPS and TIPS methods with different polymer concentrations. As shown in Fig. 2-12(a), comparing the CPK membranes prepared by TIPS and NIPS methods using the same polymer concentration of 25 wt% (N-25 and T-25), the water permeability of the membrane prepared by TIPS (400 L $m^{-2}h^{-1}bar^{-1}$) was much higher than that of NIPS (5 L $m^{-2}h^{-1}bar^{-1}$) because of the porous surface structure, the larger pore size (90.7 nm) and higher porosity (64.8 %) of the T-25 membrane (Fig. 2-12b and Fig. S2-4). Even though the CPK concentration was increased to 30 wt%, the CPK membrane (T-30) still demonstrated acceptable water permeability (89 L $m^{-2}h^{-1}bar^{-1}$). The water permeabilities of the HPK homopolymer membranes showed a trend similar to that of CPK membranes. That is, the T-25 membrane showed much higher water permeability than the N-25 membrane. It is well-know that the dope composition and cooling rate mainly determine the membrane structure in the TIPS process resulting in a uniform structure with less defects and a narrower pore size distribution than other phase inversion process, which has also been stated many times in other articles [52-54]. For the membrane prepared by NIPS technique, it often exhibits a wider pore size distribution due to the existence of the macrovoids or defects that resulted from unstable and nonuniform solvent nonsolvent exchange [52, 55]. However, in this work membrane prepared by NIPS has shown a narrower pore size distribution than that prepared by TIPS method at the same PK concentration for both HPK and CPK membrane, which contradicts above-mentioned statement. This opposite results might originate from the differences in the preparation procedure. In this work, the instantaneous liquid-liquid demixing dominated membrane preparation process to form the dense upper surface in membrane with small pore size and narrow pore size distributions shown in Fig. S2-3. For the TIPS preparation process in this work, the usage of preheated stainless-steel plate prevents

the evaporation of diluent to form a dense upper surface. L-L phase separation process dominated the formation of the overall structure of the membrane. As a result, both the upper and bottom surface formed a porous structure with a big pore size and wide pore size distribution. Due to the limitation of our knowledge, as for the deeper reasons, we are not clear at present, we will do more research in this respect in the future. Comparing the water permeabilities of the membranes prepared by the NIPS method, the HPK membranes (N-15 and N-25) showed higher water permeability than the CPK membranes because of the pore formation at the upper surface (Figs. 2-11(a-2 and b-2)).

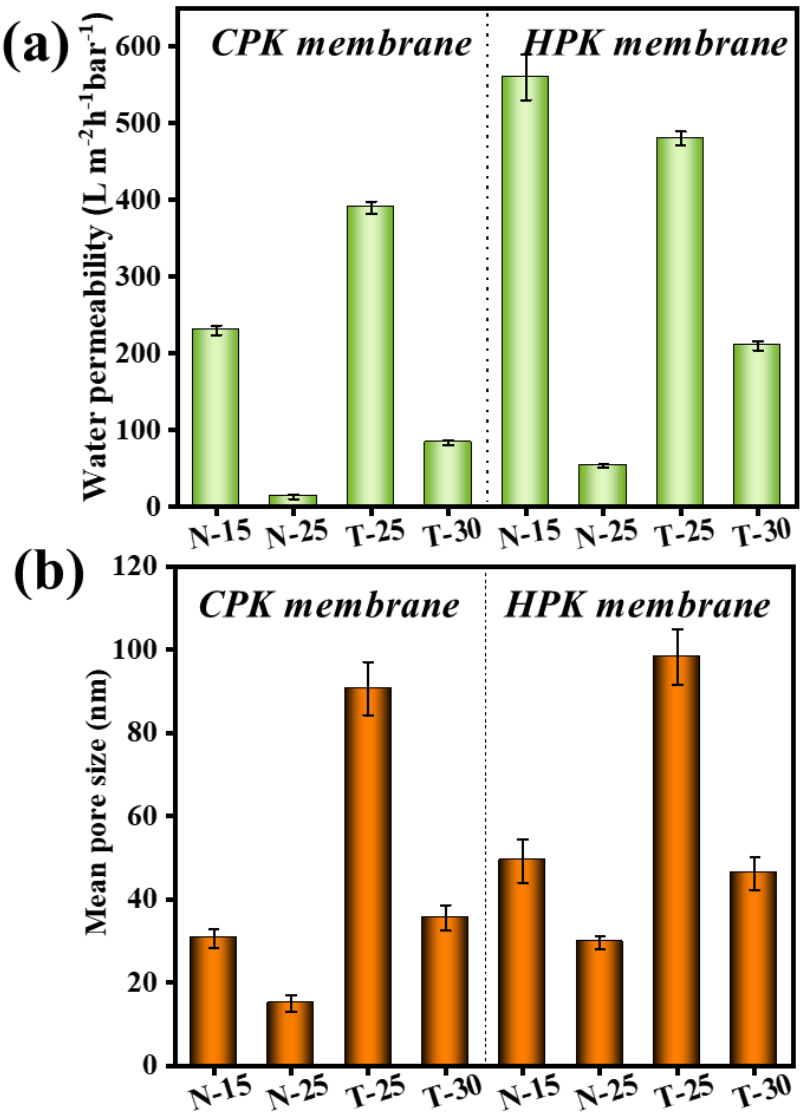


**Fig. 2-12** Performance of the CPK and HPK flat sheet membranes. Pure water permeability (a), mean pore size (b).

As shown in Fig. 2-13(a) and 2-13(b), the membrane tensile strength gradually increased with increasing polymer concentrations in the dope solutions for both membranes prepared by the NIPS and TIPS methods. Basically, the elongation at break also increases with increasing polymer concentration. However, the elongation at break of the T-30 membranes was slightly lower than that of T-25 because of their slight brittleness. Regarding the tensile strength and elongation at break, the difference

between the membranes prepared by the TIPS method (T-25) and those prepared by the NIPS method (N-25) is not obvious.

The T-30 membrane prepared by the TIPS method showed higher water permeability and tensile strength than the N-25 membrane prepared by the NIPS method in both CPK and HPK cases.

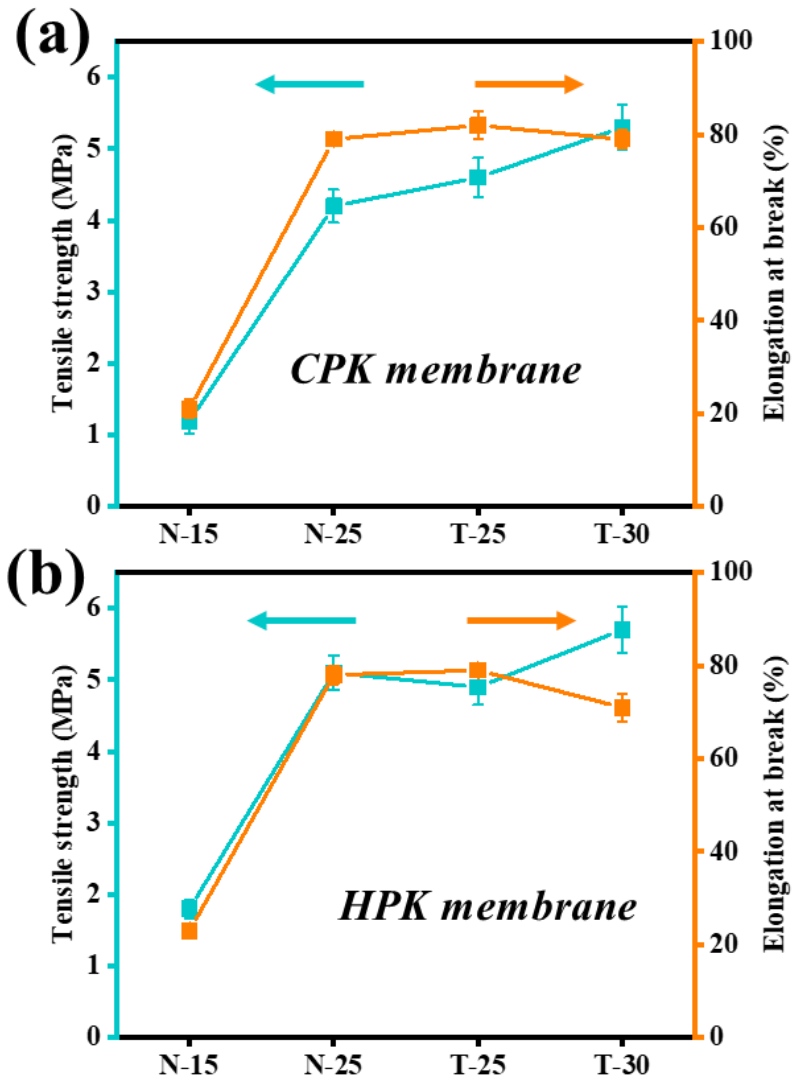


**Fig. 2-13** Tensile strength and elongation at break of CPK membrane (a) and HPK membrane (b).

### *2.4 Conclusions*

In this study, two types of PK membranes were prepared using TIPS methods. Diluents suitable for PK polymers in the TIPS method were first screened. The focus was on diluents that induce L-L phase separation in the TIPS method. For the copolymer PK, polyethylene glycol 300 and di-*n*-propyl phthalate were found to induce L-L phase separation, whereas only polyethylene glycol 200 could induce L-L phase separation in homopolymer PK.

The phase diagrams of the copolymer and homopolymer PKs were investigated in detail. For homopolymer PK, the effects of nonsolvent addition to the dope solution on the phase diagrams were also investigated. The PK type, cooling rate, and polymer concentration could affect the porous structures of the membranes prepared by L-L phase separation using the TIPS method.

Finally, the porous structure, water permeance, and mechanical properties of the membranes prepared by the NIPS and TIPS methods were compared. Even when using a dope solution with a higher PK concentration of 30 wt%, membrane preparation was possible using the TIPS method, and the resultant membranes showed high pure water permeability and high mechanical strength.

### *References*

[1] A. Wakker, Lower critical demixing of a polyketone in hexafluoroisopropanol, Polymer, 32 (1990) 279-283.

[2] G. Memsitieri, M.A.D. Noblie, A. Sommazzi, L. Nicolais, Water transport in a polyketone terpolymer, J. Polym. Sci. B Polym. Phys., 33 (1995) 1365-1370.

[3] J.M. Lagaron, A.K. Powell, N.S. Davidson, Characterization of the structure and crystalline polymorphism present in aliphatic polyketones by raman spectroscopy, Macromolecules, 33 (2000) 1030-1035.

[4] P. Gupta, J.T. Schulte, J.E. Flood, J.E. Spruiell, Development of high-strength fibers from aliphatic polyketones by melt spinning and drawing, J. Appl. Polym. Sci., 82

(2001) 1794-1815.

[5] L. Cheng, A.R. Shaikh, L.F. Fang, S. Jeon, C.J. Liu, L. Zhang, H.C. Wu, D.M. Wang, H. Matsuyama, Fouling-resistant and self-cleaning aliphatic polyketone membrane for sustainable oil-water emulsion separation, ACS Appl. Mater. Interfaces, 10 (2018) 44880-44889.

[6] L.E. Govaert, P.J.D. Vries, P.J. Fennis, W.F. Nijenhuis, J.P. Keustermans, Influence of strain rate, temperature and humidity on the tensile yield behaviour of aliphatic polyketone, Polymer, 41 (2000) 1959-1962.

[7] W.C.J. Zuiderduin, D.P.N. Vlasveld, J. Huétink, R.J. Gaymans, Mechanical properties of polyketone terpolymer/rubber blends, Polymer, 45 (2004) 3765-3779.

[8] L. Zhang, L. Cheng, H. Wu, T. Yoshioka, H. Matsuyama, One-step fabrication of robust and anti-oil-fouling aliphatic polyketone composite membranes for sustainable and efficient filtration of oil-in-water emulsions, J. Mater. Chem. A, 6 (2018) 24641-24650.

[9] Y. Jia, K. Guan, P. Zhang, Q. Shen, T. Istirokhatun, Y. Lin, H. Matsuyama, Nanostructural manipulation of polyphenol coatings for superwetting membrane surfaces, ACS Sustain. Chem. Eng., 9 (2021) 14525-14536.

[10] Y. Jia, K. Guan, L. Zhang, Y. Lin, Q. Shen, P. Zhang, H. Matsuyama, Enabling polyketone membrane with underwater superoleophobicity via a hydrogel-based modification for high-efficiency oil-in-water emulsion separation, J. Membr. Sci., 618 (2021) 118705.

[11] C. Liu, D. Saeki, L. Cheng, J. Luo, H. Matsuyama, Polyketone-based membrane support improves the organic solvent resistance of laccase catalysis, J. Colloid Interface Sci., 544 (2019) 230-240.

[12] K. Guan, L. Zhang, S. Wang, R. Takagi, H. Matsuyama, Controlling the formation of porous polyketone membranes via a cross-linkable alginate additive for oil-in-water emulsion separations, J. Membr. Sci., 611 (2020) 118362.

[13] C. Liu, R. Takagi, D. Saeki, L. Cheng, T. Shintani, T. Yasui, H. Matsuyama, Highly

improved organic solvent reverse osmosis (OSRO) membrane for organic liquid mixture separation by simple heat treatment, J. Membr. Sci., 618 (2021) 118710.

[14] W. Kushida, R.R. Gonzales, T. Shintani, A. Matsuoka, K. Nakagawa, T. Yoshioka, H. Matsuyama, Organic solvent mixture separation using fluorine-incorporated thin film composite reverse osmosis membrane, J. Mater. Chem. A, 10 (2022) 4146-4156.

[15] K. Guan, Y. Sasaki, Y. Jia, R.R. Gonzales, P. Zhang, Y. Lin, Z. Li, H. Matsuyama, Interfacial polymerization of thin film selective membrane layers: Effect of polyketone substrates, J. Membr. Sci., 640 (2021) 119801.

[16] L. Zhang, Y. Lin, S. Wang, L. Cheng, H. Matsuyama, Engineering of ultrafine polydopamine nanoparticles in-situ assembling on polyketone substrate for highly-efficient oil-water emulsions separation, J. Membr. Sci., 613 (2020) 118501.

[17] C. Wang, M.J. Park, D.H. Seo, S. Phuntsho, R.R. Gonzales, H. Matsuyama, E. Drioli, H.K. Shon, Inkjet printed polyelectrolyte multilayer membrane using a polyketone support for organic solvent nanofiltration, J. Membr. Sci., 642 (2022) 119943.

[18] D.R. Lloyd, Microporous membrane formation via thermally induced phase separation. I. solid-liquid phase separation, J. Membr. Sci., 52 (1990) 239-261.

[19] D.R. Lloyd, S.S. Kim, K.E. Kinzer, Microporous membrane formation via thermally induced phase separation. II. Liquid-liquid phase separation, J. Membr. Sci., 64 (1991) 1-11.

[20] S. Jeon, H. Karkhanechi, L. Fang, L. Cheng, T. Ono, R. Nakamura, H. Matsuyama, Novel preparation and fundamental characterization of polyamide 6 self-supporting hollow fiber membranes via thermally induced phase separation (TIPS), J. Membr. Sci., 546 (2018) 1-14.

[21] W. Yave, R. Quijada, D. Serafini, D. Lloyd, Effect of the polypropylene type on polymer–diluent phase diagrams and membrane structure in membranes formed via the TIPS process Part II. Syndiotactic and isotactic polypropylenes produced using metallocene catalysts, J. Membr. Sci., 263 (2005) 154-159.

[22] W. Yave, R. Quijada, M. Ulbricht, R. Benavente, Syndiotactic polypropylene as potential material for the preparation of porous membranes via thermally induced phase separation (TIPS) process, Polymer, 46 (2005) 11582-11590.

[23] Y.J. Wang, Z.P. Zhao, Z.Y. Xi, S.Y. Yan, Microporous polypropylene membrane prepared via TIPS using environment-friendly binary diluents and its VMD performance, J. Membr. Sci., 548 (2018) 332-344.

[24] G. Ji, L. Zhu, B. Zhu, C. Zhang, Y. Xu, Structure formation and characterization of PVDF hollow fiber membrane prepared via TIPS with diluent mixture, J. Membr. Sci., 319 (2008) 264-270.

[25] P. Zhang, S. Xiang, H. Wang, Y. Wang, J. Zhang, Z. Cui, J. Li, B. He, Understanding the multiple functions of styrene-co-maleic anhydride in fabricating polyvinylidene fluoride hollow fiber membrane via coupled phase inversion process and its effect on surface infiltration behavior and membrane permeability, J. Membr. Sci., 590 (2019) 117269.

[26] K. Umakoshi, R.R. Gonzales, N. Kato, P. Zhang, T. Ono, H. Matsuyama, Effect of polymer-solvent compatibility on polyamide hollow fiber membranes prepared via thermally induced phase separation, Colloids Surf. A Physicochem. Eng. Asp., 642 (2022) 128704.

[27] J. Pan, W. Ma, L. Huang, R. Li, Q. Huang, C. Xiao, Z. Jiang, Fabrication and characterization of ECTFE hollow fiber membranes via low-temperature thermally induced phase separation (L-TIPS), J. Membr. Sci., 634 (2021) 119429.

[28] I.J. Roh, S. Ramaswamy, W.B. Krantz, A.R. Greenberg, Poly(ethylene chlorotrifluoroethylene) membrane formation via thermally induced phase separation (TIPS), J. Membr. Sci., 362 (2010) 211-220.

[29] M. Shang, H. Matsuyama, T. Maki, M. Teramoto, D.R. Lloyd, Preparation and characterization of poly(ethylene-co-vinyl alcohol) membranes via thermally induced liquid-liquid phase separation, J. Appl. Polym. Sci., 87 (2003) 853-860.

[30] C.Y. Gao, A. Li, L.X. Feng, X.S. Yi, J.C. Shen, Factors controlling surface

morphology of porous polystyrene membranes prepared by thermally induced phase separation, Polym. Int., 49 (2000) 323-328.

[31] Q.Y. Wu, L.S. Wan, Z.K. Xu, Structure and performance of polyacrylonitrile membranes prepared via thermally induced phase separation, J. Membr. Sci., 409-410 (2012) 355-364.

[32] H.Q. Liang, H.N. Li, H.H. Yu, Y.T. Zhou, Z.K. Xu, Polysulfone membranes via thermally induced phase separation, Chin. J. Chem. Eng., 35 (2017) 846-856.

[33] Z. Liu, Z. Cui, Y. Zhang, S. Qin, F. Yan, J. Li, Fabrication of polysulfone membrane via thermally induced phase separation process, Mater. Lett., 195 (2017) 190-193.

[34] H. Matsuyama, T. Maki, M. Teramoto, K. Kobayashi, Effect of PVP additive on porous polysulfone membrane formation by immersion precipitation method, Sep Sci Technol, 38 (2003) 3449-3458.

[35] Y. Park, W. Jang, J. Choi, Y. Woo, J. Hou, S. Jeon, H. Byun, Fabrication of organic solvent resistant polyketone hollow fiber membranes, Membrane Journal, 31 (2021) 363-370.

[36] N. Kato, R.R. Gonzales, A. Nishitani, Y. Negi, T. Ono, H. Matsuyama, Single-step preparation of nanocomposite polyamide 6 hollow fiber membrane with integrally skinned asymmetric structure for organic solvent nanofiltration, Colloids Surf. A Physicochem. Eng. Asp., 620 (2021) 126538.

[37] W. Ma, J. Zhang, B.V.d. Bruggen, X. Wang, Formation of an interconnected lamellar structure in PVDF membranes with nanoparticles addition via solid-liquid thermally induced phase separation, J. Appl. Polym. Sci., 127 (2013) 2715-2723.

[38] T. Xiao, P. Wang, X. Yang, X. Cai, J. Lu, Fabrication and characterization of novel asymmetric polyvinylidene fluoride (PVDF) membranes by the nonsolvent thermally induced phase separation (NTIPS) method for membrane distillation applications, J. Membr. Sci., 489 (2015) 160-174.

[39] Y. Lin, Y. Tang, H. Ma, J. Yang, Y. Tian, W. Ma, X. Wang, Formation of a bicontinuous structure membrane of polyvinylidene fluoride in diphenyl carbonate

diluent via thermally induced phase separation, J. Appl. Polym. Sci., 114 (2009) 1523-1528.

[40] S. Rajabzadeh, D. Ogawa, Y. Ohmukai, Z. Zhou, T. Ishigami, H. Matsuyama, Preparation of a PVDF hollow fiber blend membrane via thermally induced phase separation (TIPS) method using new synthesized zwitterionic copolymer, Desalination Water Treat., 54 (2014) 2911-2919.

[41] H. Matsuyama, M. Teramoto, T. Uesaka Membrane formation and structure development by dry-cast process, J. Membr. Sci., 135 (1997) 271-288.

[42] M. Gu, J. Zhang, X. Wang, H. Tao, L. Ge, Formation of poly(vinylidene fluoride) (PVDF) membranes via thermally induced phase separation, Desalination, 192 (2006) 160-167.

[43] X. Fu, H. Matsuyama, M. Teramoto, H. Nagai, Preparation of hydrophilic poly(vinyl butyral) hollow fiber membrane via thermally induced phase separation, Sep. Purif. Technol., 45 (2005) 200-207.

[44] X.Y. Fu, T. Sotani, H. Matsuyama, Effect of membrane preparation method on the outer surface roughness of cellulose acetate butyrate hollow fiber membrane, Desalination, 233 (2008) 10-18.

[45] Z. Wu, Z. Cui, T. Li, S. Qin, B. He, N. Han, J. Li, Fabrication of PVDF-based blend membrane with a thin hydrophilic deposition layer and a network structure supporting layer via the thermally induced phase separation followed by non-solvent induced phase separation process, Appl. Surf. Sci., 419 (2017) 429-438.

[46] C. Wang, M.J. Park, R.R. Gonzales, S. Phuntsho, H. Matsuyama, E. Drioli, H.K. Shon, Novel organic solvent nanofiltration membrane based on inkjet printing-assisted layer-by-layer assembly, J. Membr. Sci., 655 (2022) 120582.

[47] S.Y. Wang, R.R. Gonzales, P. Zhang, T. Istirokhatun, R. Takagi, A. Motoyama, L.F. Fang, H. Matsuyama, Surface charge control of poly(methyl methacrylate-co-dimethyl aminoethyl methacrylate)-based membrane for improved fouling resistance, Sep. Purif. Technol., 279 (2021) 119778.

[48] C.M. Hansen, Hansen solubility parameters: a user's handbook, second ed., CRC press, New York, 2007.

[49] K.S. McGuire, D.R. Lioyd, G.B.A. Lim, Microporous membrane formation via thermally induced phase separation. VII. Effect of dilution, cooling rate, and nucleating agent addition on morphology, J. Membr. Sci., 79 (1993) 27-34.

[50] K.S. McGuire, A. Laxminarayan, Douglas R. Lloyd, Kinetics of droplet growth in liquid-liquid phase separation of polymer-diluent systems: experimental results, Polymer, 36 (1995) 4951-4960.

[51] H. Matsuyama, K. Ohga, T. Maki, M. Tearamoto, S. Nakatsuka, Porous cellulose acetate membrane prepared by thermally induced phase separation, J. Appl. Polym. Sci., 89 (2003) 3951-3955.

[52] J. Zhao, J.Y. Chong, L. Shi, R. Wang, Explorations of combined nonsolvent and thermally induced phase separation (N-TIPS) method for fabricating novel PVDF hollow fiber membranes using mixed diluents, J. Membr. Sci., 572 (2019) 210-222.

[53] G.T. Caneba, D.S. Soong, Polymer membrane formation through the thermal-inversion process. 1. experimental study of membrane structure formation, macromolecules, 18 (1985) 2538-2545.

[54] J.F. Kim, J.H. Kim, Y.M. Lee, E. Drioli, Thermally induced phase separation and electrospinning methods for emerging membrane applications: A review, AIChE J., 62 (2016) 461-490.

[55] J.T. Jung, H.H. Wang, J.F. Kim, J. Lee, J.S. Kim, E. Drioli, Y.M. Lee, Tailoring nonsolvent-thermally induced phase separation (N-TIPS) effect using triple spinneret to fabricate high performance PVDF hollow fiber membranes, J. Membr. Sci., 559 (2018) 117-126.

***Supporting information***

**Table S2-1** Phase separation condition, Hansen solubility parameters and *R*a values of

HPK, CPK and pure solvents

| | For HPK | For CPK | $\delta_d$ $(MPa)^{0.5}$ | $\delta_p$ $(MPa)^{0.5}$ | $\delta_h$ $(MPa)^{0.5}$ | Ra (HPK) $(MPa)^{0.5}$ | Ra (CPK) $(MPa)^{0.5}$ |
|---|---|---|---|---|---|---|---|
| HPK | | | 19.2 | 17.9 | 6.8 | | |
| CPK | | | 19.9 | 17.9 | 6.8 | | |
| PC | S-L | S-L | 20 | 18 | 4.1 | 3.1 | 2.7 |
| SFL | S-L | S-L | 17.8 | 17.4 | 8.7 | 3.5 | 4.6 |
| CPL | S-L | S-L | 19.4 | 13.8 | 3.9 | 5 | 5.1 |
| $DMSO_2$ | S-L | S-L | 19 | 19.4 | 12.3 | 5.7 | 6 |
| DMP | S-L | S-L | 18.6 | 10.8 | 4.9 | 7.5 | 7.8 |
| DEP | S-L | S-L | 17.6 | 9.6 | 4.5 | 9.2 | 9.8 |
| DPrP | insoluble | L-L | 17.4 | 7.3 | 3.3 | 11.8 | 12.2 |
| DPC | S-L | S-L | 18.7 | 3.6 | 7.5 | 14.4 | 14.5 |
| TEG | S-L | S-L | 16 | 12.5 | 18.6 | 14.5 | 15.1 |
| DEG | insoluble | insoluble | 16.6 | 12 | 19 | 14.5 | 15.1 |
| DBS | insoluble | insoluble | 16.7 | 4.5 | 4.1 | 14.6 | 15.1 |
| GTA | insoluble | insoluble | 16.5 | 4.5 | 9.1 | 14.7 | 15.2 |
| TEC | insoluble | insoluble | 16.5 | 4.9 | 12 | 15 | 15.6 |
| ATEC | insoluble | insoluble | 16.6 | 3.5 | 8.6 | 15.4 | 15.1 |
| ATBC | insoluble | insoluble | 16.7 | 2.5 | 7.4 | 16.2 | 16.7 |
| DIBA | insoluble | insoluble | 16.7 | 2.5 | 6.2 | 16.2 | 16.7 |
| PEG300 | insoluble | L-L | 16.6 | 4.4 | 14.5 | 16.4 | 16.9 |
| PEG400 | insoluble | insoluble | 16.6 | 3.7 | 13.3 | 16.5 | 17 |
| PEG600 | insoluble | insoluble | 16.6 | 3.2 | 12.1 | 16.5 | 17 |
| PEG200 | L-L | S-L | 16.7 | 5.6 | 16.7 | 16.6 | 17.1 |
| PPG400 | insoluble | insoluble | 16.8 | 10.4 | 21.3 | 17 | 17.5 |
| DPM | insoluble | insoluble | 19.5 | 1 | 1 | 17.9 | 17.9 |

| | | | | | | | |
|---|---|---|---|---|---|---|---|
| EG | insoluble | insoluble | 17 | 11 | 26 | 20.9 | 21.2 |
| Glycerol | insoluble | insoluble | 17.4 | 11.3 | 27.2 | 21.8 | 22 |

**Note:** Homopolymer and copolymer of polyketones (HPK and CPK), propylene carbonate (PC), sulfolane (SFL), caprolactam (CPL), dimethyl sulfone (DMSO2), dimethyl phthalate (DMP), diethyl phthalate (DEP), di-n-propyl phthalate (DPrP), diphenyl carbonate (DPC), triethylene glycol (TEG), diethylene glycol (DEG), dibutyl sebacate (DBS), glycerol triacetate (GTA), triethyl citrate (TEC), acetyl triethyl citrate (ATEC), acetyl tributyl citrate (ATBC), diisobutyl adipate (DIBA), Polyethylene glycol (PEG200, PEG300, PEG400, and PEG600), propylene glycol 400 (PPG400), diphenylmethane (DPM), and ethylene glycol (EG).

**Table S2-2** Phase separation condition, Hansen solubility parameters and *R*a values of mixed solvents

| Mixed solvent | Solvent ratio (w/w) | Phase separation for HPK | $\delta_d$ $(MPa)^{0.5}$ | $\delta_p$ $(MPa)^{0.5}$ | $\delta_h$ $(MPa)^{0.5}$ | *R*a (HPK) $(MPa)^{0.5}$ |
|---|---|---|---|---|---|---|
| PEG200/PEG300 | 9/1 | L-L | 16.7 | 5.5 | 16.5 | 16.5 |
| PEG200/PEG300 | 8/2 | L-L | 16.7 | 5.4 | 16.3 | 16.5 |
| PEG200/PEG300 | 6/4 | L-L | 16.7 | 5.1 | 15.8 | 16.5 |
| PEG200/PEG400 | 9/1 | L-L | 16.7 | 5.4 | 16.4 | 16.6 |
| PEG200/PEG600 | 9/1 | L-L | 16.7 | 5.4 | 16.2 | 16.4 |

The solubility parameters of polyketone (HPK and CPK) were estimated by the group contributions given by van Krevelen [1], using the following Eqs. (S2-1)- (S2-3).

$$\delta_D = \frac{\sum F_{Di}}{V} \quad \text{(S2-1)}$$

$$\delta_P = \frac{(\sum F_{Pi}^2)^{1/2}}{V} \quad \text{(S2-2)}$$

$$\delta_H = (\frac{\sum E_{Hi}}{V})^{1/2} \quad \text{(S2-3)}$$

where $\delta_D$, $\delta_P$ and $\delta_H$ represent dispersion force, polar and hydrogen bond, respectively, $V$ is molar volume of polymer ($cm^3\ mol^{-1}$) and i is the number of structure group. The group contributions including $F_{Di}$, $F_{Pi}$ and $E_{Hi}$ were shown in Table S2-3 [1], corresponding to the structure group of polyketone. $V$ of polyketone is calculated according to the method expressed by Coleman [2, 3], based on the molecular weight of constitutional unit and density of polymer. The densities of HPK and CPK were 1.3 g $cm^{-1}$ and 1.24 g $cm^{-1}$ [4, 5], respectively.

**Table S2-3** Group contribution value for estimation of Hansen solubility parameters (Hoftyzer-Van Krevelen method)

| Structure group | $F_{Di}$ $(MJ/m^3)^{1/2}\ mol^{-1}$ | $F_{Pi}$ $(MJ/m^3)^{1/2}\ mol^{-1}$ | $E_{Hi}$ J/mol |
|---|---|---|---|
| -CH3 | 420 | 0 | 0 |
| -CH2- | 270 | 0 | 0 |
| >CH- | 80 | 0 | 0 |
| -CO- | 290 | 770 | 2000 |

The solubility parameters of diluents in this work mainly refer to the Hansen Solubility Parameters databases [6]. The parameters of DPrP was estimated by software (Hansen Solubility Parameters in Practice, HSPiP) based on the molecular structure. The parameters of PEG200, PEG300, PEG400 and PEG600 were referred from the published work [7]. The parameters of DPC was referred from the published work [8].

The solubility parameters of mixed diluents were calculated by Eqs. (S2-4)- (S2-6) [6, 9].

$$\delta_{DM} = \varphi_1\delta_{D1} + \varphi_2\delta_{D2} \quad \text{(S2-4)}$$

$$\delta_{PM} = \varphi_1\delta_{P1} + \varphi_2\delta_{P2} \quad \text{(S2-5)}$$

$$\delta_{HM} = \varphi_1\delta_{H1} + \varphi_2\delta_{H2} \quad \text{(S2-6)}$$

where M, 1 and 2, represent the mixed diluent system, diluent 1 and diluent 2, respectively. $\varphi_1$ and $\varphi_2$ are the volume fraction of diluent 1 and diluent 2, respectively.

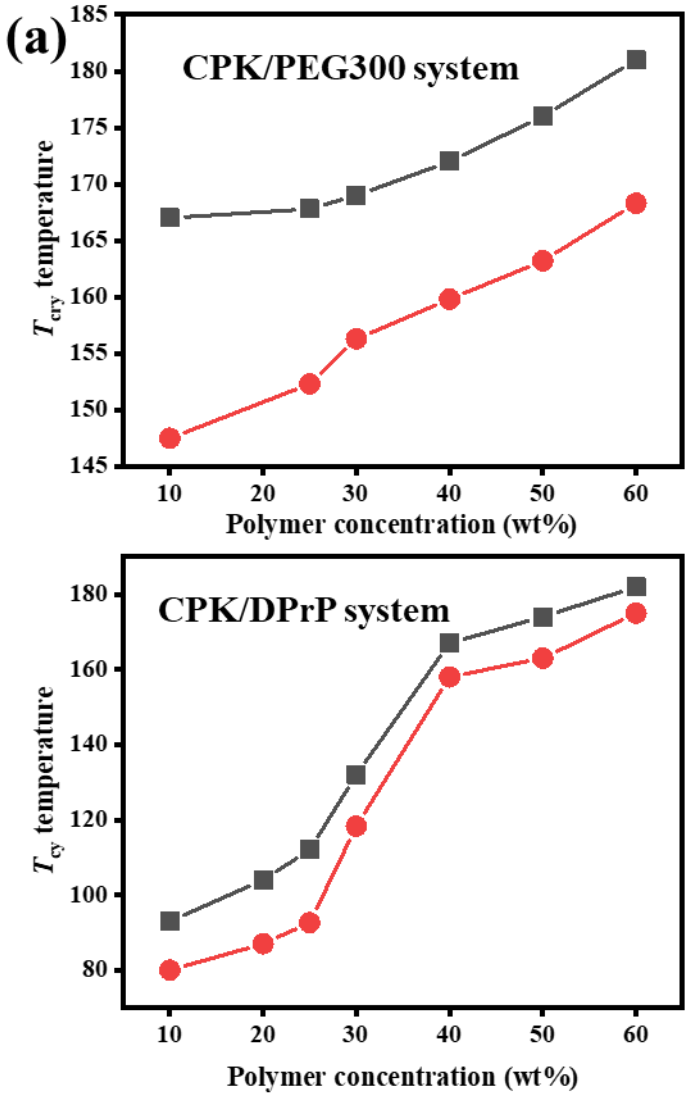


**Fig. S2-1** Crystallization temperature of CPK/PEG300 system (a) and CPK/DPrP system (b) using different cooling rates of 10 °C $min^{-1}$ (black line) and 50 °C $min^{-1}$ (red line).

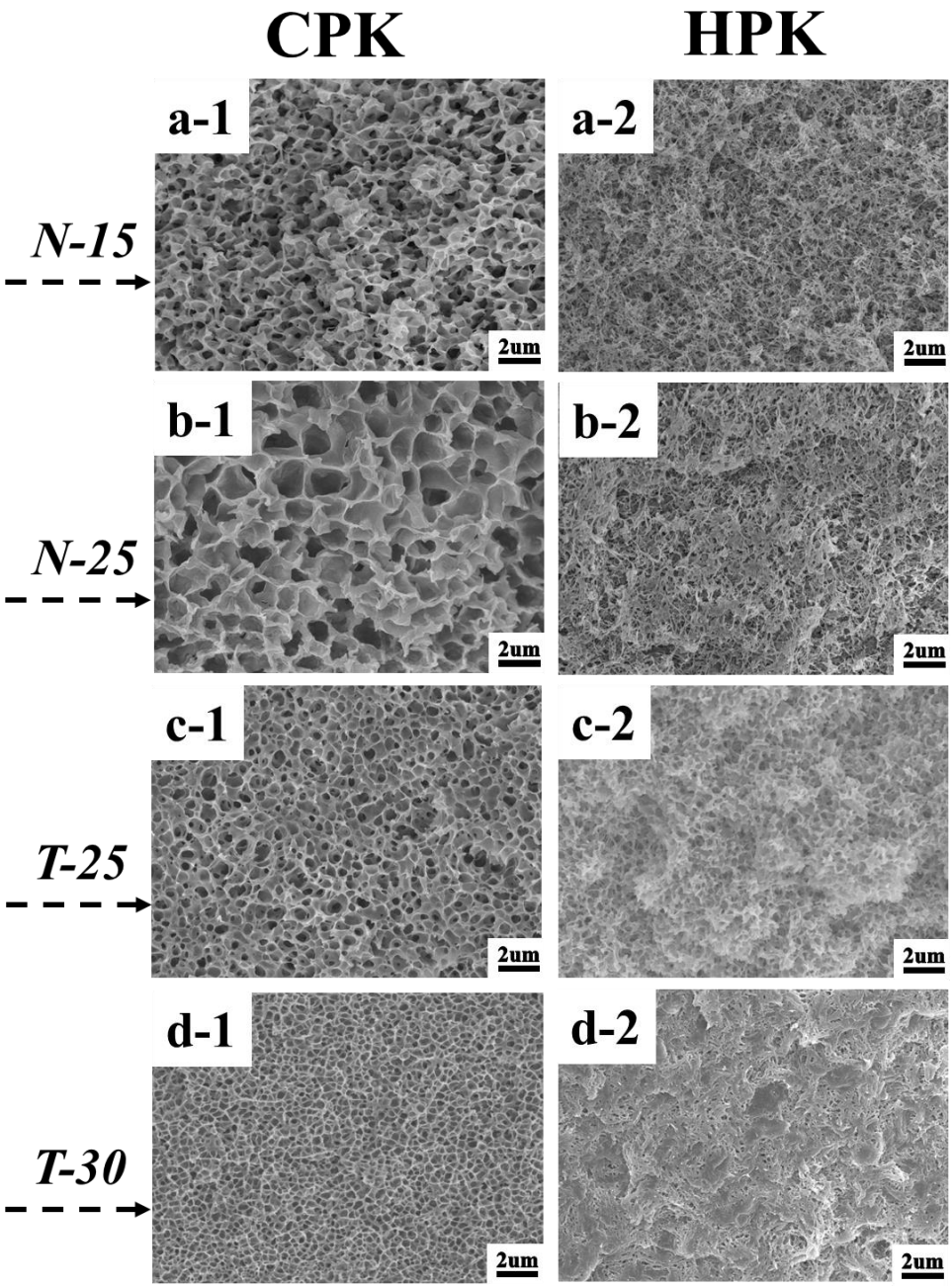


**Fig. S2-2** Enlarged cross-section morphology of CPK and HPK membranes prepared by NIPS and TIPS methods under different polymer concentrations. 1 and 2 represent CPK membrane and HPK membrane, respectively.

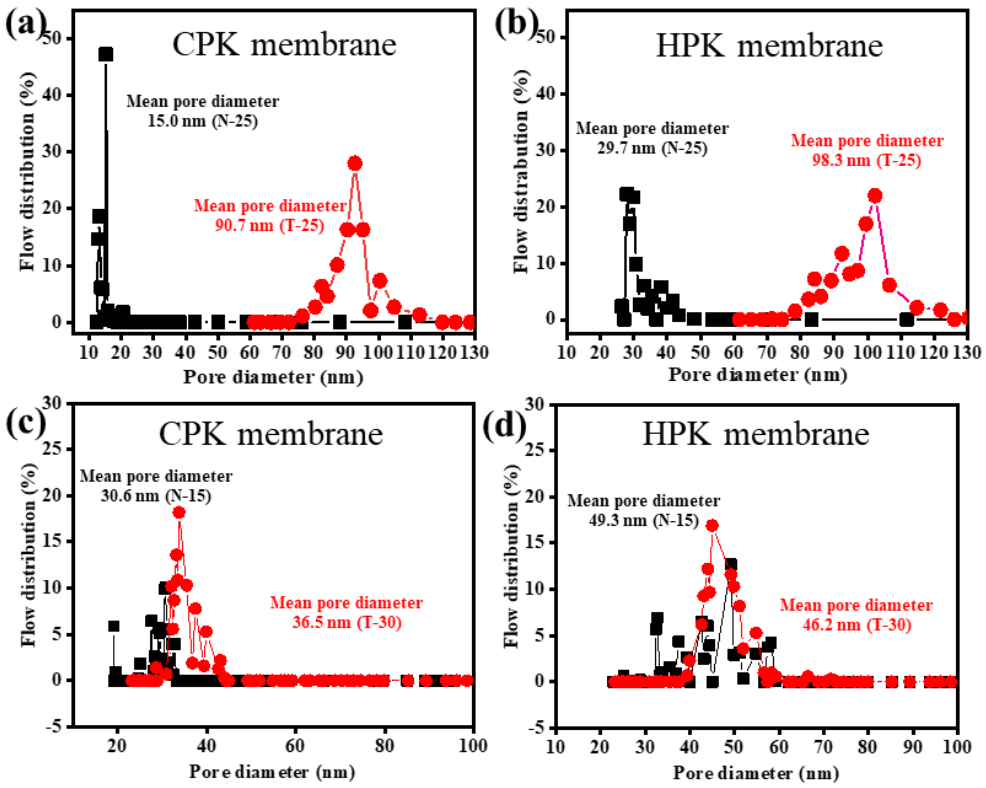


**Fig. S2-3** Pore diameters of membranes prepared by NIPS and TIPS methods with different PK concentrations. (a) CPK membrane (N-25 and T-25) and (b) HPK membrane (N-25 and T-25), (c) CPK membrane (N-15 and T-30) and (d) HPK membrane (N-15 and T-30).

The porosity of the prepared flat sheet membranes was measured by gravimetric method. Membranes were weighted dry and wet after the immersion in 1-Butanol for 12 h. Porosity was calculated by the following Eq. (S2-7) [10]:

$$\varepsilon = \frac{(m_w - m_d)/\rho_w}{(m_w - m_d)/\rho_w + m_d/\rho} \times 100\% \qquad \text{(S2-7)}$$

where $m_d$ and $m_w$ was the weight of the dry and wet flat membrane, respectively. $\rho_w$ was the 1-Butanol density (0.81 g cm$^{-3}$) and ρ was the density of polyketone include CPK (1.24 g cm$^{-3}$) and HPK (1.33 g cm$^{-3}$).

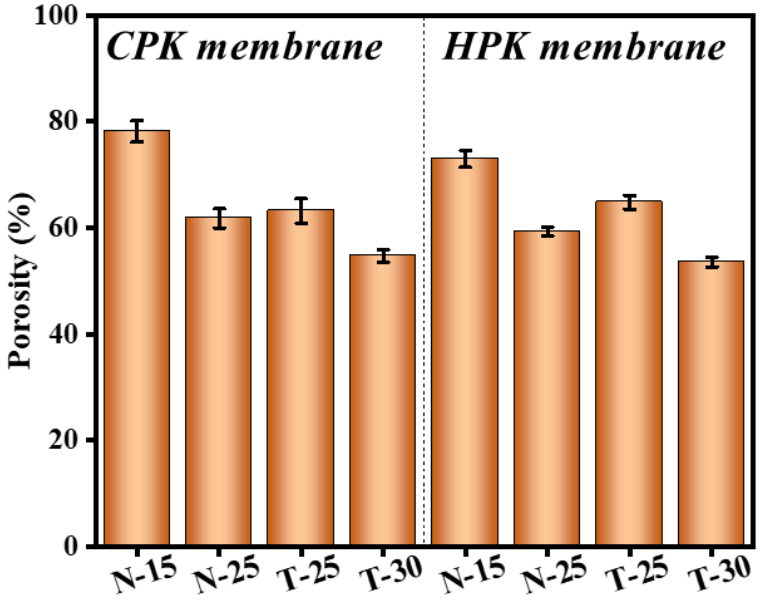


**Fig. S2-4** The porosity of the CPK and HPK flat sheet membranes.

## References

[1] D.W.V. krevelen, K.T. Nijenhuis, Properties of Polymers: Their correlation with chemical structure; their numerical estimation and prediction from additive group contributions, Fourth ed., Elsevier B.V., Amsterdam, Noord-Holland, 2008.

[2] M.M. Coleman, J.F. Graf, P.C. Painter, Specific interactions and the miscibility of polymer blends, Technomic Publishing, Lancaster, Pennsylvania, 1991.

[3] M.M. Coleman, X. Yang, H. Zhang, P.C. Painter, Ethyleneco-vinyl alcohol blends, J. Macromol. Sci. Phys. B, 32 (1993) 295-326.

[4] M. Yasukawa, S. Mishima, M. Shibuya, D. Saeki, T. Takahashi, T. Miyoshi, H. Matsuyama, Preparation of a forward osmosis membrane using a highly porous polyketone microfiltration membrane as a novel support, J. Membr. Sci., 487 (2015) 51-59.

[5] W.C.J. Zuiderduin, D.P.N. Vlasveld, J. Hue´tink, R.J. Gaymans, Mechanical properties of polyketone terpolymer/rubber blends, polymer, 45 (2004) 3765-3779.

[6] C.M. Hansen, Hansen solubility parameters: a user's handbook, second ed., CRC Press, New York, 2007.

[7] Bo Liu, Qiangguo Du, Y. Yang, The phase diagrams of mixtures of EVAL and PEG in relation to membrane formation, J. Membr. Sci., 180 (2000) 81-92.

[8] C. Fang, S. Jeon, S. Rajabzadeh, L. Cheng, L. Fang, H. Matsuyama, Tailoring the surface pore size of hollow fiber membranes in the TIPS process, J. Mater. Chem. A, 6 (2018) 535-547.

[9] H. Zhang, X. Lu, Z. Liu, Z. Ma, S. Wu, Z. Li, X. Kong, C. Wu, Study of the dual role mechanism of water-soluble additive in low temperature thermally-induced phase separation, J. Membr. Sci., 543 (2017) 1-9.

[10] J. Pan, C. Xiao, Q. Huang, H. Liu, J. Hu, ECTFE porous membranes with conveniently controlled microstructures for vacuum membrane distillation, J. Mater. Chem. A, 3 (2015) 23549-23559.

# Chapter 3

## Lowering spinning temperature for polyketone (PK) hollow fiber membrane fabrication with low-toxic diluent system via thermally induced phase separation

### *3.1 Introduction*

Over the past half-century, membrane separation technology has gained increasing attention as a solution to address resource scarcity and environmental concerns due to its cost-effectiveness and low energy consumption [1-4]. The phase separation method, which includes non-solvent induced phase separation (NIPS) and thermally induced phase separation (TIPS), has been widely used to fabricate polymeric porous membranes [5-7]. Compared with NIPS, TIPS, based on heat transfer, offers numerous advantages for membrane fabrication, including a wide range of polymeric materials, a straightforward preparation process, and resulting membranes with strong mechanical properties [8, 9].

In the TIPS process, a polymer is first dissolved by a diluent at elevated temperatures to create a homogeneous solution. This solution is then shaped into the desired form, such as hollow fibers or flat sheets, and immersed in a cold quenching bath, causing either solid-liquid (S-L) or liquid-liquid (L-L) phase separation, leading to the formation of the primary membrane. After removing the diluent from the primary membrane, the final porous membrane is obtained [8-10]. During the TIPS process, if the diluent has a strong interaction with polymer, the S-L phase separation will occur upon cooling leading to the formation of the spherulite structure. On the contrary, when

diluent possesses a weak interaction with polymer, the L-L phase separation will happen resulting in an interconnected network structure or cellular structure. Compared with the spherulite structure, the interconnected network structure and the cellular structure typically exhibit high mechanical properties. Besides the kinds of diluent, the polymer concentration and cooling rate also have a significant impact on membrane structure. In addition, several polymers, such as polyvinylidene fluoride (PVDF) [11-13], polypropylene (PP) [14-16], poly (vinyl butyral) (PVB) [17], polyamide (PA) [18-20], polyethylene (PE) [21-23], poly (ethylene-co-vinyl alcohol) (EVOH) [24, 25], poly (ethylene chlorotrifluoroethylene) (ECTFE) [26], polystyrene (PS) [27], polysulfone (PSF) [28, 29], polyphenylene sulfide (PPS) [30], and polymethyl methacrylate (PMMA) [31], have been used to create porous membrane through the TIPS method.

Compared to the aforementioned materials, polyketone (PK), a semi-crystalline polymer known for its chemical resistance and mechanical properties, shows great potential for producing high-performance porous membranes [5, 32]. Although PK flat porous membranes with excellent permeance have been prepared using the NIPS method [33, 34], the use of toxic solvents and complex processes has significantly increased production costs and hindered the development and application of PK membranes, primarily due to environmental and safety concerns [35, 36]. Therefore, there is growing interest in utilizing low-toxic or non-toxic solvents in phase separation methods [37-39]. Given its simple preparation process and potential low toxicity, the TIPS process is an ideal candidate for creating high-performance PK porous membranes. In our prior study, more than 10 pure diluents, involving both S-L and L-L phase separation systems, were examined, and a PK flat sheet membrane was prepared via the L-L TIPS process [36]. For example, polyethylene glycol 300 (PEG300), characterized by a high boiling point (approximately 250°C) and low toxicity, was selected as a diluent based on the L-L phase separation system due to its weak interaction with PK (*R*a value of 16.9 $(MPa)^{0.5}$). The impact of PK concentration on the phase diagram, structure, and performance of the resulting PK membrane was

meticulously studied. However, L-L phase separation typically requires a high membrane formation temperature, often surpassing the melting point of polymer in certain cases [36, 40]. This is because the polymeric solution, while passing through a metastable region, forms a diluent-lean phase and a diluent-rich phase before reaching the crystallization temperature in the L-L phase separation process. Consequently, the high-temperature preparation process and prolonged exposure to organic solvents can lead to PK decomposition, significantly limiting the application of the TIPS technique in PK membrane preparation. Furthermore, the elevated preparation temperature significantly increases energy consumption and equipment requirements. Therefore, it is essential to reduce the formation temperature for PK membrane production. This not only conserves energy but also, more importantly, for PK, mitigates the risk of PK decomposition, resulting in a more stable membrane structure and improved performance.

To lower the membrane fabrication temperature in the L-L phase separation based on the TIPS method, several approaches have been explored. Identifying a new diluent capable of dissolving the polymer and inducing phase separation at lower temperatures is the most direct and effective method. For instance, in PVDF/ Diphenyl carbonate (DPC)/PC system, increasing the PC concentration sharply reduces the cloud point temperature resulting from the enhanced interaction with PVDF and mixed diluents system, suggesting a potential reduction in membrane formation temperature. These findings indicate that membrane formation temperature can be controlled by simply introducing a secondary diluent that interacts effectively with the polymer while preserving the desired network structure resulting from L-L phase separation. Thus, it becomes possible to apply this concept to create PK membranes with interconnected structures at lower spinning temperatures in the TIPS process by mixing in another good solvent.

Based on our previous solvent screening results, several diluents were found to induce S-L phase separation upon cooling for PK. These diluents include PC, dimethyl

phthalate (DMP), DPC, TEG, sulfolane (SFL), caprolactam (CPL), dimethyl sulfone ($DMSO_2$), and diethyl phthalate (DEP) [36]. Among them, TEG, a water-soluble low-toxic diluent with a high boiling point (285°C), exhibits better interaction with PK than PEG300. Considering their low toxicity and cost-effectiveness, we aimed to incorporate TEG into the PK/PEG300 system to reduce the spinning temperature. In this study, we have successfully manufactured PK hollow fiber membranes using a mixture of PEG300 and TEG at a relatively low formation temperature through the TIPS process. We systematically investigated the impact of TEG concentration and PK concentration in the mixed diluents on the phase diagram, membrane structure, pore size, mechanical property, and filtration performance. The addition of TEG to the diluent successfully controlled the spinning temperature to below 200ºC. To further enhance membrane water permeability, we varied the bore liquid composition to create porous inner surface structure and studied its influence on PK hollow fiber membranes. Finally, we evaluated the solvent-resistant properties of PK hollow fiber membranes by immersion in various solvents. This work aims to reduce the formation temperature of PK hollow fiber membranes using low-toxic mixed solvents while achieving solvent-resistant PK hollow fiber membrane with stable structures and performance.

## *3.2 Experimental*

### *3.2.1 Materials*

Polyketone (M630A) was supplied by Hyosung Corporation Co., Ltd (South Korea). Polyethylene glycol 300 (PEG300), triethylene glycol (TEG), propylene carbonate (PC), toluene, acetone, dimethylformamide (DMF), dimethyl sulfoxide (DMSO), hexane, and ethanol were purchased from Tokyo Chemical Industry Co., Ltd. (Japan). Methanol (MeOH), chloroform, isopropanol (IPA), and tetrahydrofuran (THF) were obtained from Wako Pure Chemical Industries (Japan). Polystyrene (PS) latex particles with standard diameters of 100 and 50 nm were supplied by Duke Scientific Corporation (USA). Pure water was generated using an ultrapure water machine (Milli-

Q IQ 7000, Millipore SAS, France). All the materials were used without further purification.

### *3.2.2 The measurement of cloud point and crystallization temperature*

Initially, the PK and diluent, in the specified ratio were weighted, mixed, and heated to create a homogeneous solution at an elevated temperature using the glass tube. Subsequently, the dope solution was rapidly quenched using liquid nitrogen to produce a solidified sample, which was then preserved under low-temperature conditions.

The cloud point temperature ($T_{cloud}$) of the dope solution was determined using an optical microscope (Olympus BX50, Olympus, Japan) and a hot stage (LK-600, Linkam, UK). In detail, approximately 5 mg of the solidified sample was cut and sandwiched between two microscope coverslips to minimize solvent evaporation. The sample was then heated to form a uniform solution and gradually cooled to room temperature (20 ºC) at a controlled rate (10 ºC $min^{-1}$) using the hot stage. During this cooling process, the optical microscope was employed to observe changes in the morphology of the dope solution. The temperature at which the first droplet separated from the homogeneous solution was recorded as the $T_{cloud}$.

Differential scanning calorimetry (DSC) (DSC-8500, Perkin Elmer, USA) was utilized to determine the crystallization temperature ($T_{cry}$) of the PK solution. About 8 mg of the solid sample was weighed and sealed in an aluminum pan, and the crystallization process of the PK was monitored using a controlled heating rate of 10 ºC $min^{-1}$. The temperature at which the exothermic peak started during the cooling process was taken as the $T_{cry}$.

### *3.2.3 Preparation of PK hollow fiber membranes*

The fabrication of the PK hollow fiber membrane was carried out using a spinning apparatus equipped with a batch-type extruder (BA-0, Imoto Co., Japan) [41]. In detail, as shown in Table 3-1, PK pellets and diluents (PEG300/TEG) were weighed in the

specified ratio and placed in a tank. The mixture was stirred and heated to form a homogeneous solution. After ensuring the removal of air bubbles, the PK solution was pushed into the spinneret by a gear pump, under a nitrogen pressure of 0.1 MPa. Simultaneously, a bore liquid was transported into the spinneret using the metering pump. The PK solution containing the bore liquid was extruded through the spinneret. The extruded material passed through an air gap and then immersed in a quenching bath, and the resulting membrane was collected by a take-up winder. Subsequently, any remaining diluent was removed by immersing the prepared membranes in ethanol. Finally, the membranes were dried and stored under ambient conditions. The detailed preparation parameters are listed in Table S3-1

**Table 3-1** Composition and preparation parameters of the membranes.

| Membrane code | Diluent | | PK (wt%) | Bore liquid | Spinning temperature (°C) |
|---|---|---|---|---|---|
| | PEG300 (wt%) | TEG (wt%) | | | |
| A1 | 80 | 0 | 20 | PEG300 | 245 |
| A2 | 60 | 20 | 20 | PEG300 | 225 |
| A3 | 40 | 40 | 20 | PEG300 | 200 |
| A4 | 20 | 60 | 20 | PEG300 | 195 |
| B1 | 40 | 40 | 20 | PEG300 | 200 |
| B2 | 38.5 | 38.5 | 23 | PEG300 | 200 |
| B3 | 36.5 | 36.5 | 27 | PEG300 | 200 |
| B4 | 35 | 35 | 30 | PEG300 | 200 |
| C1 | 40 | 40 | 20 | 100/0 | 200 |
| C2 | 40 | 40 | 20 | 70/30 | 200 |
| C3 | 40 | 40 | 20 | 40/60 | 200 |
| C4 | 40 | 40 | 20 | 0/100 | 200 |

Note: Bore liquid consists of PEG300 and PC with different weight percent.

### *3.2.4 Characterization of membranes*

3.2.4.1 Membrane morphology and crystalline structure

To assess the morphology of the membrane surface and cross-section, a field-emission scanning electron microscope (FE-SEM) (JSF-7500F, JEOL Co., Japan) was used. Initially, the hollow fiber membranes were fractured in a liquid nitrogen environment to create cross-section samples. All samples, including the cross-section and membrane surface, were vacuum-dried for approximately 24 hours. Following this, cesium tetroxide was applied, and the samples were examined using FE-SEM. The crystalline phase of the hollow fiber membrane was characterized using a Fourier transform infrared spectroscopy spectrometer (FTIR-ATR, Alpha Bruker, USA) and X-ray diffraction (XRD, D2 PHASER, Bruker, USA). The viscosity of bore liquid was measured by EMS Viscomter (EMS-1000S, Kyoto Electronics Manufacturing Co.,) at 25°C.

3.2.4.2 Surface roughness, hydrophilicity, pore size, and porosity of membrane

The surface roughness of the hollow fiber membranes was determined using a laser microscope (VK-X3000, Keyence, Japan). To evaluate membrane hydrophilicity, the water contact angle on the membrane surface was measured with a contact angle goniometer (Drop Master, Kyowa Interface Science Co., Japan). The mean pore size of the hollow fiber membrane was determined using a liquid–liquid porometer (LLP-1100A, PIM, USA). Overall porosity was confirmed using the gravimetric method. All measurements were conducted three times, and the average values were calculated.

3.2.4.3 Membrane performance

The mechanical strength of the hollow fiber membrane was assessed using a precision strength tester (AGS-J, Shimadzu Co., Japan). This involved clamping the membrane with two pairs of tweezers spaced 20 mm apart and stretching it at a controlled rate (10 mm $min^{-1}$) until it broke. Each sample was measured three times,

and the average value was calculated.

A laboratory-scale measurement device was employed to determine the pure water permeability (PWP) and particle rejection of the hollow fiber membranes [43]. To measure the PWP, a dry hollow fiber membrane, 10 cm in length, was immersed in ethanol for 10 minutes. Subsequently, the membrane was tested under an inside-to-outside filtration model with a filtration pressure of 1 bar. Three membrane samples for each specimen were selected and measured to calculate the average value. PWP (L $m^{-2}h^{-1}bar^{-1}$) was calculated using Equation (3-1):

$$PWP=\frac{V}{A\times\Delta t\times P} \tag{3-1}$$

where $V$ represents the volume of the permeate solution (L). $A$, $\Delta t$ and $P$ are the efficient filtration area ($m^2$), operating time (h), and operating pressure (bar), respectively.

To assess particle rejection properties, standard PS particles with sizes of 50 nm and 100 nm were used. A PS particle aqueous solution (1 g $L^{-1}$) was prepared by adding 0.1 wt% of the nonionic surfactant Triton X-100 and stirring for approximately 3 hours at 1000 rpm. During the same filtration process as the PWP measurement, the permeation solution was collected. The concentration of PS particles in both the feed and permeation solutions was measured three times using a Hitachi U-200 ultraviolet (UV) spectrophotometer at a wavelength of 380 nm. Particle rejection was calculated using Equation (3-2):

$$R=\frac{C_f-C_p}{C_f}\times 100\% \tag{3-2}$$

where $R$ represents the rejection of PS particles (%). $C_p$ and $C_f$ are the PS particle concentrations (g $L^{-1}$) of permeate and feed solution, respectively.

To evaluate the resistance of PK hollow fiber membranes to different organic solvents (including MeOH, toluene, acetone, DMF, DMSO, hexane, chloroform, IPA, and THF), a representative sample (C4) was selected and soaked in these solvents for 10 days at room temperature (25°C). Following soaking, the PK membrane was cleaned with either pure water or ethanol and then dried. Finally, the PWP and mechanical

strength of the samples (original membrane and soaked membrane) were measured using the same process as described earlier.

### *3.3 Results and discussion*

#### *3.3.1 Phase diagram*

To reduce the spinning temperature, TEG, a solvent that induces S-L phase separation for PK as reported in previous research [36], was added into the PVDF/PEG300 system. Fig. 3-1 illustrates the phase diagram of PK/PEG300/TEG ternary system with different PEG300/TEG ratios, while maintaining a fixed PK concentration of 20 wt%. It is evident that as the ratio of PEG300/TEG decreased (indicating an increased TEG concentration), the $T_{cloud}$ dramatically decreased. When the ratio reached 20/60 (wt%/wt%) in the diluent mixture, droplets appeared before PK crystals, suggesting that the PK solution system would undergo L-L phase separation. When the ratio of PEG300/TEG exceeded a certain threshold in the mixed diluent, in cases where excessive TEG was added, only the crystallization process of PK was observed during the cooling process, indicating S-L phase separation.

This behavior in the PK/PEG300/TEG system aligns with the findings reported by Zhang et al. for the PVDF/DPC/PC system [10]. The primary focus of this study is on the L-L phase separation process because it leads to an interconnected structure within the bulk of the PK membrane. It is noteworthy that the $T_{cloud}$ decreased from 235ºC (80/0) to 172ºC (20/60) as the TEG concentration in the PK solution increased, while $T_{cry}$ experienced only a slight change. Consequently, the spinning temperature for PK membrane fabrication was significantly reduced to below 200ºC. This reduction effectively mitigated or slowed down the decomposition process of PK, resulting in a smoother spinning process and a more uniform membrane structure.

As demonstrated in our prior research, S-L phase separation occurs in the PK/TEG binary system at any composition due to the strong interaction between PK and TEG. Table 3-2 presents the interaction parameter (*R*a), which is used to gauge the

compatibility between PK and the mixed diluent. A lower *R*a value signifies better compatibility. In comparison to the *R*a value of PK and PEG300 (16.9 $MPa^{0.5}$), the smaller *R*a value between PK and TEG (15.1 $MPa^{0.5}$) indicates that TEG exhibits superior compatibility with PK. Consequently, with an increase in the TEG ratio in the diluent, the *R*a values between PK and mixed diluent gradually decreased. The $\Delta G^E$ value was calculated to further evaluate the interaction between PK and solvents, as shown in Table 3-2. In contrast to the slight reduction in the *R*a value, the $\Delta G^E$ value between PK and mixed diluent significantly decreases from 252.4 J $m^{-3}$ to 185.3 J $m^{-3}$ with an increase in the TEG ratio in the diluent, reconfirming that the decreased spinning temperature resulted from the enhanced interaction between PK and the diluent. Thus, by incorporating TEG into the solution, a lower spinning temperature for the PK/PEG300 system can be achieved based on the L-L phase separation system.

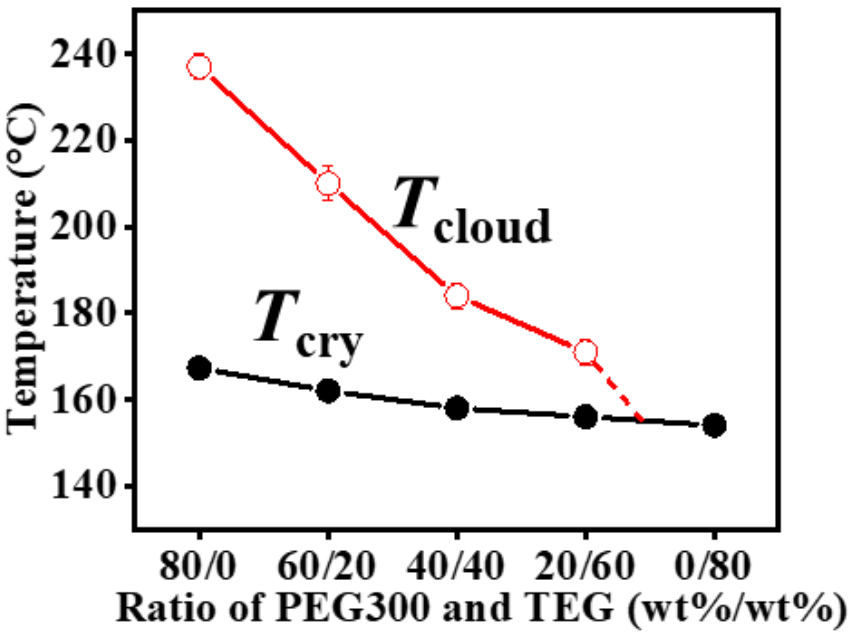


**Fig. 3-1** Cloud point and crystallization temperature of PK/PEG300/TEG systems with different ratios of PEG300/TEG. PK concentration was fixed at 20 wt%.

**Table 3-2** Hansen solubility parameters, *R*a value of PK and solvents, and Gibbs free

energy of mixing ($\Delta G^E$) of PK and solvents.

| | $\delta_d$ (MPa)$^{0.5}$ | $\delta_p$ (MPa)$^{0.5}$ | $\delta_h$ (MPa)$^{0.5}$ | $Ra$ (MPa)$^{0.5}$ | $\Delta G^E$ (J m$^{-3}$) |
|---|---|---|---|---|---|
| PK | 19.9 | 17.9 | 6.8 | | |
| TEG | 16.0 | 12.5 | 18.6 | 15.1 | 183.6 |
| PEG300 | 16.6 | 4.4 | 14.5 | 16.9 | 252.4 |
| PEG300/TEG (80/0) | 16.6 | 4.4 | 14.5 | 16.9 | 252.4 |
| PEG300/TEG (60/20) | 16.5 | 6.4 | 15.5 | 16.0 | 219.7 |
| PEG300/TEG (40/40) | 16.3 | 8.5 | 16.6 | 15.4 | 197.3 |
| PEG300/TEG (20/60) | 16.2 | 10.5 | 17.6 | 15.1 | 185.3 |

Note: Calculation methods of the solubility parameter of mixed diluent, $Ra$, and $\Delta G^E$ are shown in equations S3-1-S3-5 in the supplementary information.

Based on the aforementioned experimental results, we have selected A3 with an 1/1 (wt%/wt%) ratio of PEG300 and TEG as the mixed diluent system for our subsequent research. This choice is based on the fact that this system possesses a cloud point temperature of 184ºC in the case of PK 20 wt%, which falls below the desired threshold of 200℃ . In addition, a long distance between $T_{cloud}$ and $T_{cry}$ implies the broad range of PK concentrations in the L-L phase separation region. Next, we investigated the influence of PK concentration on both the cloud point temperature and crystallization temperatures of the PK/PEG300/TEG system. As shown in Fig. 3-2, as the PK concentration increases, the cloud point temperature shows a characteristic decrease. The point where the cloud point curve intersects with the crystallization curve represents the monotectic point, which occurs at 170.3℃ and 31 wt%. This implies that L-L phase separation still occurs within the PK solution during the cooling process as long as the PK concentration is lower than that at the monotectic point.

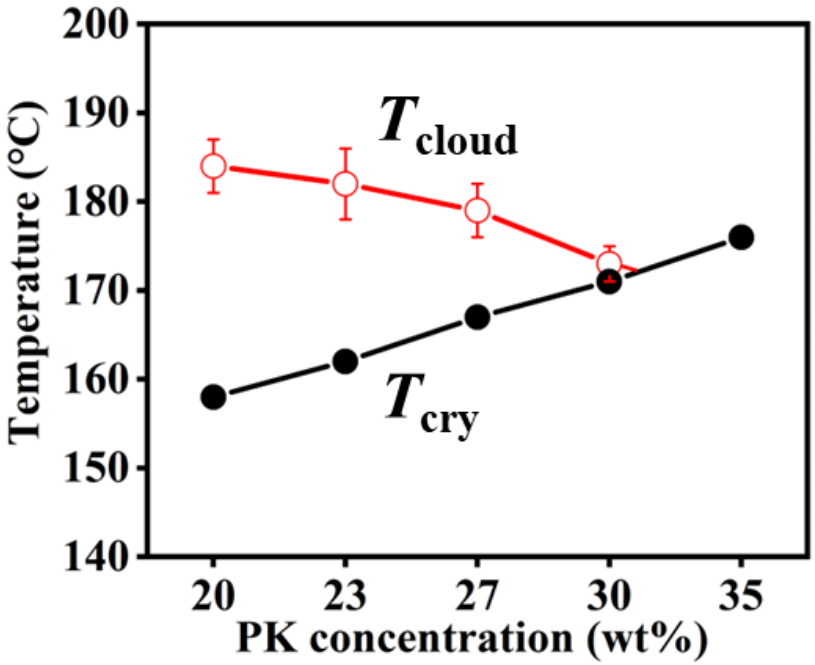


**Fig. 3-2** Cloud point and crystallization temperature of PK/PEG300/TEG systems with different PK concentrations. The ratio of PEG300/TEG was fixed at 1/1 (wt%/wt%).

To provide a clear visualization of the changes in cloud point temperature and crystallization temperature, the phase diagrams of PK/PEG300 and PK/PEG300/TEG systems are presented in Fig. 3-3. The data of PK/PEG300 system were derived from previous work [36]. It is evident that the PK/PEG300 system exhibits a high $T_{cloud}$ and monotectic point (53 wt%), which implies a broad range of PK/diluent compositions capable of inducing L-L phase separation, primarily due to the weak interaction between PK and PEG300. In contrast, the increased proportion of TEG in the PK/PEG300/TEG system significantly reduces the $T_{cloud}$. This reduction is attributed to the enhanced interaction between PK and the mixed diluent, as discussed earlier. Ultimately, the PK/PEG300/TEG system with a 1/1 ratio of PEG300/TEG exhibits a low $T_{cloud}$ (170.3°C) at the monotectic point, which is the primary factor contributing to the lowering of the spinning temperature. As a trade-off, the monotectic point decreases to 31 wt%.

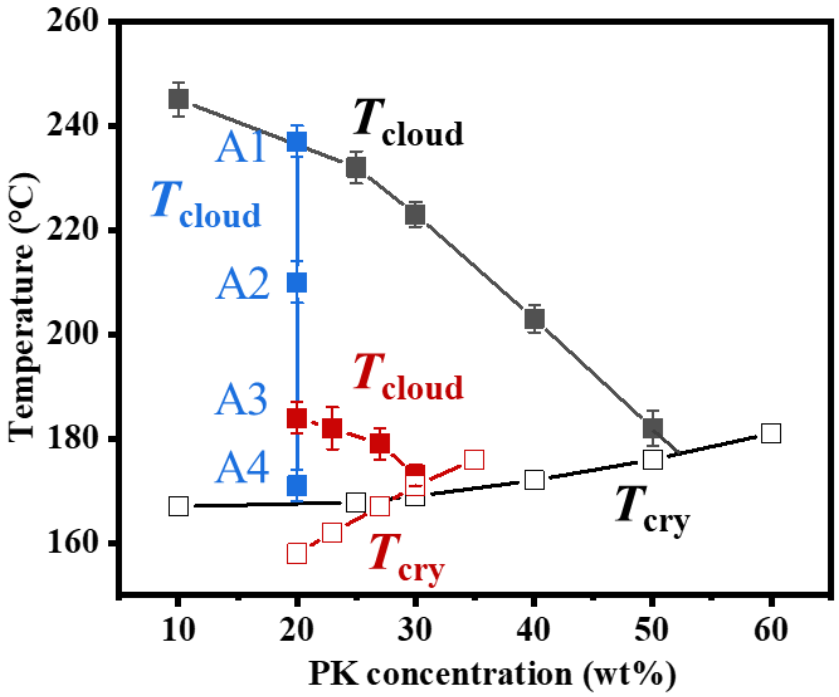


**Fig. 3-3** Cloud point temperature and crystallization temperature of PK/PEG300 and PK/PEG300/TEG system. The black line represents the PK/PEG300 system with different PK concentrations from the previous work [36]. The blue line represents the different ratios of PEG300/TEG and PK concentration is fixed at 20 wt%. The red line represents the PK/PEG300/TEG system with different PK concentrations based on the fixed ratio of PEG300 and TEG (1/1 wt%/wt%) in the diluent.

### *3.3.2 Membrane characterizations*

Fig. 3-4 presents the morphology of the PK hollow fiber membranes prepared using a mixed diluent with varying ratios of PEG300 and TEG, while maintaining a constant PK concentration of 20 wt%. In all the samples, the middle of the cross-section is predominantly characterized by cellular structures resulting from the L-L phase separation in Fig. 3-4(III). As the TEG concentration increases in the dope solution, the smaller cellular structure was obtained compared with membrane A1-I to A1-IV. This

change is mainly ascribed to the short coarsening process of the diluent-rich phase. As discussed in the phase diagram in Fig. 3-1, the addition of TEG significantly reduces the distance between $T_{cloud}$ and $T_{cry}$, resulting in a shorter time for the growth of the diluent-rich phase before PK crystallization to form the small cellular structure. A similar phenomenon is observed in the cross-section near the inner surface, as shown in Fig. 3-4(IV).

However, the cross-section near the outer surface exhibits a smaller interconnected structure than that in the middle of the cross-section. Two factors contribute to this difference in cross-section structure. Firstly, the cooling rate along the thickness direction differs. The region near the outer surface of the membrane experiences rapid cooling when it enters the quenching bath, resulting in a shorter coarsening period for the diluent-rich phase before the crystallization of PK. This shorter period reduces the size of the network structure. Secondly, there is a loss of diluent at the outer surface of the primary membrane, including evaporation at the air gap and outflow in the quenching bath. This causes a higher PK concentration at the outer surface of the membrane, which also shortens the time for the L-L phase separation, as illustrated in Fig. 3-1. The membrane structure is strongly influenced by the growth period of the diluent-rich phase and polymer-rich phase, resulting in a smaller network structure near the outer surface compared to the bulk.

Fig. 3-4(V) and 3-4(VI) display the outer and inner surface morphology of the PK hollow fiber membranes by varying the ratios of PEG300/TEG in the dope solution. A1-V exhibits a dense outer surface with few pores, while the amount of surface pores gradually increases with the increase in TEG concentration in the dope solution. This difference is attributed to the extremely high spinning temperature (245ºC) of A1 case (Table 3-2), which accelerates the evaporation of the diluent (PEG300) at the membrane outer surface during passing through the air gap, resulting in a higher PK concentration and the formation of a dense outer surface. Conversely, as the ratio of TEG in the mixed diluents increases, the spinning temperature significantly decreases, slowing down the

evaporation of the diluent on the primary membrane surface. Additionally, the higher boiling point (280°C) of TEG increases the difficulty of diluent evaporation, leading to the formation of more porous structures on the membrane outer surface. The porous inner surface of all the prepared membranes (Fig. 3-4(VI)) can be observed due to the utilization of the same solvent, PEG300, in the bore liquid, because of the penetrating bore liquid into the dope solution.

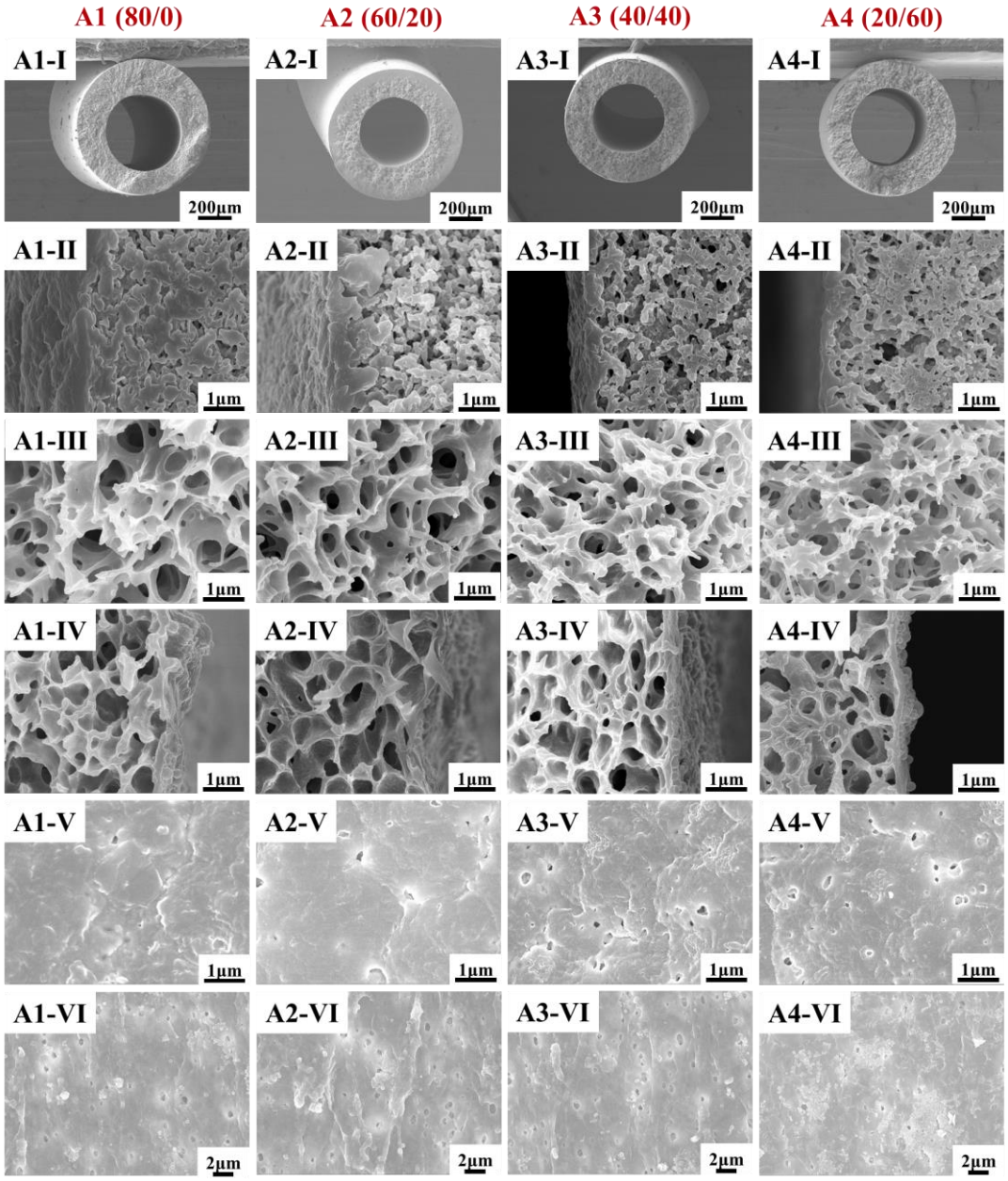

**Fig. 3-4** Cross-section and surface morphology of PK hollow fiber membrane prepared by the different ratios of PEG300/TEG in diluent. A1, A2, A3 and A4 represent the ratio of PEG300/TEG are 80/0, 60/20, 40/40 and 20/60 (wt%/wt%), respectively. I, II, III, IV, V, and VI represent the whole structure, near outer surface, center part, near inner surface, the outer and inner surfaces of the membranes, respectively. The PK concentration was 20 wt%. Bore liquid was PEG300.

The addition of TEG successfully reduced the spinning temperature, however, it comes at the cost of shifting the monotectic point to a lower concentration. This means that the range of polymer-diluent compositions capable of inducing L-L phase separation is narrowed. Therefore, we also investigated the effect of PK concentration on the membrane structure in detail. Fig. 3-5 shows the cross-section and surface morphology of the PK hollow fiber membranes prepared by different PK concentrations in the PK/PEG300/TEG system, with a fixed ratio of PEG300/TEG ratio at 1/1 (wt%/wt%). In each prepared membrane, a cellular structure is observed, which is the result of L-L phase separation and corresponds to the phase diagram results (Fig. 3-2). As the PK concentration increases, the size of the cellular structure decreases. This can be attributed to the decrease in $T_{cloud}$, which approaches the $T_{cry}$ of the dope solution, as shown in Fig. 3-2. Particularly, in the case of membrane B4, the $T_{cloud}$ (173ºC) and $T_{cry}$ (171ºC) are so close that the PK solidifies and forms a smaller cellular structure before the droplets have time to grow. In addition, as the PK concentration increases, the thickness of both the outer and inner skin layers increases, and the outer and inner surfaces become denser, displaying fewer pores.

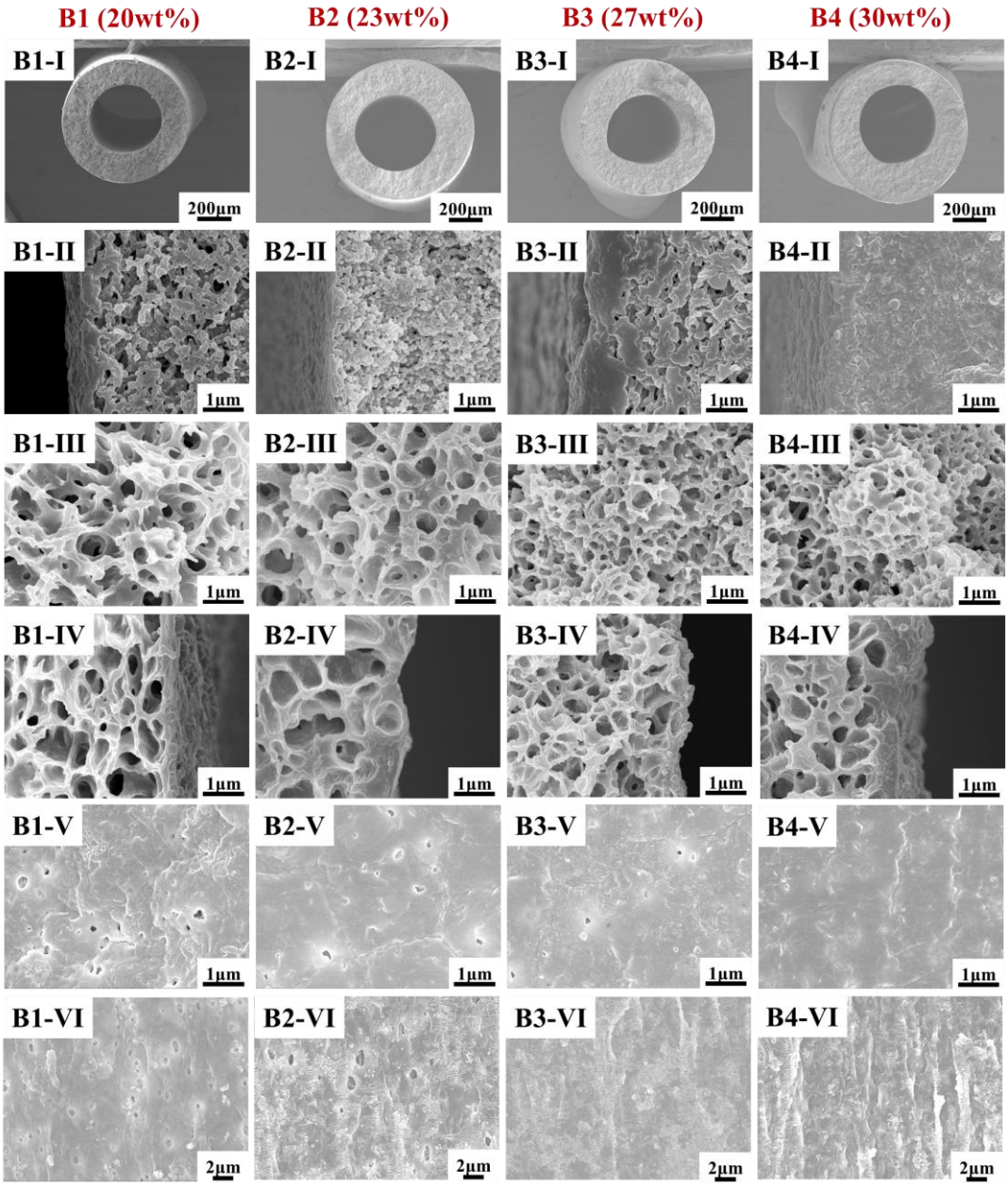


**Fig. 3-5** Cross-section and surface morphology of PK hollow fiber membrane prepared by different PK concentrations. B1, B2, B3, and B4 represent the PK concentration are 20, 23, 27, and 30 wt%, respectively. I, II, III, IV, V and VI represent the whole structure, near outer surface, center part, near inner surface, the outer and inner surfaces of the membranes, respectively. The ratio of PEG300/TEG was fixed at 1/1 (wt%/wt%). Bore liquid was PEG300.

Fig. 3-6 presents the cross-sectional and surface morphology of the PK hollow fiber

membranes prepared by varying the composition of the bore liquids. The PK/PEG300/TEG ratio in the dope solution was held constant at 20/40/40 (wt%/wt%/wt%). A general interconnected structure can be observed near the outer surface (Fig. 3-6(II)) and the center part (Fig. 3-6(III)), resulting from the L-L phase separation during the cooling process. There is almost no change in the membrane bulk and the outer surface structure for all prepared membranes using different bore liquids, indicating that the bore liquid has a minimal effect on the main bulk of the membrane and its outer surface.

Regarding the membrane structure near the inner surface, compared to the membrane prepared using pure PEG300 used as the bore liquid (Fig. 3-6(C1-IV)), an increase in the PC ratio in the bore liquid led to the elimination of the inner skin layer and a rougher appearance in membranes C2-IV and C3-IV. In membrane C4-IV, macrovoid structures, appeared near the inner surface when pure PC was used as the bore liquid. It also can be observed from Fig. 3-6(VI) that the addition of PC transformed the inner surface structure from a dense structure with fewer small pores to a porous structure with larger pores. In the case of membrane C4, the inner surface pores are so large that the overall structure can be observed even at a much lower magnification as shown in Fig. S3-1.

The low molecular weight and liquid status of the bore liquid make it highly to penetrate into the inner surface of the primary PK hollow fiber membranes. As shown in Table 3-3, the bore liquid with a 100/0 (wt%/wt%) ratio of PEG300/PC had a high viscosity. For sample C4, the viscosity of pure PC is 20 times lower than pure PEG300 (sample C1). Consequently, when pure PC was used as bore liquid, PC rapidly penetrated into the inner surface region, significantly reducing the inner surface PK concentration and causing the PC penetrated region to cool down faster. This resulted in the formation of macrovoid structure on the inner surface.

Fig. 3-6(V) and 3-6(VI) display the outer and inner surface morphology of the PK hollow fiber membranes by different ratios of PEG300/PC in the diluent. The similar structures, a dense outer surface with few pores, can be observed in 6(V), due to the

less effect on the outer surface with varying bore liquid. On the contrary, the inner surface porosity rapidly increased from 8.3 to 69.0% as shown in Table S3-2, resulting from the decreased viscosity promoting the bore liquid to penetrate into the inner surface region as mentioned above. In addition, spherulite structures were formed on the inner surface of membrane in C3-VI and C4-VI, resulting from the increased interaction between PK and bore liquid, as shown in Table S3-3.

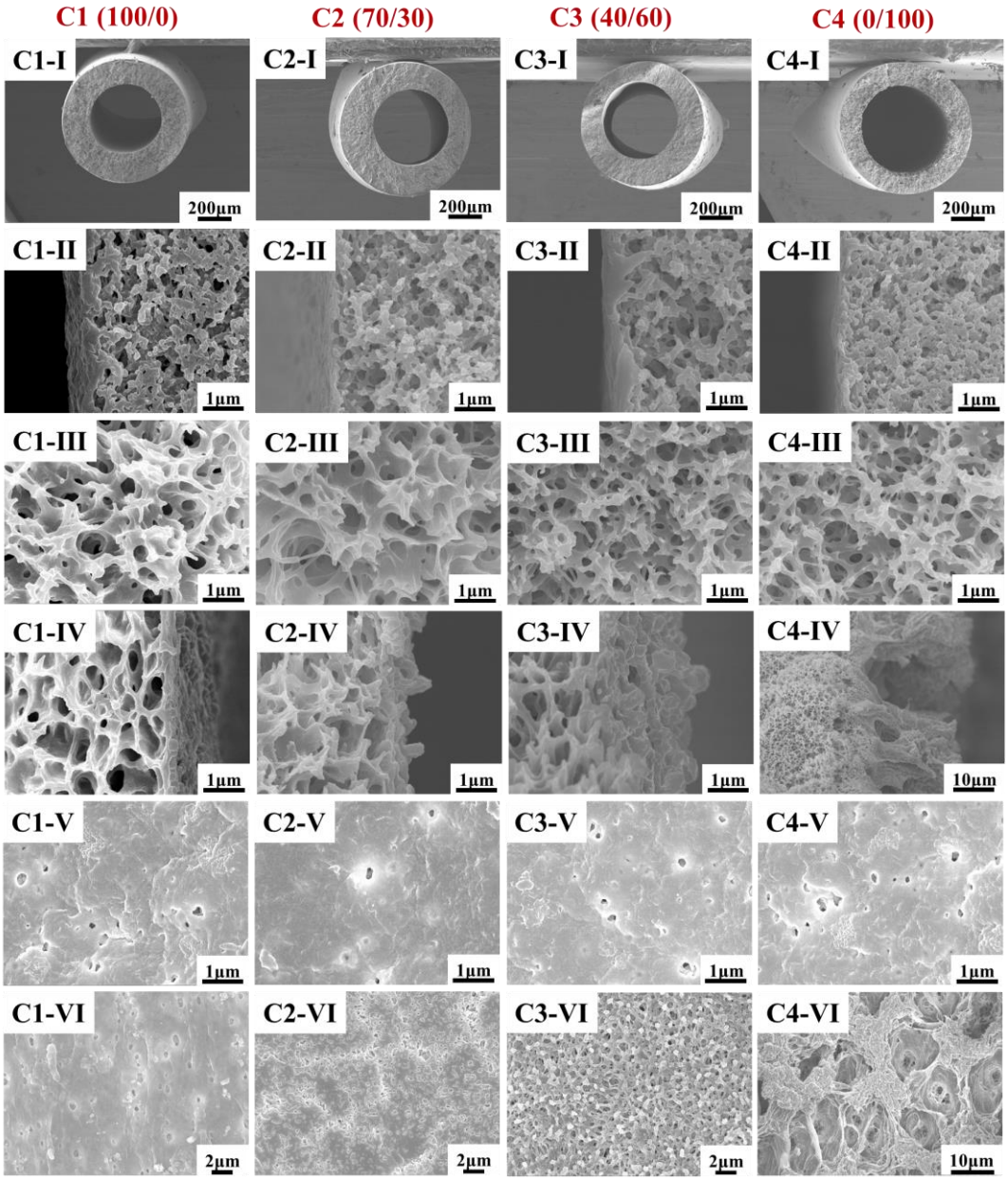


**Fig. 3-6** Cross-section and surface morphology of PK hollow fiber membrane prepared by different bore liquids. C1, C2, C3, and C4 represent the ratio of PEG300/PC are

100/0, 70/30, 40/60 and 0/100 (wt%/wt%) in bore liquid, respectively. I, II, III, IV, V and VI represent the whole structure, near outer surface, center part, near inner surface, the outer and inner surfaces of the membranes, respectively. The ratio of PK/PEG300/TEG (dope solution) was fixed at 20/40/40 (wt%/wt%/wt%).

**Table 3-3** Viscosity of bore liquid at 25°C conditions.

| Bore liquid (PEG300/PC wt%/wt%) | Viscosity (η) mPa.s |
|---|---|
| 100/0 | 80.3 |
| 70/30 | 53.2 |
| 40/60 | 28 |
| 0/100 | 2.8 |

XRD analysis was performed to examine the crystal structures of the PK hollow fiber membranes. PK can exist in two crystalline forms known as $\alpha$ and $\beta$, depending on processing conditions. As shown in Fig. 3-7(a), the XRD peaks appear at the identical diffraction angles $2\theta$ of 21.7°, 24.6°, 26.1°, 32.6°, and 39.3°, corresponding to the crystal planes of (110), (111), (200), (210), (212), respectively. These peaks indicate that all prepared PK membranes exhibited the characteristic $\alpha$ form. The formation of $\alpha$ form in these PK membranes is likely due to the crystallization process of PK occurring in the solution [42]. The crystal structure was further elucidated by using FT-IR measurement, as shown in Fig. 3-1(b). Absorption bands at approximately 593, 811, 1056, 1334, 1408, 1692, and 2912 $cm^{-1}$ were observed in all samples, which are related to the α-phase of PK crystals [42, 43]. The intensity of the characteristic peaks showed negligible changes, and there were no new typical peaks observed when changing the mixed diluent, PK concentration, or bore liquid. This indicates the α-form crystal was consistently formed in the PK hollow fiber membranes during the cooling process and was less affected by variations in mixed diluent, PK concentration, or bore liquid. The presence of the $\alpha$ crystal form in the PK hollow fiber membrane is significant because

it has a denser packing compared to the $\beta$ form, with shorter inter-atomic distances, and is more stable at room temperature [43]. Therefore, the presence of $\alpha$ crystal form contributes to stronger mechanical properties and stability of the hollow fiber membrane.

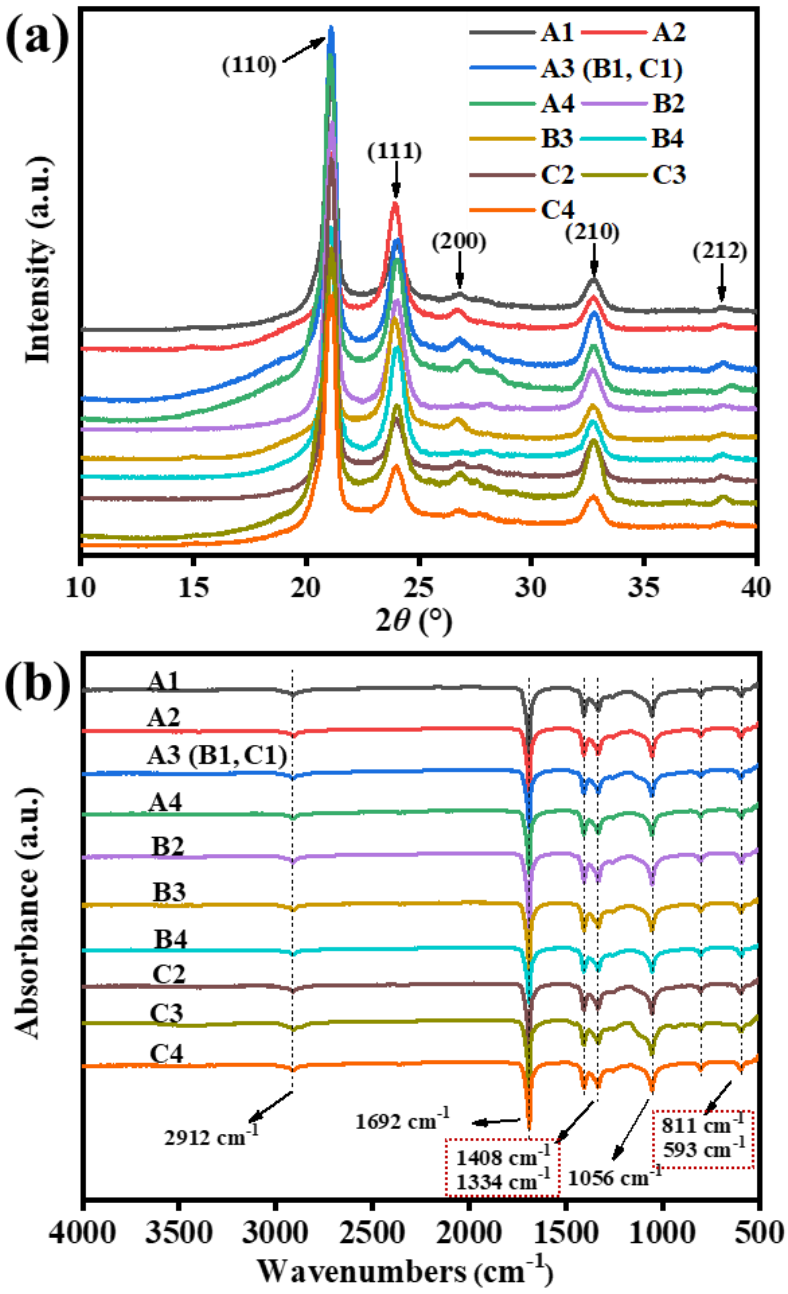


**Fig. 3-7** XRD patterns (a) and FTIR spectra (b) of PK hollow fiber membrane.

The effect of mixed diluent, PK concentration, and mixed bore liquid on the fundamental properties of the prepared PK membrane, including mean pore size, porosity, surface roughness, and water contact angle (WCA), were analyzed. The mean pore size (Fig. 3-8) of the PK hollow fiber membranes increased from 67 to 75 nm with the addition of TEG in the PK solution. This increase can be mainly attributed to changes in PK/mixed diluent miscibility and the evaporation of diluent, as shown in Table 3-2. When pure PEG300 was used as the diluent, the low PK/diluent interaction led to a high $T_{cloud}$. This resulted in a longer time for the growth of the diluent-rich phase, producing larger cellular structures. In contrast, the use of mixed diluent PEG300/TEG, which has a stronger PK/mixed diluent interaction and a lower $T_{cloud}$, led to a shorter time for L-L phase separation, producing a smaller structure after diluent extraction. This tendency agrees well with the previously reported work [10]. More importantly, the decreased spinning temperature diminishes the evaporation of the diluent, loading a porous outer surface. Finally, the mean pore size gradually increased as the increased TEG ratio in the PK solution. However, the membrane mean pore size exhibited a decline with the increase in PK concentration in the dope solution. This is due to the increment of PK fraction in the unit volume, which not only reduced $T_{cloud}$ (Fig. 3-2) but also formed a dense skin layer at the outer surface during the phase separation process (Fig. 3-5(V)). The denser skin layer resulted in diminished mean pore size and overall porosity of the prepared PK membranes, as shown in Fig. 3-8 and Table 3-4.

The increased addition of PC in the bore liquid had a positive effect on the mean pore size, which increased gradually from 75 to 89 nm. The lower viscosity of the bore liquid with higher PC concentration allowed more bore liquid to penetrate into the inner surface region of the primary PK hollow fiber during passage through the air gap. As a result, the inner surface formed a very porous structure with a larger mean pore size and higher porosity.

For the hydrophilic material PK, the hydrophilicity of the membrane depends on the

surface microstructure. As shown in Table 3-4, the TEG ratio in the mixed diluent and PC concentration in the bore liquid showed negligible effects on the membrane surface roughness and water contact angle due to minimal changes in the outer surface structures of membranes. However, increasing the PK concentration from 20 to 30 wt% resulted in a decrease in the roughness of the outer surface (84.5 to 38 nm) and a significant increase in the WCA value (60.7º to 75.1º) [44]. This was due to the formation of a dense outer surface and the elimination of surface pores (Fig. 3-5(V)).

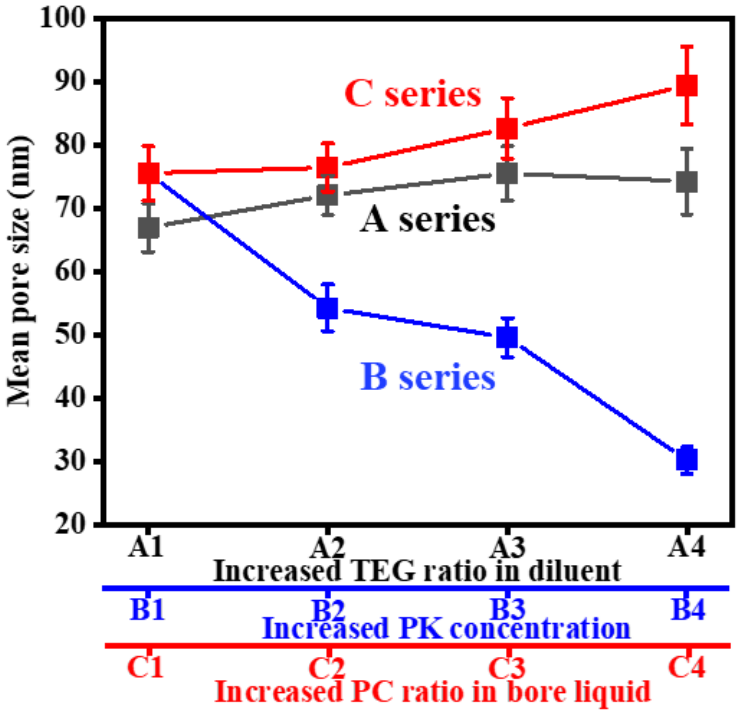


**Fig. 3-8** Mean pore size of PK hollow fiber membrane.

**Table 3-4** Surface roughness parameter (*RMS*), water contact angle, porosity of PK hollow fiber membrane.

| Samples | *RMS* (nm) | Water contact angle (º) | Overall porosity (%) |
|---|---|---|---|
| A1 | 75.8±3.2 | 64.7±3.2 | 77.3±1.8 |
| A2 | 82.5±7.1 | 62.1±2.7 | 76.8±2.1 |

| | | | |
|---|---|---|---|
| A3 | 84.5±5.3 | 60.7±3.1 | 75.2±1.9 |
| A4 | 80.3±6.2 | 61.2±2.8 | 74.5±1.8 |
| B1 | 84.5±5.3 | 60.7±3.1 | 75.2±1.9 |
| B2 | 72±5.3 | 64.2±2.4 | 72.3±1.3 |
| B3 | 53±3.2 | 69.3±1.9 | 69±1.6 |
| B4 | 38±6.1 | 75.1±1.2 | 64±1.4 |
| C1 | 84.5±5.3 | 60.7±3.1 | 75.2±1.9 |
| C2 | 82.7±6.2 | 60.2±2.6 | 76.6±1.8 |
| C3 | 86.3±3.4 | 58.7±2.0 | 77.1±1.7 |
| C4 | 91.8±7.2 | 56.4±3.7 | 83.2±2.8 |

The pure water permeability (PWP) of the prepared hollow fiber membrane and their rejection properties for PS particles of different sizes were assessed, as well as their mechanical properties, and the results are shown in Fig. 3-9. The PWP of the PK hollow fiber membrane slightly increased from 93 to 122 L $m^{-2}h^{-1}bar^{-1}$ as the TEG concentration in the dope solution increased. This increase was primarily attributed to the larger pore size and increased surface pores resulting from the addition of TEG. However, when the PK concentrations increased from 20 wt% to 30 wt%, the PWP decreased significantly to 18 L $m^{-2}h^{-1}bar^{-1}$. This reduction was due to the decreased pore size and formation of dense skin layer on the outer surface of the membrane, which increased the filtration resistance. For the fixed dope solution system in Table 3-1, the PWP of the membrane sharply increased from 124 to 820 L $m^{-2}h^{-1}bar^{-1}$, as the ratio of PEG300/PC of bore liquid changed from 100/0 to 0/100 (wt%/wt%). It can mainly be attributed to the increase pore size and surface porosity of the membrane inner surface. In detail, as the PEG300/PC ratio in bore liquid changed from 100/0 to 0/100 (wt%/wt%), the membrane pore size increased from 74.3 to 89 nm, and the inner surface porosity rapidly increased from 8.3 to 69.0%, which significantly reduced the water filtration resistance and increased the water flux. Finally, the membrane exhibits

a high permeability with the increased PC ratio in bore liquid.

The PS particles with standard diameters of 100 and 50 nm were used to evaluate the membrane rejection. As shown in Fig. 3-9(b), the membrane exhibited good rejection of PS particles with a standard diameter of 100 nm, with rejections higher than 90% for most samples. However, when the PS particle size was reduced to 50 nm, the rejection decreased, particularly for membranes with varying bore liquids. The rejection of PS particles corresponded to the pore size of the membrane, with larger pores resulting in lower rejection.

The effect of membrane preparation conditions such as different diluents, PK concentration and bore liquid on tensile strength, and elongation at the break of PK hollow fiber membranes were shown in Fig. 3-9(c) and 3-9(d), respectively. The tensile strength and elongation at break of the PK hollow fiber membranes were influenced by different factors. Increasing the TEG ratio in the diluent had a minor effect on mechanical strength, with slight variations in tensile strength (3.12 to 3.3 MPa) and elongation at break (121 to 135 %) at a PK concentration of 20 wt%. An increase in PK concentration from 20 to 30 wt% led to higher tensile strength (3.3 to 8.4 MPa) and a slight decrease in elongation at break slightly (125 to 110%). Changing the bore liquid composition had a significant impact on mechanical properties, with a gradual decrease in tensile strength and elongation at break when the ratio of PEG300/PC in bore liquid changed from 100/0 to pure PC 0/100 (wt%/wt%). This decrease was attributed to the formation of macrovoid structures on the inner surface.

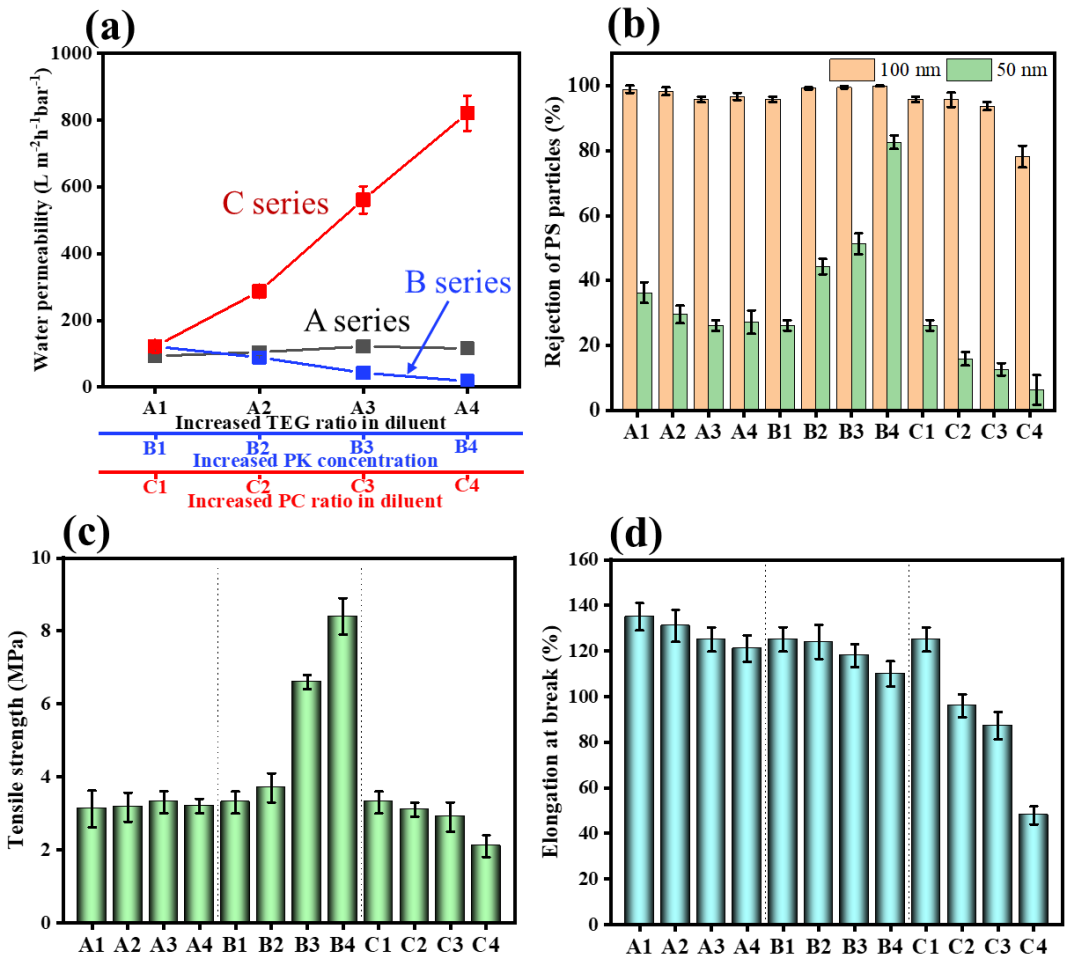


**Fig. 3-9** Filtration performance and mechanical properties of the PK membranes. (a) pure water permeability, (b) rejection of PS particles with standard diameters of 100 and 50 nm, (c) tensile strength, and (d) elongation at break.

The solvent resistance of the PK hollow fiber membrane, specifically sample C4, was evaluated by immersion in various organic solvents, including MeOH, toluene, acetone, DMF, DMSO, hexane, chloroform, IPA, and THF, for 10 days at room temperature. Fig. 3-10 (a) and (b) show the water permeability and mechanical properties of the membranes before and after immersing into different organic solvents. After immersion in the different organic solvents, there was almost no change in water permeability for sample C4. The water permeability remained in the range of 793 to 867 L $m^{-2}h^{-1}bar^{-1}$, which is quite similar to the original membrane (C4) before solvent

immersion. This indicates that the PK hollow fiber membrane maintained its water permeability even after exposure to various solvents. The mechanical properties of the membrane also showed negligible changes after immersion in the organic solvents. Both tensile strength and elongation at break remained stable, indicating that the membrane retained its mechanical integrity and strength.

These results suggest that the PK hollow fiber membrane, prepared using the TIPS method, exhibited excellent resistance to a variety of organic solvents. This resistance can be attributed to the presence of ketone functionality and the high crystallinity with dense packing of PK molecular chains, which result from the strong intramolecular and intermolecular interactions formed by the ketone groups on the PK molecular structure.

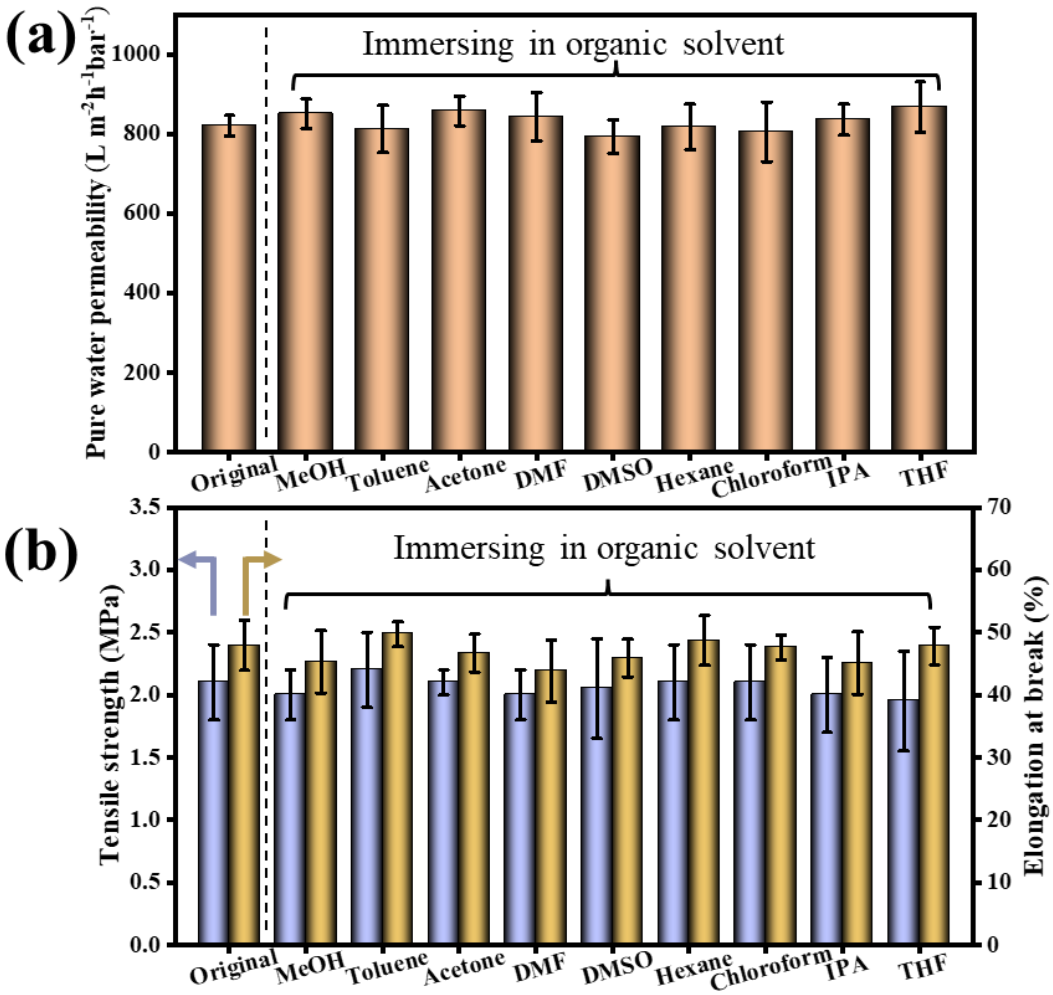

**Fig. 3-10** Performance of PK membrane (C4) including original membrane and the membrane immersing in organic solvents for 10 days at room temperature. (a) water permeability, and (b) tensile strength and elongation at break. The organic solvents are MeOH, toluene, acetone, DMF, DMSO, hexane, chloroform, IPA, and THF, respectively.

### *3.4 Conclusions*

This study focused on the preparation of PK hollow fiber membranes using the TIPS method with a low-toxic PEG300/TEG diluent system, based on the traditional spinneret, as shown in Fig. S3-2. Several key findings and conclusions can be drawn from this research. The addition of TEG to the dope solution significantly lowered the spinning temperature of PK/diluents from 245°C to 200°C. This temperature reduction helped prevent PK decomposition during the spinning process, resulting in smoother and more uniform membrane structures. The L-L phase separation led to the formation of interconnected membranes with minimal changes in performance. This interconnected structure was characterized by the presence of cellular and network-like structures, contributing to the properties of the membrane.

The effects of PK concentration and bore liquid composition on the phase diagram, membrane structure, and performance have also been extensively investigated. Increasing the PK concentration in the dope solution led to denser outer surfaces and reduced mean pore sizes. This resulted in decreased pure water permeability but increased tensile strength. Varying the composition of the bore liquid, specifically the addition of PC, had a notable effect on the inner surface structure. This addition resulted in increased surface porosity and significantly improved pure water permeability. The prepared PK hollow fiber membrane demonstrated excellent stability when immersed in various organic solvents, including MeOH, toluene, acetone, DMF, DMSO, hexane, chloroform, IPA, and THF. This resistance is attributed to the ketone functionality and high crystallinity of PK.

Overall, this work provides valuable insights into the preparation and properties of PK hollow fiber membranes, offering a promising approach for applications where solvent resistance, water permeability, and mechanical strength are essential.

***References***

[1] J.F. Kim, J.H. Kim, Y.M. Lee, E. Drioli, Thermally induced phase separation and electrospinning methods for emerging membrane applications: A review, AIChE J., 62 (2016) 461-490.

[2] Z. Cui, W. Li, H. Zeng, X. Tang, J. Zhang, S. Qin, N. Han, J. Li, Fabricating PVDF hollow fiber microfiltration membrane with a tenon-connection structure via the thermally induced phase separation process to enhance strength and permeability, Eur. Polym. J., 111 (2019) 49-62.

[3] M. Liu, S. Liu, Z. Xu, Y. Wei, H. Yang, Formation of microporous polymeric membranes via thermally induced phase separation: A review, Front Chem Sci Eng, 10 (2016) 57-75.

[4] Y. Tang, Y. Lin, W. Ma, X. Wang, A review on microporous polyvinylidene fluoride membranes fabricated via thermally induced phase separation for MF/UF application, J. Membr. Sci., 639 (2021) 119759.

[5] K. Guan, L. Zhang, S. Wang, R. Takagi, H. Matsuyama, Controlling the formation of porous polyketone membranes via a cross-linkable alginate additive for oil-in-water emulsion separations, J. Membr. Sci., 611 (2020) 118362.

[6] A.A. Alwattari, D.R. Lloyd, Microporous membrane formation via thermally induced phase separation. VI. Effect of diluent morphology and relative crystallization kinetics on polypropylene membrane structure, J. Membr. Sci., 64 (1991) 55-68.

[7] S.S. Kim, D.R. Lloyd, Microporous membrane formation via thermally induced phase separation. III. Effect of thermodynamic interactions on the structure of isotactic polypropylene membranes, J. Membr. Sci., 64 (1991) 13-29.

[8] D.R. Lloyd, Microporous membrane formation via thermally induced phase

separation. I. solid-liquid phase separation, J. Membr. Sci., 52 (1990) 239-261.

[9] D.R. Lloyd, S.S. Kim, K.E. Kinzer, Microporous membrane formation via thermally induced phase separation. II. Liquid-liquid phase separation, J. Membr. Sci., 64 (1991) 1-11.

[10] P. Zhang, C. Fang, S. Rajabzadeh, W. Liu, Y. Jia, Q. Shen, L. Zhang, S. Wang, N. Kato, H. Matsuyama, Effect of polymer molecular weight on structure and performance of PVDF hollow fiber membranes prepared via TIPS process with co-extrusion of solvent using triple orifice spinneret, J. Membr. Sci., 620 (2021) 118854.

[11] G. Ji, L. Zhu, B. Zhu, C. Zhang, Y. Xu, Structure formation and characterization of PVDF hollow fiber membrane prepared via TIPS with diluent mixture, J. Membr. Sci., 319 (2008) 264-270.

[12] M. Gu, J. Zhang, X. Wang, H. Tao, L. Ge, Formation of poly(vinylidene fluoride) (PVDF) membranes via thermally induced phase separation, Desalination, 192 (2006) 160-167.

[13] P. Zhang, S. Rajabzadeh, Q. Song, R.R. Gonzales, Y. Jia, S. Xiang, Z. Li, H. Matsuyama, Development of loose nanofiltration PVDF hollow fiber membrane for dye/salt separation, Desalination, 549 (2023) 116315.

[14] W. Yave, R. Quijada, D. Serafini, D. Lloyd, Effect of the polypropylene type on polymer–diluent phase diagrams and membrane structure in membranes formed via the TIPS process Part II. Syndiotactic and isotactic polypropylenes produced using metallocene catalysts, J. Membr. Sci., 263 (2005) 154-159.

[15] W. Yave, R. Quijada, M. Ulbricht, R. Benavente, Syndiotactic polypropylene as potential material for the preparation of porous membranes via thermally induced phase separation (TIPS) process, Polymer, 46 (2005) 11582-11590.

[16] Y.J. Wang, Z.P. Zhao, Z.Y. Xi, S.Y. Yan, Microporous polypropylene membrane prepared via TIPS using environment-friendly binary diluents and its VMD performance, J. Membr. Sci., 548 (2018) 332-344.

[17] Y.R. Qiu, H. Matsuyama, G.Y. Gao, Y.W. Ou, C. Miao, Effects of diluent molecular

weight on the performance of hydrophilic poly(vinyl butyral)/Pluronic F127 blend hollow fiber membrane via thermally induced phase separation, J. Membr. Sci., 338 (2009) 128-134.

[18] S. Jeon, H. Karkhanechi, L. Fang, L. Cheng, T. Ono, R. Nakamura, H. Matsuyama, Novel preparation and fundamental characterization of polyamide 6 self-supporting hollow fiber membranes via thermally induced phase separation (TIPS), J. Membr. Sci., 546 (2018) 1-14.

[19] N. Kato, R.R. Gonzales, A. Nishitani, Y. Negi, T. Ono, H. Matsuyama, Single-step preparation of nanocomposite polyamide 6 hollow fiber membrane with integrally skinned asymmetric structure for organic solvent nanofiltration, Colloids Surf. A Physicochem. Eng. Asp., 620 (2021) 126538.

[20] K. Umakoshi, R.R. Gonzales, N. Kato, P. Zhang, T. Ono, H. Matsuyama, Effect of polymer-solvent compatibility on polyamide hollow fiber membranes prepared via thermally induced phase separation, Colloids Surf. A Physicochem. Eng. Asp., 642 (2022) 128704.

[21] M.A. Kivi, H. Alinia, Y. Jafarzadeh, R. Yegani, High-density polyethylene membranes embedded with carboxylated and polyethylene glycol-grafted nanodiamond to be used in membrane bioreactors, J. Appl. Polym. Sci., 136 (2019) 47914.

[22] Y. Jafarzadeh, R. Yegani, S.B. Tantekin-Ersolmaz, Effect of $TiO_2$ nanoparticles on structure and properties of high density polyethylene membranes prepared by thermally induced phase separation method, Polym. Adv. Technol., 26 (2015) 392-398.

[23] Y. Jafarzadeh, R. Yegani, M. Sedaghat, Preparation, characterization and fouling analysis of ZnO/polyethylene hybrid membranes for collagen separation, Chem. Eng. Res. Des., 94 (2015) 417-427.

[24] Mengxian Shang, Hideto Matsuyama, Masaaki Teramoto, Junpei Okuno, Douglas R. Lloyd, N. Kubota, Effect of diluent on poly(ethylene-co-vinyl alcohol) hollow-fiber membrane formation via thermally induced phase separation, J. Appl. Polym. Sci., 95

(2005) 219-225.

[25] M. Shang, H. Matsuyama, M. Teramoto, D.R. Lloyd, N. Kubota, Preparation and membrane performance of poly(ethylene-co-vinyl alcohol) hollow fiber membrane via thermally induced phase separation, Polymer, 44 (2003) 7441-7447.

[26] J. Pan, W. Ma, L. Huang, R. Li, Q. Huang, C. Xiao, Z. Jiang, Fabrication and characterization of ECTFE hollow fiber membranes via low-temperature thermally induced phase separation (L-TIPS), J. Membr. Sci., 634 (2021) 119429.

[27] G.C. You, L. An, F.L. Xian, Y.X. Su, S.J. Cong, Factors controlling surface morphology of porous polystyrene membranes prepared by thermally induced phase separation, Polym. Int., 49 (2000) 323-328.

[28] H.Q. Liang, H.N. Li, H.H. Yu, Y.T. Zhou, Z.K. Xu, Polysulfone membranes via thermally induced phase separation, Chin. J. Chem. Eng., 35 (2017) 846-856.

[29] H. Matsuyama, T. Maki, M. Teramoto, K. Kobayashi, Effect of PVP additive on porous polysulfone membrane formation by immersion precipitation method, Sep Sci Technol, 38 (2003) 3449-3458.

[30] T. Fan, Z. Li, B. Cheng, J. Li, Preparation, characterization of PPS micro-porous membranes and their excellent performance in vacuum membrane distillation, J. Membr. Sci., 556 (2018) 107-117.

[31] Hideto Matsuyama, Yusuke Takida, Taisuke Maki, M. Teramoto, Preparation of porous membrane by combined use of thermally induced phase separation and immersion precipitation, Polymer, 43 (2002) 5243-5248.

[32] L. Cheng, A.R. Shaikh, L.F. Fang, S. Jeon, C.J. Liu, L. Zhang, H.C. Wu, D.M. Wang, H. Matsuyama, Fouling-resistant and self-cleaning aliphatic polyketone membrane for sustainable oil-water emulsion separation, ACS Appl. Mater. Interfaces, 10 (2018) 44880-44889.

[33] L. Zhang, Y. Lin, L. Cheng, Z. Yang, H. Matsuyama, A comprehensively fouling- and solvent-resistant aliphatic polyketone membrane for high-flux filtration of difficult oil-in-water micro- and nanoemulsions, J. Membr. Sci., 582 (2019) 48-58.

[34] Y. Jia, K. Guan, L. Zhang, Y. Lin, Q. Shen, P. Zhang, H. Matsuyama, Enabling polyketone membrane with underwater superoleophobicity via a hydrogel-based modification for high-efficiency oil-in-water emulsion separation, J. Membr. Sci., 618 (2021) 118705.

[35] L. Zhang, Y. Lin, S. Wang, L. Cheng, H. Matsuyama, Engineering of ultrafine polydopamine nanoparticles in-situ assembling on polyketone substrate for highly-efficient oil-water emulsions separation, J. Membr. Sci., 613 (2020) 118501.

[36] S. Xiang, P. Zhang, S. Rajabzadeh, R.R. Gonzales, Z. Li, Y. Shi, S. Zhou, M. Hu, K. Guan, H. Matsuyama, Development of porous polyketone membrane via liquid–liquid thermally induced phase separation, J. Membr. Sci., 677 (2023) 121639.

[37] Z. Cui, Y. Cheng, K. Xu, J. Yue, Y. Zhou, X. Li, Q. Wang, S.P. Sun, Y. Wang, X. Wang, Z. Wang, Wide liquid-liquid phase separation region enhancing tensile strength of poly(vinylidene fluoride) membranes via TIPS method with a new diluent, Polymer, 141 (2018) 46-53.

[38] N.T. Hassankiadeh, Z. Cui, J.H. Kim, D.W. Shin, S.Y. Lee, A. Sanguineti, V. Arcella, Y.M. Lee, E. Drioli, Microporous poly(vinylidene fluoride) hollow fiber membranes fabricated with PolarClean as water-soluble green diluent and additives, J. Membr. Sci., 479 (2015) 204-212.

[39] Z. Cui, N.T. Hassankiadeh, S.Y. Lee, J.M. Lee, K.T. Woo, A. Sanguineti, V. Arcella, Y.M. Lee, E. Drioli, Poly(vinylidene fluoride) membrane preparation with an environmental diluent via thermally induced phase separation, J. Membr. Sci., 444 (2013) 223-236.

[40] G.L. Ji, C.H. Du, B.K. Zhu, Y.Y. Xu, Preparation of porous PVDF membrane via thermally induced phase separation with diluent mixture of DBP and DEHP, J. Appl. Polym. Sci., 105 (2007) 1496-1502.

[41] S. Rajabzadeh, C. Liang, Y. Ohmukai, T. Maruyama, H. Matsuyama, Effect of additives on the morphology and properties of poly(vinylidene fluoride) blend hollow fiber membrane prepared by the thermally induced phase separation method, J. Membr.

Sci., 423-424 (2012) 189-194.

[42] O. Ohsawa, K. Lee, B. Kim, S. Lee, I. Kim, Preparation and characterization of polyketone (PK) fibrous membrane via electrospinning, Polymer, 51 (2010) 2007-2012.

[43] S. De Vito, F. Ciardelli, E. Benedetti, E. Bramanti, Thermal phase transitions of carbon monoxide-ethylene alternating copolymer: an FT/IR study, Polym. Adv. Technol., 8 (1997) 53-62.

[44] C. Li, J. Zhang, J. Han, B. Yao, A numerical solution to the effects of surface roughness on water-coal contact angle, Sci Rep, 11 (2021) 459.

***Supporting information***

The solubility parameters of mixed diluents were calculated by Eqs. (S3-1)- (S3-3) [1].

$$\delta_{dM}=\varphi_1\delta_{d1}+\varphi_2\delta_{d2} \quad \text{(S3-1)}$$

$$\delta_{pM}=\varphi_1\delta_{p1}+\varphi_2\delta_{p2} \quad \text{(S3-2)}$$

$$\delta_{hM}=\varphi_1\delta_{h1}+\varphi_2\delta_{h2} \quad \text{(S3-3)}$$

where M, 1 and 2, represent the mixed diluent system, diluent 1 and diluent 2, respectively. $\varphi_1$ and $\varphi_2$ are the volume fraction of diluent 1 and diluent 2, respectively. $\delta_d$, $\delta_p$ and $\delta_h$ represent dispersion force, polar and hydrogen bond, respectively.

The *R*a value of two compositions was obtained by Eq. (S3-4) [1].

$$Ra=(4(\delta_{d1}-\delta_{d2})^2+\left(\delta_{p1}-\delta_{p2}\right)^2+(\delta_{h1}-\delta_{h2})^2)^{0.5} \quad \text{(S3-4)}$$

where 1 and 2, represent the composition 1 and composition 2, respectively. $\delta_d$, $\delta_p$ and $\delta_h$ represent dispersion force, polar and hydrogen bond, respectively.

The Gibbs free energy of mixing ($\Delta G^E$) value of PK and various solvents by the following Eq. (S3-5) [2].

$$\Delta G^E=(\delta_{d1}-\delta_{d2})^2+(\delta_{p1}-\delta_{p2})^2+(\delta_{h1}-\delta_{h2})^2 \quad \text{(S3-5)}$$

where $\delta_d$, $\delta_p$, and $\delta_h$ represent the dispersion, polar, and hydrogen bonding, respectively; while 1 and 2 respectively denote PK and solvents.

**Table S3-1** spinning conditions of hollow fiber membrane.

| Preparation conditions | Parameters |
|---|---|
| Air gap (cm) | 1 |
| Extrusion rate of polymer solution (m/s) | 0.9 |
| Extrusion pressure of polymer solution (MPa) | 0.1 |
| Bore liquid flow rate (m/s) | 0.16 |
| Bore liquid temperature (°C) | Room temperature |
| Quenching bath | PC/water (20/80 wt%/wt%) |
| Quenching bath temperature (°C) | Room temperature |
| Take-up speed (m/s) | 0.31 |

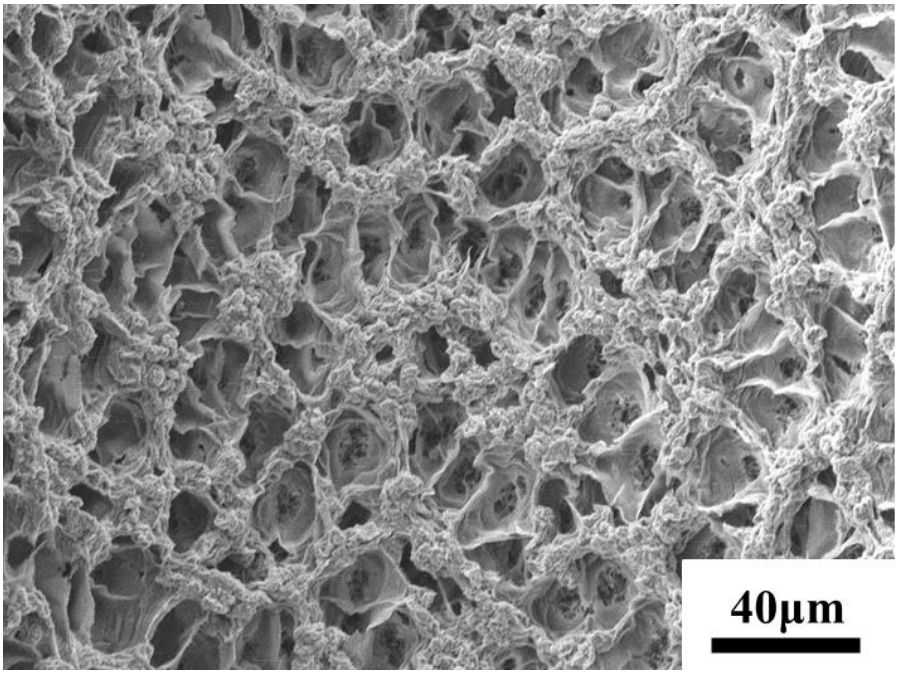


**Fig. S3-1** The inner surface morphology of PK hollow fiber membrane (sample C4) with low magnification. Pure PC was used as bore liquid, and the ratio of PK/PEG300/TEG (dope solution) was fixed at 20/40/40 (wt%/wt%/wt%).

**Table S3-2** Surface porosity of PK hollow fiber membrane (part C).

| Membrane | Bore liquid | Inner surface porosity (%) |
|---|---|---|
| C1 | PEG300/PC (100/0 wt%/wt%) | 8.3 |
| C2 | PEG300/PC (70/30 wt%/wt%) | 30.7 |
| C3 | PEG300/PC (40/60 wt%/wt%) | 56.2 |
| C4 | PEG300/PC (0/100 wt%/wt%) | 69.0 |

Noted: The surface porosity was measured by ImageJ.

**Table S3-3** The *R*a value between PK and bore liquid.

| | | $\delta_d$ $(MPa)^{0.5}$ | $\delta_p$ $(MPa)^{0.5}$ | $\delta_h$ $(MPa)^{0.5}$ | *R*a $(MPa)^{0.5}$ |
|---|---|---|---|---|---|
| PK | | 19.9 | 17.9 | 6.8 | |
| The ratio of | 100/0 (C1) | 16.6 | 4.4 | 14.5 | 16.9 |
| PEG300 and | 70/30 (C2) | 17.6 | 8.5 | 11.4 | 11.4 |
| PC | 40/60 (C3) | 18.6 | 12.6 | 8.3 | 6.1 |
| (wt%/wt%) (bore liquid) | 0/100 (C4) | 20 | 18 | 4.1 | 2.7 |

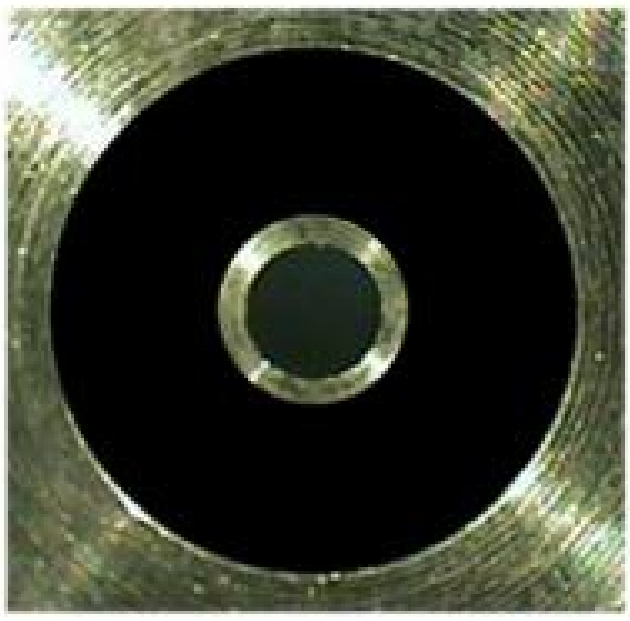

**Fig. S3-2** Diagram of a traditional spinneret with double orifice.

**Reference**

[1] C.M. Hansen, Hansen solubility parameters: a User's handbook, CRC Press, (2007).

[2] H. Zhang, X. Lu, Z. Liu, Z. Ma, S. Wu, Z. Li, X. Kong, C. Wu, Study of the dual role mechanism of water-soluble additive in low temperature thermally-induced phase separation, J. Membr. Sci., 543 (2017) 1-9.

# Chapter 4

## Fabrication of high-permeance polyketone (PK) hollow fiber membrane using the triple-orifice spinneret via the thermally induced phase separation

### *4.1 Introduction*

Polymeric porous membranes play a crucial role in diverse industrial and scientific applications, from conventional water and wastewater treatment to emerging technologies such as membrane contactor processes [1-3], membrane-based power generation [4, 5], and gas separation [6-8]. Their popularity stems from the simple fabrication process, low cost, and excellent performance [9, 10]. Commonly used polymer materials for membrane preparation include regenerated cellulose, cellulose acetate, polyamide, polysulfone, polycarbonate, poly(ether imide), polyimide, polytetrafluoroethylene, polypropylene, and poly(vinylidene fluoride) (PVDF) [11]. Among the available polymeric membrane materials, PVDF is widely used to manufacture polymer porous membranes with wide applications, especially in wastewater treatment, where PVDF membranes account for over 60% of the usage, due to its excellent inherent properties such as good processability, high thermal stability, and great chemical resistance [10, 12, 13]. While PVDF is a popular choice for membrane material, environmental concerns due to its fluorinated nature [14] have led to increased interest in alternatives.

Polyketone (PK), a semi-crystalline polymer, presents itself as a promising candidate due to its good mechanical properties and chemical resistance [15, 16]. Compared with

PVDF, the low-cost feedstock of synthetic polyketone, including ethylene, carbon monoxide, and about 6 mol% of propylene, as shown in Fig. 4-1. makes it highly competitive [17]. In addition, its hydrophilicity and excellent solvent resistance [18] make it suitable for filtration process with low fouling tendency [19, 20]. Despite the advantages of PK, there are challenges in PK membrane preparation, particularly with methods like non-solvent induced phase separation (NIPS), which involves toxic solvents and complex procedures [21, 22]. The thermally induced phase separation (TIPS) method, utilizing low-toxicity solvents, including polyethylene glycol 300 (PEG300), triethylene glycol (TEG), and PC, offers a simpler and more controllable membrane fabrication process [23, 24]. However, it often results in a dense outer surface, impacting filtration resistance and water permeability [24]. Since high permeability is an important membrane performance parameter, it is necessary to find a simple and controllable method to reduce the thickness of the outer surface layer and increase the surface porosity.

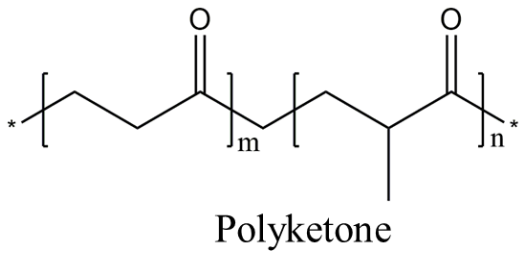


Polyketone

**Fig. 4-1** PK molecular structure including 6 mol % of propylene.

To enhance the porosity of the outer surface of hollow fiber membranes, plenty of studies have been reported. For example, Cha et al [25] prepared a PVDF hollow fiber membrane that possessed a porous outer surface or skinless porous surface structure by adding a solvent (dimethyl acetamide) in the water quenching bath, resulting in the change of crystalline structure of the polymer. Hassankiadeh et al [26] developed microporous PVDF hollow fiber membranes by using water-soluble diluent PolarClean

and additive polyvinyl pyrrolidone (PVP). They found that increasing the quenching bath temperature could induce mass transfer and result in the formation of finger-like structures with very thin skin layers at the outer surface of the hollow fibers. In addition, adding PVP in PVDF solution resulted in the enrichment of PVP at the outer layer of the nascent fiber and increased the surface porosity after PVP was extracted. Recently, Chen et al [27] prepared PVDF hollow fiber membranes via the TIPS method by adding amphiphilic and hydrophilic water-soluble non-solvent, TEG, and PEG400 in PVDF solution. When the PVDF solution was immersed in a water quenching bath, the water-soluble non-diluents diffused or migrated to the outer surface, leading to a reduction in polymer concentration on the outer surface. This resulted in the formation of a membrane with a porous outer surface. While the aforementioned methods could effectively increase surface porosity based on different mechanisms, there were still shortcomings, such as the extensive use of organic solvents and weakened mechanical properties.

Co-extrusion of solvents, particularly with a triple-orifice spinneret, has gained prominence for its potential to control outer surface structure and hollow fiber membrane properties [28-30]. In comparison with the traditional spinneret consisting of two channels, the triple-orifice spinneret features a third channel that allows the extrusion of solvent on the outside of the PK solution. This method, avoiding the evaporation of diluent, can produce porous outer surfaces. The interaction between the extruded solvent and polymer or diluent plays a crucial role in determining the outer surface structure. Fang et al [31, 32] found that if the extruded solvent exhibits a better interaction with polymer (PVDF) than the diluent, the PVDF molecular chains would aggregate near the outside of the PVDF solution to induce a dense outer surface as the solvent was extruded on the outside of the PVDF solution. On the contrary, when the extruded solvent has a good interaction with the diluent, rather than PVDF, the diluent aggregates on the interface between the PK solution and extruded solvent to induce a porous outer surface. Finally, the pore size of the membrane could effectively be

regulated by simply changing the type of solvent extruded [32].

In this research, co-extrusion technology with a triple-orifice spinneret was applied to enhance the permeance of the PK hollow fiber membranes. Different solvents, selected based on their interactions with PK and diluent, were extruded to investigate their impact on membrane structure and performance. The study delves into the mechanism behind the formation of the outer surface structure. Additionally, the research explores the influence of the air gap distance on the structure and properties of the PK membrane, revealing the combined effects of the solubility parameters and viscosity of the extrusion solvent on PK membranes.

## *4.2 Experimental*

### *4.2.1 Materials*

Polyketone (PK, grade M630A) was purchased from Hyosung Corporation Co., Ltd, South Korea. Polyethylene glycol (PEG300, and PEG600), sulfolane (SFL), propylene carbonate (PC), dimethyl phthalate (DMP), diethyl phthalate (DEP), triethylene glycol (TEG), and ethanol were purchased from Tokyo Chemical Industry Co., Ltd. (Japan). Pure water uses throughout the experiment was prepared in our lab using the Millipore MilliQ unit. In this work, all the chemicals without further treatment prior to use.

### *4.2.2 Preparation of PK hollow fiber membranes*

The PK hollow fiber membranes were prepared by a spinning apparatus consisting of a triple-orifice spinneret reported in our previous study [27]. In this study, the PK solution consists of PK/PEG300/TEG with a fixed ratio of 20/40/40 wt%/wt%wt%, and pure PC was used as the bore liquid. In detail, under the protection of nitrogen atmosphere, PK resins were dissolved into mixed diluent (PEG300/TEG) at 200℃ for 2 h to get a homogeneous solution. Subsequently, PK solution and bore liquid were extruded into the middle and inner channels of the triple-orifice spinneret by the metering pump. Meanwhile, the different types of solvents, including PC, SFL, DMP,

DEP, TEG, PEG300, and PEG600, were extruded into the outermost channel of the spinneret to control outer surface structure of PK hollow fiber membranes, respectively. After passing through the air gap, the primary PK membrane entered the water quenching bath and was collected by the take-up winder. The prepared membrane was moved into an ethanol bath to extract the diluent, then dried and stored the PK hollow fiber membrane in the air environment. The detailed preparation conditions are shown in Table 4-1. In addition, the interaction parameters of PK, diluent, and extruded solvent and the viscosity of extruded solvent are shown in Table 4-2. The viscosity of extruded solvents was tested by the EMS Viscomter (EMS-1000S, Kyoto Electronics Manufacturing Co., Ltd).

**Table 4-1** The spinning conditions for PK hollow fiber membranes

| Preparations conditions | Parameters |
|---|---|
| PK concentration (wt%) | 20 |
| Diluent composition (PEG300/TEG wt%/wt%) | 40/40 |
| Spinning temperature (℃) | 200 |
| Air gap (cm) | 1, 5 and 10 |
| Bore liquid | PC |
| Bore liquid temperature (℃) | 23 |
| Extruded solvent | Listed in Table 4-2 |
| Extruded solvent temperature (℃) | 23 |
| Quenching bath | water |
| Quenching bath temperature (℃) | 23 |

**Table 4-2** Interaction parameters of PK, diluent, and extruded solvent, and the viscosity of extruded solvent at 25 °C.

| | | $\delta_d$ $(MPa)^{0.5}$ | $\delta_p$ $(MPa)^{0.5}$ | $\delta_h$ $(MPa)^{0.5}$ | $Ra_{(solvent\text{-}PK)}$ $(MPa)^{0.5}$ | $Ra_{(solvent\text{-}diluent)}$ $(MPa)^{0.5}$ | $Ra_{(solvent\text{-}diluent)}$ $/Ra_{(solvent\text{-}PK)}$ | Viscosity (η) mPa.s |
|---|---|---|---|---|---|---|---|---|
| Polyketone | PK | 19.9 | 17.9 | 6.8 | | | | |
| Diluent | Diluent | 16.3 | 8.5 | 16.6 | | | | |
| Polyethylene glycol 300 | PEG300 | 16.6 | 4.4 | 14.5 | 16.9 | 4.6 | 0.27 | 80.3 |
| Triethylene glycol | TEG | 16 | 12.5 | 18.6 | 15.1 | 4.6 | 0.3 | 35.2 |
| Polyethylene glycol 600 | PEG600 | 16.6 | 3.2 | 12.1 | 17 | 6.9 | 0.41 | 146 |
| Diethyl phthalate | DEP | 17.6 | 9.6 | 4.5 | 9.8 | 12.4 | 1.3 | 11.8 |
| Dimethyl phthalate | DMP | 18.6 | 10.8 | 4.9 | 7.8 | 12.7 | 1.6 | 13.6 |
| Sulfolane | SFL | 17.8 | 17.4 | 8.7 | 4.6 | 12.3 | 2.7 | 11.2 |
| Propylene carbonate | PC | 20 | 18 | 4.1 | 2.7 | 17.3 | 6.4 | 2.8 |

Note: Diluent consists of PEG300 and TEG (1/1 wt%/wt%).

### *4.2.3 Membrane morphology*

The morphology of the PK hollow fiber membranes was observed by a field-emission scanning electron microscope (FE-SEM) (JSF-7500F, JEOL Co., Japan). To be specific, liquid nitrogen drying conditions were employed to obtain clear and smooth cross-section part samples of the membrane. Before observation, all samples were dried in a vacuum at 60℃ and coated with osmium tetroxide. Image J was used to measure the surface porosity of the PK hollow fiber membrane.

The contact angle goniometer (Drop Master, Kyowa Interface Science Co., Japan) was used to measure the dynamic water contact angle (DWAC) of the PK hollow fiber membrane. The overall porosity of the membrane was measured based on the gravimetric method [30]. The density of PK was 1.24 g $cm^{-1}$ [31]. The liquid-liquid porometer (LLP-1100A, PIM, USA) was used to determine the mean pore size of the PK membrane. Fourier transform infrared spectroscopy spectrometer (FTIR-ATR, Alpha Bruker, USA) was employed to test the membrane crystalline phase.

The precision strength tester (AGS-J, Shimadzu Co., Japan) was employed to determine the mechanical strength of the PK membrane. PK hollow fiber membranes with a length of approximately 20 mm are tested using a fixed extension rate (10 mm $min^{-1}$). Three samples for each membrane were chosen and tested. The tensile strength $B$ (MPa) and elongation at break $E$ (%) of the PK membrane were calculated by Eqs. (4-1) and (4-2):

$$B=\frac{F}{S} \tag{4-1}$$

$$E=\frac{L_1-L_0}{L_0}\times 100 \tag{4-2}$$

where $F$ and $S$ represent the breaking force (N), and the cross-sectional area of the membrane ($mm^2$), respectively. $L_1$ and $L_0$ represent the length at break and initial (mm), respectively.

### *4.2.4 Membrane performance*

Pure water permeance (PWP) of the PK hollow fiber membranes was determined using laboratory-scale measurement equipment [27]. After pre-wetting in ethanol for about 10 mins, the PK membrane with a length of 10 cm was measured under 0.5 bar filtration pressure under the outside-to-inside filtration model. Three samples were tested for each specimen to get the average value. The PWP (L $m^{-2}h^{-1}bar^{-1}$) of the PK hollow fiber membranes were calculated by Eq. (4-3):

$$PWP = \frac{V}{A \times \Delta t \times P} \tag{4-3}$$

where $V$ and $A$ are the volume of permeate solution (L) and filtration area ($m^2$), respectively. $\Delta t$ and $P$ represent the filtration time (h), and filtration pressure (bar), respectively.

## *4.3 Results and discussion*

### *4.3.1 Effect of the kinds of extruded solvent on membrane morphology*

Building on our prior investigation of the PK/PEG300/TEG trinary system, where the addition of TEG effectively reduces the spinning temperature, resulting in liquid-liquid phase separation during cooling, a PK/PEG300/TEG mixture (20/40/40 wt%/wt%/wt%) was chosen for PK hollow fiber membrane preparation [24]. Despite achieving well-connected bulk and a highly porous inner surface using PC as the bore liquid, attempts to enhance outer surface porosity by adding 20 wt% PC to the water quenching bath yielded limited success, constraining the high permeance of the membrane [24]. Consequently, a co-extrusion technique was employed to optimize the outer surface structure for high-permeance PK membrane fabrication, involving the extrusion of another solvent at the outermost layer of the triple-orifice spinneret.

Initially, various solvents, including PC, SFL, DMP, DEP, TEG, PEG300, and PEG600, were individually extruded at the outermost layer of a triple-orifice spinneret to prepare the PK hollow fiber membranes. For comparison, a membrane named “Normal” was prepared without extruding any solvent, maintaining an air gap distance

of 5 cm. The whole cross-section structure, outer surface, and inner surface of the membranes are summarized in Fig. 4-2 and Fig. S4-2 – S4-5.

The Normal sample, without any extruded solvent, displayed a dense skin layer at the outer surface without pores. In contrast, all membranes prepared using co-extrusion technology exhibited a porous outer surface without a distinguishable skin layer near the outer surface of the cross-section, with surface porosity ranging from 7.6 to 31.8%. However, the outer surface morphology varied significantly depending on the extruded solvent. Circular pore structures were uniformly distributed on the membrane surface when solvents PC and SFL were extruded, with SFL-extruded membrane showing smaller surface pore size. Membranes prepared with DMP and DEP displayed irregular and heterogeneous porous structures. TEG-extruded membranes presented relatively small pore structures visible only under high magnification (Fig. S4-6). For PEG300 and PEG600, the membranes exhibited fibrous-like structures parallel to the spinning direction, with pores between the fibers. Notably, the PEG300-formed membrane had more pores between the fiber structures compared to those formed by PEG600 extrusion.

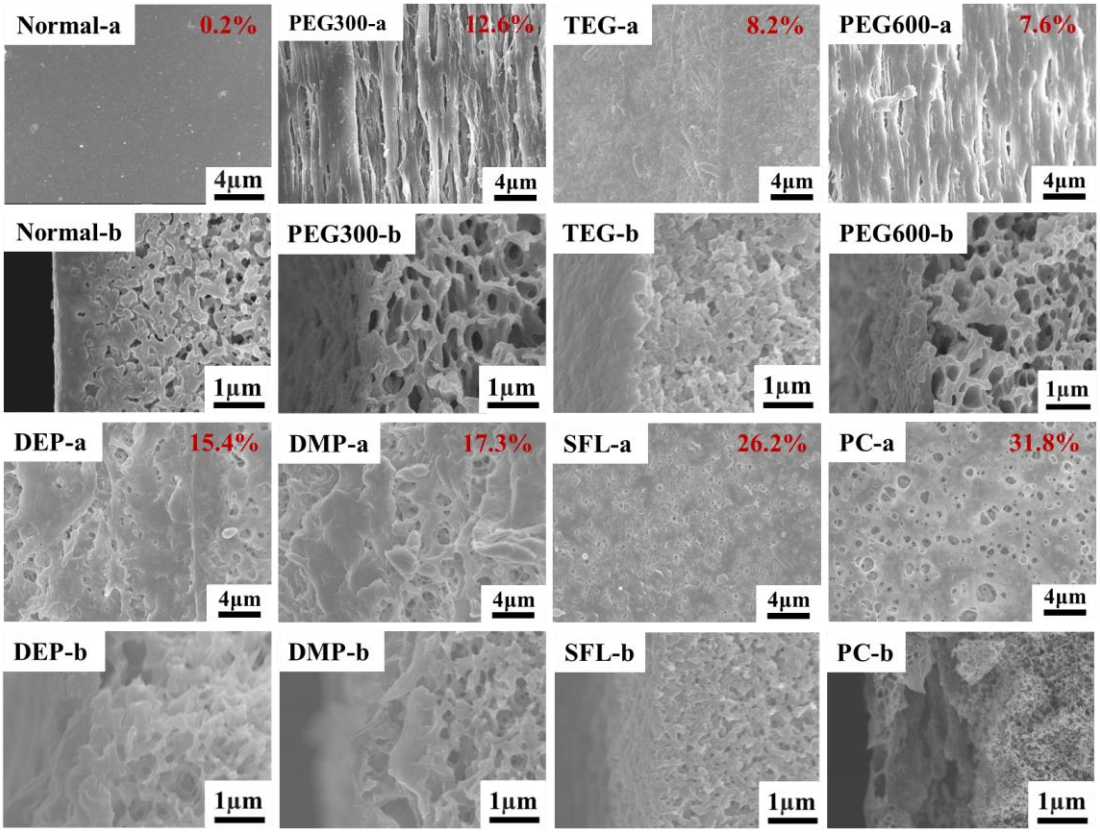


**Fig. 4-2** (a) Outer surface morphology and (b) cross-section part near the outer surface of PK membrane fabricated using different kinds of extrusion solvent, including PC, SFL, DMP, DEP, TEG, PEG300, and PEG600, respectively. The value of surface porosity was inserted into the SEM images. The air gap distance was fixed at 5 cm.

To elucidate the mechanisms behind the outer surface structure obtained through co-extrusion technology, the solubility parameter distances (*R*a values) between the extruded solvent and polymer PK ($Ra_{(Solvent\text{-}PK)}$) and between the extruded solvent and PEG300/TEG mixed diluent ($Ra_{(Solvent\text{-}Diluent)}$), were calculated using the Skaarup equation using their respective partial solubility parameter component [37]. Fig. 4-3 illustrates the relationship between $Ra_{(Solvent\text{-}PK)}$ versus $Ra_{(Solvent\text{-}Diluent)}$ for different solvents extruded at the outermost layer of the triple-orifice spinneret. In Fig. 4-3, the diagonal line divides the plot into two regions. The upper red region indicates that solvents in this region have a stronger interaction with the diluent than with PK. Conversely, the lower blue region suggests a stronger interaction with polymer PK than

with the diluent.

For extruded solvents PEG300, TEG, and PEG600, located in the red region, their compatibility with the mixed diluent (PEG300/TEG) was higher than that with PK. Consequently, during PK membrane preparation, these solvents caused the mixed diluent to segregate toward the surface region instead of PK due to their higher compatibility. This led to a decreased PK concentration at the outer surface, resulting in a porous structure, aligning with previous studies [31, 32]. On the contrary, solvents PC, SFL, DMP, and DEP, situated in the blue region below the diagonal line, exhibited higher compatibility with PK than with the diluent. This would typically lead to the formation of a less porous or dense skin layer at the membrane's outer surface, since PK molecules are likely to migrate to the membrane surface, increasing the PK concentration at the surface region. However, in this study, all membranes formed porous structures even when the extruded solvents were in the blue region, indicating that the formation of pores is not solely dictated by the relative magnitude of interactions among the extruded solvent, diluent, and PK.

Notably, as indicated in Table 2, the viscosity values of extruded solvents PC, SFL, DMP, and DEP are much lower than those of PEG300, TEG, and PEG600. Solvents with low viscosity facilitate penetration into the membrane surface. Therefore, in this case, when the outer solvent and the PK solution are extruded simultaneously, there may be a competitive behavior between the movement of polymer molecules to the membrane surface in the air gap. The former is likely to produce a dense surface structure, while the latter tends to form a porous structure because of the surface polymer dilution effect.

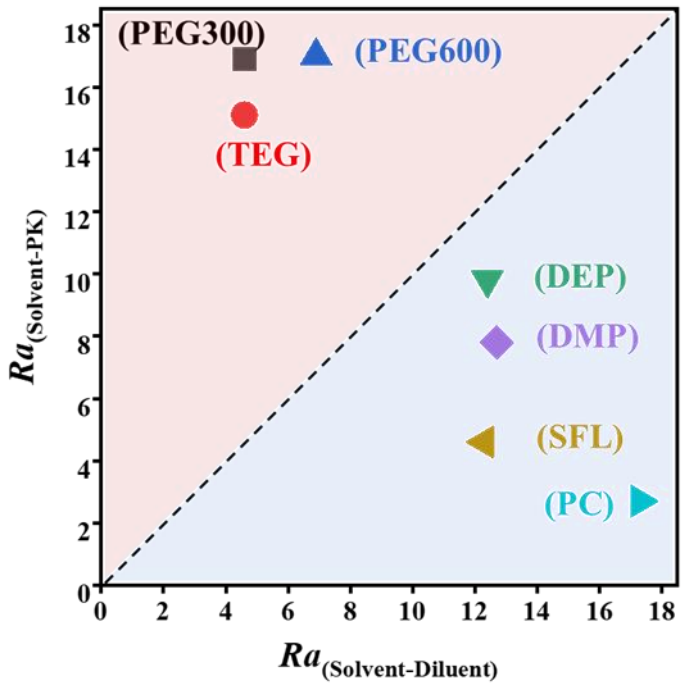


**Fig. 4-3** Interaction parameters among extruded solvents, PK, and diluent.

When PEG300, TEG, and PEG600 were extruded at the outermost layer of the triple-orifice spinneret, their higher viscosity values rendered them less prone to penetrate from the outer layer to the membrane surface region. Consequently, the diluent in the polymer solution might migrate to the surface, driven by its strong interaction with the outer solvent, thereby predominantly influencing the formation of porous structures on the membrane surface. The difficulty in penetration of these high-viscosity solvents allows the diluent to take precedence in dictating surface morphology.

On the other hand, when extruding PC, SFL, DMP, and DEP, the extremely low viscosity of these solvents hinders PK molecules from reaching the membrane surface due to their significantly higher molecular weight. In this scenario, the rapid penetration of the extruded solvent to the membrane surface replaces the polymer concentration on the surface, ultimately resulting in the creation of large and more numerous pores. Despite these solvents exhibiting better interaction with PK, their low viscosity plays a

dominant role in determining the final membrane surface morphology. Therefore, in the PK/PEG300/TEG trinary system, the penetration of the outer layer extruded solvent has a substantial impact on the membrane surface morphology due to its low viscosity, even if the solvent exhibits better interaction with PK. The proposed mechanism for the formation of the outer surface of the PK hollow fiber membrane is illustrated in Fig. 4-4.

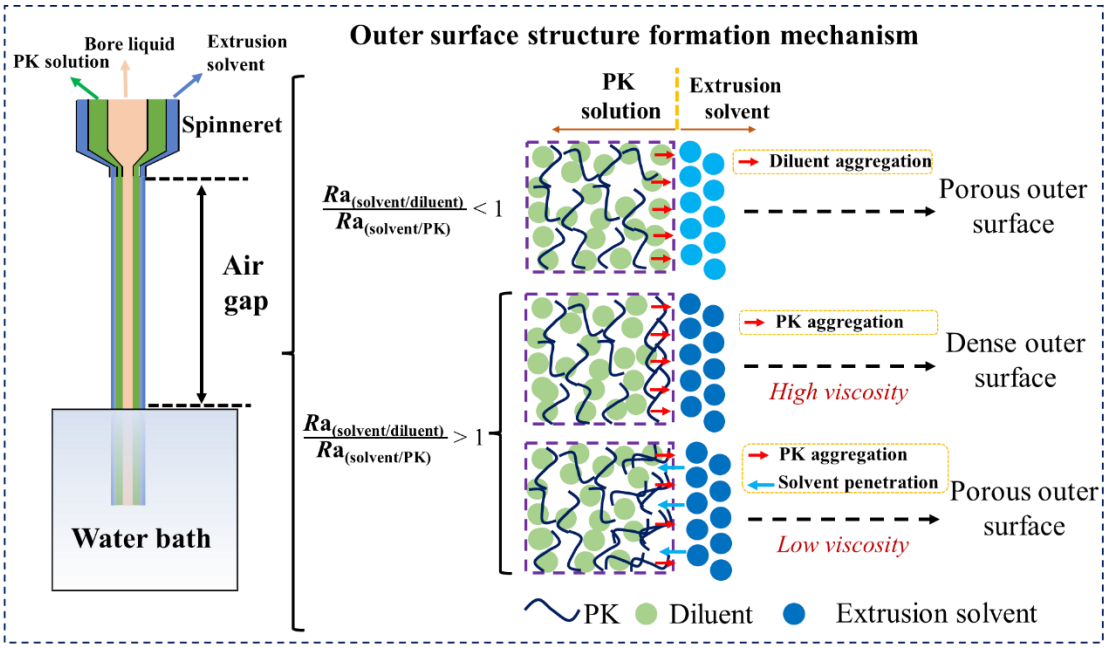


**Fig. 4-4** Formation mechanism of the outer surface of PK hollow fiber membrane using different extruded solvents.

### *4.3.2 Characterization and performances of PK membranes with different solvents*

The crystal structure is an important parameter of polymeric membranes significantly affecting its mechanical strength. FTIR analysis was employed to analyze the effect of extrusion solvent on the outer surface crystal structures of the PK hollow fiber membranes. As shown in Fig. S4-7, the FTIR spectra, including the Normal sample (no extruded solvent) and extruded solvent samples, exhibited identical absorption bands at 2911, 1692, 1408, 1334, 1056, 811, and 594 $cm^{-1}$, and the corresponding characteristic peaks are $CH_2$, C=O, $CH_2$, $CH_2$, $CH_2$-CO, C-C, and C-C [38], indicating

the $\alpha$ crystal type of PK. The extrusion solvent had a minimal impact on the crystal morphology of the outer surface, and the $\alpha$ crystal form, known for denser packing, contributed to improving the mechanical strength of hollow fiber membranes.

Dynamic water contact angle (DWCA) measurements were used to characterize the hydrophilicity of PK hollow fiber membranes. The DWCA measurements indicated the hydrophilic properties of all PK membranes, as shown in Fig. 4-5(a). The initial water contact angle was lower than 80° for Normal and extruded solvent samples, attributed to the presence of hydrophilic carbonyl groups on PK molecular chains. The water contact angle rapidly decreased to 0° after droplet contact with PK membranes, with PC extrusion achieving this in 4.5 s compared to 23 s for the Normal sample, showcasing the impact of the porous structure on hydrophilicity.

Overall porosity is one of the important parameters for PK hollow fiber membranes. Since PK concentration is 20 wt% and the densities of PK and mixed diluent are 1.24 and 1.13 g $cm^{-1}$, respectively, the overall porosity was estimated as 81.4%. The overall porosity reached 81 to 83%, as shown in Fig. 4-5(b), using extruded solvent. Extruded solvent prevented diluent evaporation, leading to porous structures at the membrane outer surface. Bore liquid penetration induced larger porous structures near the inner surface, further enhancing overall porosity.

Mean pore diameters varied from 21.3 nm for the Normal PK membrane to 89.4 nm for TEG and 114.9 nm for PC when extruding different solvents at the outermost layer (Fig. 4-5(c)). This variation in pore size influenced the water permeance of the membranes.

The effect of extruded solvents on the water permeance of PK hollow fiber membranes was investigated. As shown in Fig. 4-5(d), PK membranes prepared with co-extruded solvents exhibited high water permeance (> 1000 L $m^{-2}h^{-1}bar^{-1}$) compared to the low water permeance (62 L $m^{-2}h^{-1}bar^{-1}$) of Normal PK membrane. This could be attributed to the large pore size, the hydrophilicity of PK, high overall porosity, and porous structure at the membrane outer surface. However, clear distinguishment was

observed in pure water permeance of prepared PK membranes when extruding different solvents at the outer layer. It was found that when solvents have strong interaction with diluent, as located above the diagonal in Fig. 4-3 (TEG, PEG300, and PEG600), the water permeance of the PK membranes ranged from 1210 to 1580 L $m^{-2}h^{-1}bar^{-1}$. Surprisingly, PC, SFL, DMP, and DEP with low viscosity resulted in higher water flux, reaching a maximum value of 2430 L $m^{-2}h^{-1}bar^{-1}$ for PC. We believe that the slightly increased pore size played a partial role in the significant enhancement of water permeance, as the mean pore diameter only increased from 89.4 to 114.9 nm, which was not enough to increase the flux more than twice. In Fig. S4-3 - S4-5, all PK membranes showed the interconnected membrane bulk structure and porous inner surface, which should have the same resistance to penetration of water molecules. Thus, the resistance was mainly derived from the different outer surface structures of the membranes and this ultimately determined the water permeance of membrane. From Fig. 4-5(c), PK membrane surface porosity was higher when extruding solvents with low viscosity, especially PC with a surface porosity of 32%. The combination of increased pore size and surface porosity improved water flux, emphasizing the importance of these parameters in determining membrane water permeance. In summary, the choice of extruded solvents significantly influenced the crystal structure, hydrophilicity, overall porosity, mean pore size, and water permeance of the PK hollow fiber membranes. The study demonstrated the intricate interplay between solvent properties, membrane structure, and performance, providing insights for optimizing membrane characteristics in various applications. In addition, the PK membrane with the highest water permeance (2430 L $m^{-2}h^{-1}bar^{-1}$) prepared by extruding solvent PC at the outermost layer of triple-orifice-spinneret was selected, and pure water permeance retention (PWPR) for PK hollow fiber membrane was measured in Fig. S4-8. After 48 hours of continuous operation, the PWPR of PK membrane was decreased to 72.8%, because the membrane compaction during the filtration process under the outside to the inside for water permeability.

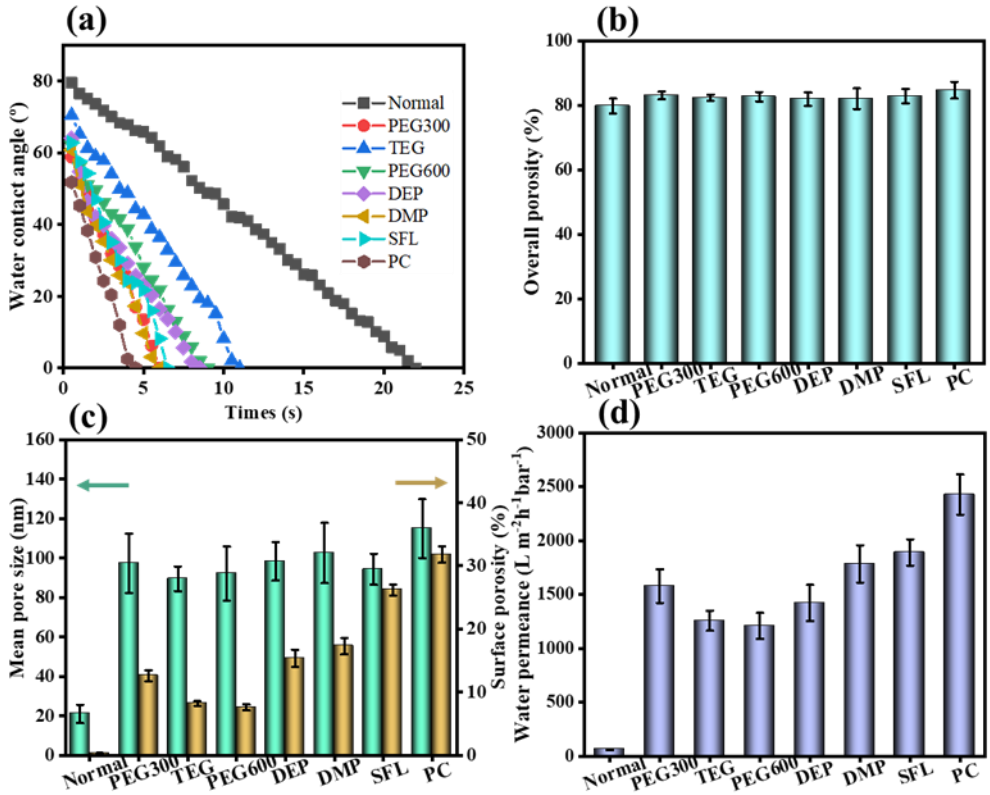


**Fig. 4-5** Performance of PK hollow fiber membranes: (a) dynamic water contact angle, (b) overall porosity, (c) mean pore size, and (d) pure water permeance. The air gap distance is 5 cm.

The impact of extrusion solvents on the tensile strength and elongation at the break of the PK hollow fiber membranes is shown in Fig. 4-6. Compared to the Normal PK membrane, the tensile strength of membranes prepared with extruded solvents was slightly reduced. This reduction is attributed to the thinner outer skin layer and the porous outer surface introduced by the extrusion process. With the exception of PC, the choice of extrusion solvent had a relatively minor impact on the tensile strength of PK hollow fiber membranes. The alteration mainly occurred in the membrane structure near the outer surface region, with minimal effects on the bulk structure. PC, when used as an extruded solvent, led to the formation of a porous structure near the outer surface, contributing to a decrease in the tensile strength of the PK membrane. The elongation

at break of PK hollow fiber membranes, prepared by extruding PC, SFL, DMP, and DEP, was lower compared to membranes prepared by extruding TEG, PEG300, and PEG600. This reduction in elongation at break is attributed to the formation of denser or fiber-like structures on the outer surface of the membrane. The specific characteristics introduced by these solvents influenced the membrane's ability to stretch before breaking. In summary, the extrusion solvents had a nuanced effect on the tensile strength and elongation at break of PK hollow fiber membranes. While the overall impact on tensile strength was slight, the choice of solvent influenced the membrane's ability to stretch before breaking, with certain solvents leading to denser or fiber-like structures on the outer surface, affecting mechanical properties. In addition, a comparison of PK hollow fiber membranes including water permeance and mechanical strength, between the literature and those prepared in this work is shown in Table S4-1. Compared with the PK hollow fiber membrane published in recent literature, the PK membrane prepared in this work exhibits excellent water permeance using the co-extrusion technology, but the tensile strength and elongation at break of the PK membrane are slightly lower.

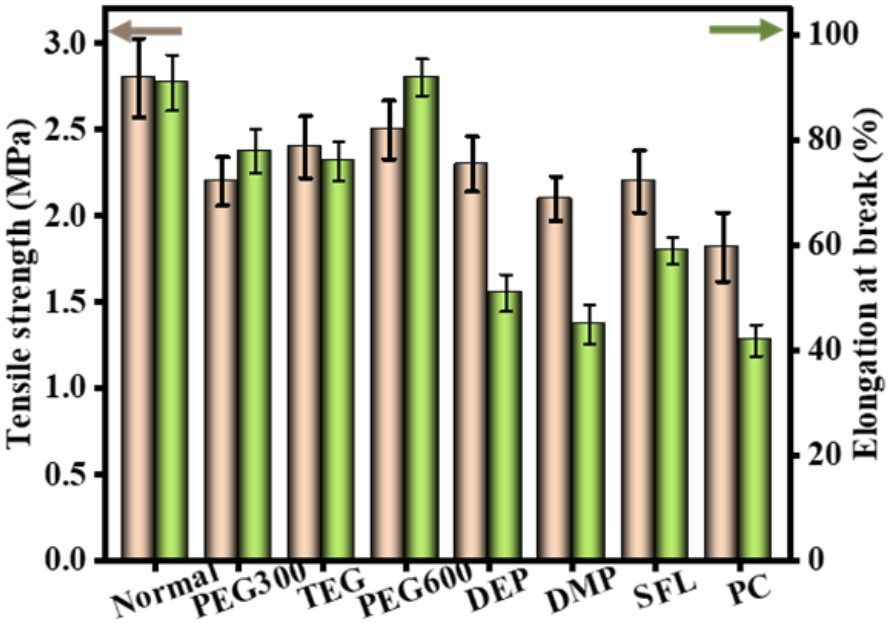


**Fig. 4-6** Tensile strength and elongation at break of PK hollow fiber membranes.

Finally, we summarized the relationship among the surface porosity, water permeance, viscosity of the extruded solvent, and the interaction of the extruded solvent with PK and mixed diluent is presented in Fig. 4-7. Two cases based on the $Ra_{(Solvent\text{-}Diluent)}/Ra_{(Solvent\text{-}PK)}$ values need to be discussed to explain the surface porosity of the PK membranes. As shown in Fig. 4-7(a), a $Ra_{(Solvent\text{-}Diluent)}/Ra_{(Solvent\text{-}PK)}$ value less than 1 indicates that the extruded solvent has a stronger interaction with the diluent than with PK. With the increase of $Ra_{(Solvent\text{-}Diluent)}/Ra_{(Solvent\text{-}PK)}$, the surface porosity of the PK membrane gradually decreases, because the tendency of the diluent to migrate toward the membrane surface weakens, contributing to reduced surface porosity. Also, high viscosity makes the penetration of the outer layer solvent to the membrane surface difficult. The order of decreasing surface porosity in this case is PEG300, TEG, and PEG600.

On the other hand, when the ratio of $Ra_{(Solvent\text{-}Diluent)}/Ra_{(Solvent\text{-}PK)}$ is larger than 1, this indicates that the penetration of the outer layer solvent dominates the formation of

porous structures on the membrane surface due to low viscosity. The limited time and high viscosity of the polymer solution make it challenging for PK molecules to move toward the surface in a short time. This is mainly because low solvent viscosity allows increased penetration of solvents into the membrane surface, diluting the polymer concentration and increasing the outer surface porosity. As a result, the water permeance of the PK membranes gradually increased with decreased extruded solvent viscosity, as shown in Fig. 4-7(b).

Fig. 4-7(c) demonstrates a strong agreement between water permeance and surface porosity of PK hollow fiber membranes. This highlights the importance of outer surface porosity for enhancing membrane permeance without increasing pore size. Fundamentally, the increased infiltration of the low-viscosity outer layer solvent increases the porosity of the outer surface, leading to improved water permeance of PK hollow fiber membranes. The figure emphasizes the intricate interplay between the extruded solvent properties, surface porosity, and water permeance in PK hollow fiber membranes, providing valuable insights into the factors influencing membrane performance.

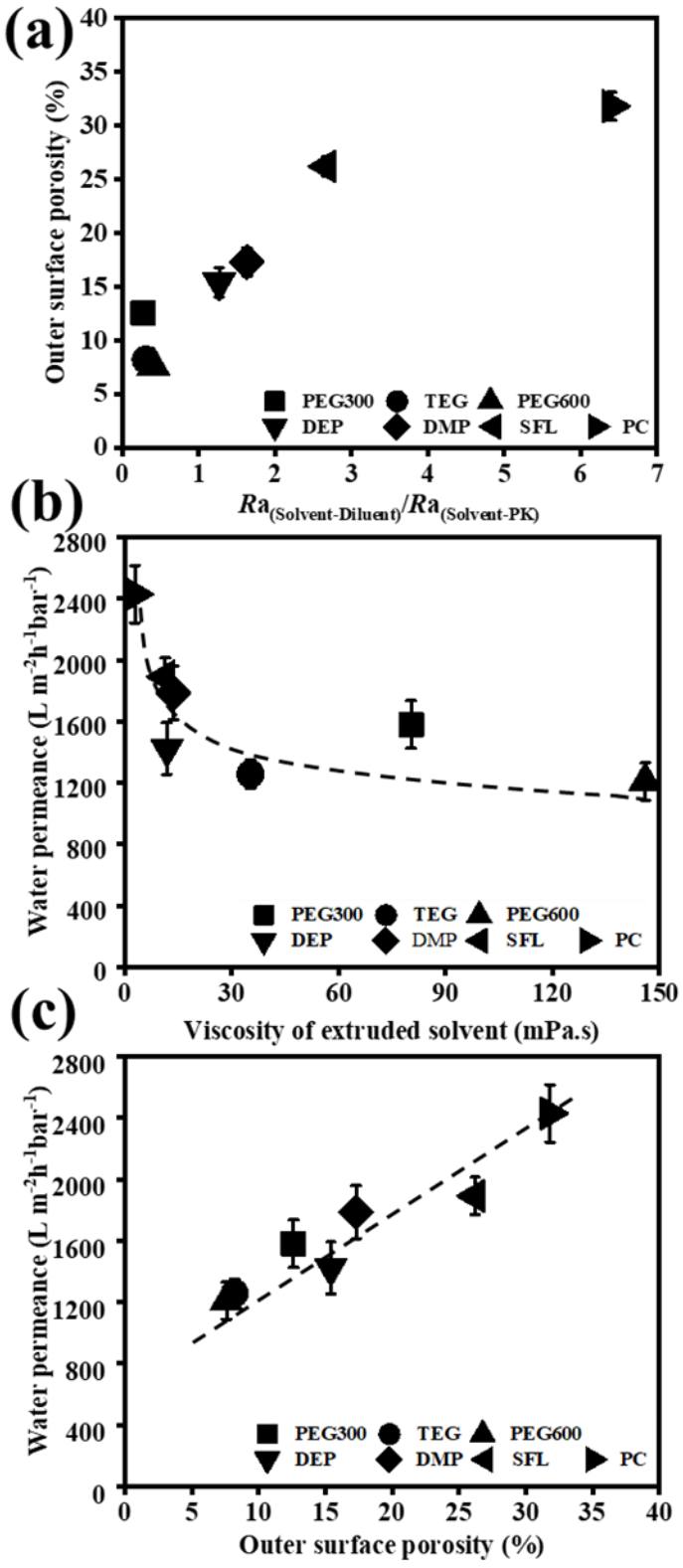


**Fig. 4-7** Relationship between the surface porosity and the interaction of extruded solvent, PK, and mixed diluent (a), water permeance and viscosity of extruded solvent (b), water permeance and surface porosity (c).

### *4.3.3 Effect of the length of the air gap membrane structure*

During the co-extrusion process, the air gap distance plays a crucial role in determining the interaction time between the outer layer solvent and the polymer solvent [33, 39]. The impact of different air gap distances (1, 5, and 10 cm) on the membrane structure and performance of PK membrane prepared using the co-extrusion method with SFL as the outer solvent was investigated. SFL was selected because the membrane prepared using SFL had the second highest permeance, following the membrane prepared using PC, and a relatively higher mechanical strength compared with the PC-extruded membrane. The membranes prepared with air gap distances of 1, 5, and 10 cm were labeled as “M1”, “M5”, and “M10”, respectively.

Fig. 4-8 and Fig. S4-8 show the FESEM images of the cross-section structure of the PK hollow fiber membranes. It can be seen that a well interconnected cellular structure could be observed in the middle of the cross-section for all samples, a result of the liquid-liquid phase separation process in the PK/PEG300/TEG system upon cooling [24]. The region close to the inner surface exhibited an almost identical macrovoid structure generated by the penetration of bore liquid (PC), indicating minimal influence of air gap length and extruded solvent on bulk structure and inner surface. Conversely, the cross-section near the outer surface exhibited significant differences. As the SFL was extruded at the outermost layer of the PK solution with an air gap length of 1 cm, a dense outer skin layer with a thickness of approximately 0.4 μm formed as shown in Fig. 4-8(M1-a), showing few pores at the outer surface. When the distance of the air gap increased to 5 cm, the dense outer skin layer disappeared in Fig. 4-8(M5-a), and a large number of pores appeared at the outer surface. As the air gap increased further to 10 cm, the number of pores on the membrane surface decreased somewhat compared to M5. Interestingly, as the air gap increased, the surface porosity of the PK membrane increased first and then decreased with increasing air gap distance when SFL was extruded at the outer layer. SFL is located below the diagonal line in Fig. 4-3, having a

ratio of $Ra_{(Solvent\text{-}Diluent)}/Ra_{(Solvent\text{-}PK)}$ larger than 1, indicating better interaction with PK than with the diluent. As such, PK molecules would move to the membrane surface forming a denser outer surface while passing through the air gap. In the case of short air gap distance (1 or 5 cm), SFL, with low viscosity (11.2 mPa.s), penetrated the membrane surface more effectively than the migration of PK from the solution, dominating the formation of a porous structure on the membrane surface. Thus, M5 exhibited more pores than M1. On the other hand, an excessively long air gap distance (10 cm) provided more time for PK in the solution to move to the surface, negatively affecting the formation of the pore structure. Thus, for M10, surface porosity decreased, suggesting that long air gaps may not favor the formation of porous structures with low-viscosity extruded solvents.

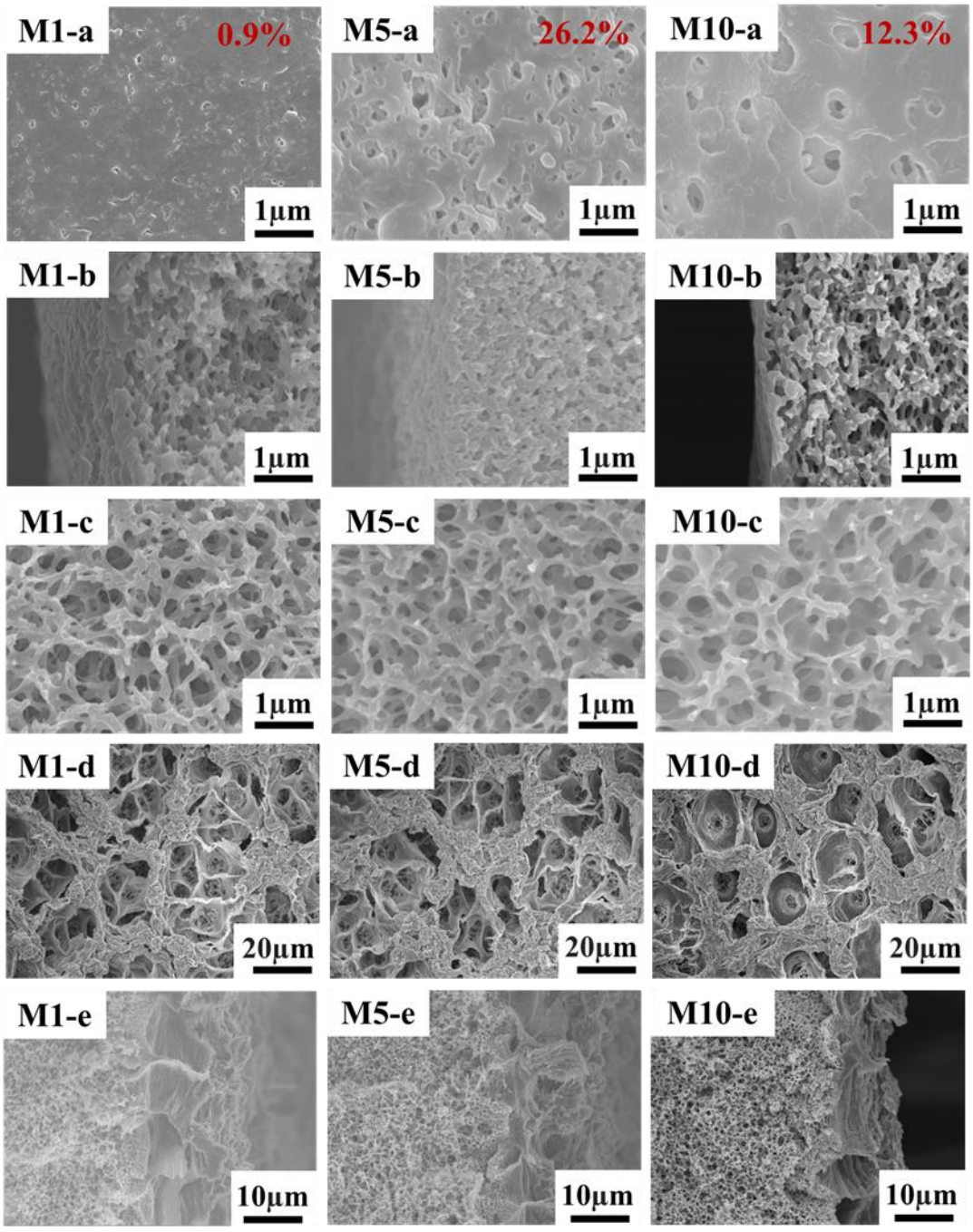


**Fig. 4-8** Morphology of PK hollow fiber membrane. M1, M5, and M10 represent the 1, 5, and 10 cm air gap distances, respectively. a, b, c, d, and e represent the near outer surface, center part, near inner surface, outer surface, and inner surface of the membranes, respectively. The extruded solvent was SFL for all membranes.

### *4.3.4 Effect of the length of air gap on membrane performance*

The air gap distance during co-extrusion significantly influenced membrane pore size

and water permeance. As shown in Fig. 4-9(a), when the SFL was extruded on the outside of the PK solution with a 1 cm air gap, the prepared PK membrane exhibited a small mean pore size (43.2 nm), attributed to the formation of the dense outer surface with small surface pores, as shown in Fig. 4-8(M1-a). When the air gap increased to 5 cm, the mean pore size of the PK hollow fiber membrane significantly increased to 94.3 nm, because larger outer surface pores formed (Fig. 4-8(M5-a)), due to the penetration of SFL. When the air gap increased to 10 cm (M10), the mean pore size was similar to M5. Surface migration of PK and penetration of the outer solvent acted simultaneously, affecting surface porosity rather than pore size. Correspondingly, as the air gap changed from 1 to 5 cm, the water permeance of the PK hollow fiber membrane increased significantly from 179 to 1892 L $m^{-2}h^{-1}bar^{-1}$, resulting from the increased overall pore size and porosity of the outer surface of the PK membrane as shown in Fig. 4-9(a). For M10, the water permeance decreased to 1120 L $m^{-2}h^{-1}bar^{-1}$ due to the reduced number of pore structures on the membrane surface.

Unlike the pore size and flux, tensile strength and elongation at the break of the PK membrane exhibited slight changes at different air gap distances and extrusion solvents, as shown in Fig. 4-9(b). Changes in the air gap and extrusion solvents primarily affected surface structure, leaving the bulk structure and inner surface relatively unchanged.

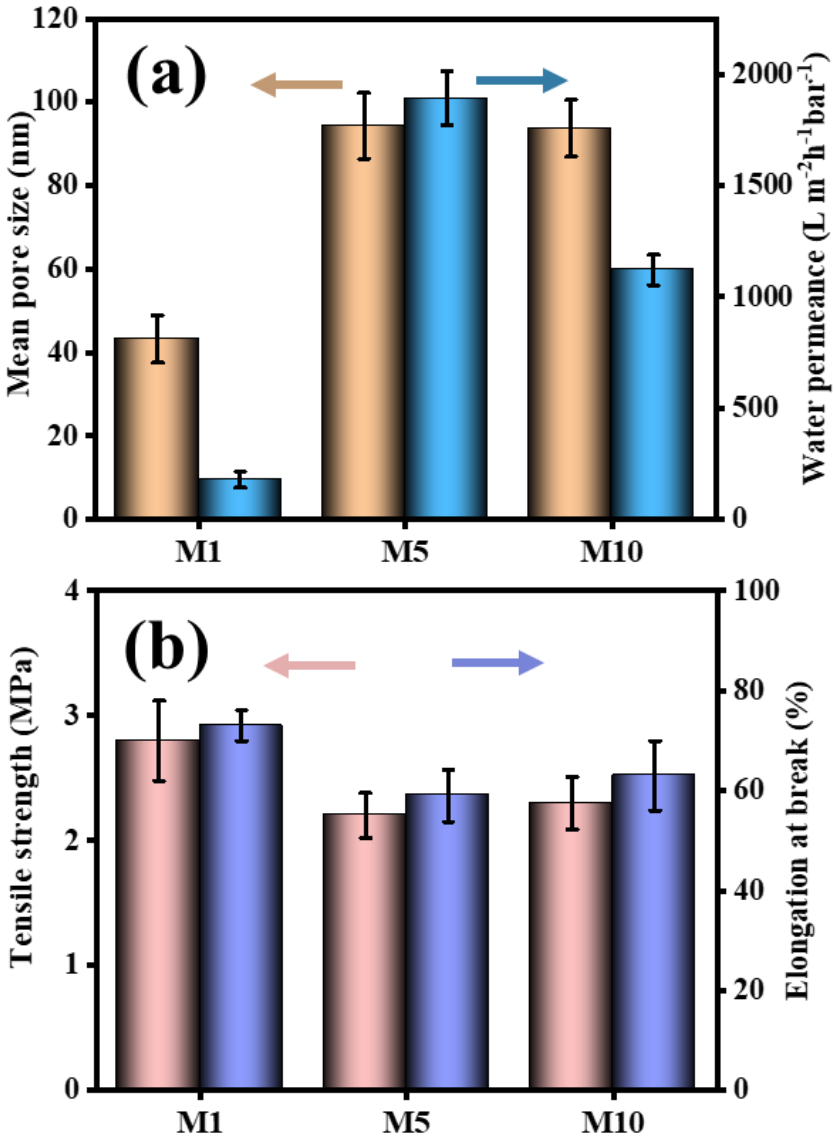


**Fig. 4-9** Performance of PK hollow fiber membranes using the fixed extruded solvent (SFL). (a) mean pore size and water permeance, (b) tensile strength and elongation at break. M1, M5, and M10 represent the 1, 5, and 10 cm air gap distances, respectively. The extruded solvent was SFL for all membranes.

### *4.4 Conclusion*

In this work, co-extrusion technology was employed to fabricate PK hollow fiber membranes with high water permeance by extruding another solvent at the outermost

layer of the triple-orifice spinneret (Fig. S4-9) via the TIPS method. By extruding different kinds of solvents, the morphology, surface porosity, pore size, and water permeance of prepared PK membranes were systematically investigated. In addition to the interaction between the PK, diluent, and the extruded solvent, the viscosity of the extruded solvent also played an important role in the membrane surface structure during the co-extrusion process. When the solvent with low viscosity was extruded at the outermost layer of the triple-orifice spinneret, the penetration of the outer solvent into the membrane surface region was highly effective in improving the membrane surface porosity by diluting the polymer concentration on the membrane surface. When PC was used as the outer layer solvent, the water permeance of the resultant PK membrane reached 2430 L $m^{-2}h^{-1}bar^{-1}$. It was also found that increasing the surface porosity of the membrane was a crucial factor in improving the membrane water flux without compromising the pore size.

***References***

[1] R. Klaassen, P. Feron, A. Jansen, Membrane contactor applications, Desalination, 224 (2008) 81-87.

[2] Y. Zhang, R. Wang, Novel method for incorporating hydrophobic silica nanoparticles on polyetherimide hollow fiber membranes for $CO_2$ absorption in a gas–liquid membrane contactor, J. Membr. Sci., 452 (2014) 379-389.

[3] A. Ovcharova, V. Vasilevsky, I. Borisov, S. Bazhenov, A. Volkov, A. Bildyukevich, V. Volkov, Polysulfone porous hollow fiber membranes for ethylene-ethane separation in gas-liquid membrane contactor, Sep. Purif. Technol., 183 (2017) 162-172.

[4] B.E. Logan, M. Elimelech, Membrane-based processes for sustainable power generation using water, Nature, 488 (2012) 313-319.

[5] Y. Jiao, L. Song, C. Zhao, Y. An, W. Lu, B. He, C. Yang, Membrane-based indirect power generation technologies for harvesting salinity gradient energy - A review, Desalination, 525 (2022) 115485.

[6] A. Brunetti, E. Drioli, Y.M. Lee, G. Barbieri, Engineering evaluation of $CO_2$ separation by membrane gas separation systems, J. Membr. Sci., 454 (2014) 305-315.

[7] F. Moghadam, E. Kamio, H. Matsuyama, High $CO_2$ separation performance of amino acid ionic liquid-based double network ion gel membranes in low $CO_2$ concentration gas mixtures under humid conditions, J. Membr. Sci., 525 (2017) 290-297.

[8] J. Zhang, J.A. Schott, S.M. Mahurin, S. Dai, Porous structure design of polymeric membranes for gas separation, Small Methods, 1 (2017) 1600051.

[9] U. Baig, M. Faizan, A. Waheed, A review on super-wettable porous membranes and materials based on bio-polymeric chitosan for oil-water separation, Adv Colloid Interface Sci, 303 (2022) 102635.

[10] Y. Tang, Y. Lin, W. Ma, X. Wang, A review on microporous polyvinylidene fluoride membranes fabricated via thermally induced phase separation for MF/UF application, J. Membr. Sci., 639 (2021) 119759.

[11] I. Pinnau, B.D. Freeman, Membrane Formation and Modification, Copyright, Advisory Board, Foreword, (1999).

[12] G.-d. Kang, Y.-m. Cao, Application and modification of poly(vinylidene fluoride) (PVDF) membranes – A review, J. Membr. Sci., 463 (2014) 145-165.

[13] P. Saxena, P. Shukla, A comprehensive review on fundamental properties and applications of poly(vinylidene fluoride) (PVDF), Adv. Compos. Mater., 4 (2021) 8-26.

[14] PVDF membranes and PFAS: what impact of the EU's REACH legislation? The MBR Site.

[15] J. Cho, I. Jeon, S.Y. Kim, S. Lim, J.Y. Jho, Improving dispersion and barrier properties of polyketone/graphene nanoplatelet composites via noncovalent functionalization using aminopyrene, ACS Appl. Mater. Interfaces, 9 (2017) 27984-27994.

[16] L. Zhang, Y. Lin, L. Cheng, Z. Yang, H. Matsuyama, A comprehensively fouling- and solvent-resistant aliphatic polyketone membrane for high-flux filtration of difficult

oil-in-water micro- and nanoemulsions, J. Membr. Sci., 582 (2019) 48-58.

[17] A. Backman, J. Lange, M. S. Hedenqvist, Transport properties of uniaxially oriented aliphatic polyketone, J Polym Sci B Polym Phys, 42 (2004) 947-955.

[18] L. Zhang, L. Cheng, H. Wu, T. Yoshioka, H. Matsuyama, One-step fabrication of robust and anti-oil-fouling aliphatic polyketone composite membranes for sustainable and efficient filtration of oil-in-water emulsions, J. Mater. Chem. A, 6 (2018) 24641-24650.

[19] C. Shen, L. Bian, P. Zhang, B. An, Z. Cui, H. Wang, J. Li, Microstructure evolution of bonded water layer and morphology of grafting membrane with different polyethylene glycol length and their influence on permeability and anti-fouling capacity, J. Membr. Sci., 601 (2020) 117949.

[20] L. Cheng, A.R. Shaikh, L.F. Fang, S. Jeon, C.J. Liu, L. Zhang, H.C. Wu, D.M. Wang, H. Matsuyama, Fouling-resistant and self-cleaning aliphatic polyketone membrane for sustainable oil-water emulsion separation, ACS Appl. Mater. Interfaces, 10 (2018) 44880-44889.

[21] K. Guan, L. Zhang, S. Wang, R. Takagi, H. Matsuyama, Controlling the formation of porous polyketone membranes via a cross-linkable alginate additive for oil-in-water emulsion separations, J. Membr. Sci., 611 (2020) 118362.

[22] Y. Jia, K. Guan, L. Zhang, Y. Lin, Q. Shen, P. Zhang, H. Matsuyama, Enabling polyketone membrane with underwater superoleophobicity via a hydrogel-based modification for high-efficiency oil-in-water emulsion separation, J. Membr. Sci., 618 (2021) 118705.

[23] S. Xiang, P. Zhang, S. Rajabzadeh, R.R. Gonzales, Z. Li, Y. Shi, S. Zhou, M. Hu, K. Guan, H. Matsuyama, Development of porous polyketone membrane via liquid–liquid thermally induced phase separation, J. Membr. Sci., 677 (2023) 121639.

[24] S. Xiang, P. Zhang, R.R. Gonzales, R. Saeid, L. Deng, Y. Shi, W. Fu, Z. Li, K. Guan, H. Matsuyama, Lowering spinning temperature for polyketone (PK) hollow fiber membrane fabrication with low-toxic diluent system via thermally induced phase

separation, J. Membr. Sci., 689 (2023) 122176.

[25] B.J. Cha, J.M. Yang, Preparation of poly(vinylidene fluoride) hollow fiber membranes for microfiltration using modified TIPS process, J. Membr. Sci., 291 (2007) 191-198.

[26] N.T. Hassankiadeh, Z. Cui, J.H. Kim, D.W. Shin, S.Y. Lee, A. Sanguineti, V. Arcella, Y.M. Lee, E. Drioli, Microporous poly(vinylidene fluoride) hollow fiber membranes fabricated with PolarClean as water-soluble green diluent and additives, J. Membr. Sci., 479 (2015) 204-212.

[27] N. Chen, J. Zhao, L. Shi, A. Goto, R. Wang, Fabrication of PVDF ultrafiltration membrane using modified thermally induced phase separation: The role of amphiphilic and hydrophilic non-solvents, J. Membr. Sci., 685 (2023) 121919.

[28] P. Zhang, C. Fang, S. Rajabzadeh, W. Liu, Y. Jia, Q. Shen, L. Zhang, S. Wang, N. Kato, H. Matsuyama, Effect of polymer molecular weight on structure and performance of PVDF hollow fiber membranes prepared via TIPS process with co-extrusion of solvent using triple orifice spinneret, J. Membr. Sci., 620 (2021) 118854.

[29] D. Zou, H.W. Kim, S.M. Jeon, Y.M. Lee, Fabrication and modification of PVDF/PSF hollow-fiber membranes for ginseng extract and saline water separations via direct contact membrane distillation, J. Membr. Sci., 644 (2022) 120101.

[30] J.T. Jung, H.H. Wang, J.F. Kim, J. Lee, J.S. Kim, E. Drioli, Y.M. Lee, Tailoring nonsolvent-thermally induced phase separation (N-TIPS) effect using triple spinneret to fabricate high performance PVDF hollow fiber membranes, J. Membr. Sci., 559 (2018) 117-126.

[31] C. Fang, S. Jeon, S. Rajabzadeh, L. Fang, L. Cheng, H. Matsuyama, Tailoring both the surface pore size and sub-layer structures of PVDF membranes prepared by the TIPS process with a triple orifice spinneret, J. Mater. Chem. A, 6 (2018) 20712-20724.

[32] C. Fang, S. Jeon, S. Rajabzadeh, L. Cheng, L. Fang, H. Matsuyama, Tailoring the surface pore size of hollow fiber membranes in the TIPS process, J. Mater. Chem. A, 6 (2018) 535-547.

[33] P. Zhang, S. Rajabzadeh, A. Venault, S. Wang, Q. Shen, Y. Jia, C. Fang, N. Kato, Y. Chang, H. Matsuyama, One-step entrapment of a PS-PEGMA amphiphilic copolymer on the outer surface of a hollow fiber membrane via TIPS process using triple-orifice spinneret, J. Membr. Sci., 638 (2021) 1119712.

[34] J. Wang, L. Wang, W. Ruan, C. Zhang, J. Ji, Rheology behavior of high‐density polyethylene/diluent blends and fabrication of hollow‐fiber membranes via thermally induced phase separation, J. Appl. Polym. Sci., 118 (2010) 2186-2194.

[35] W.C.J. Zuiderduin, D.P.N. Vlasveld, J. Huétink, R.J. Gaymans, Mechanical properties of polyketone terpolymer/rubber blends, Polymer, 45 (2004) 3765-3779.

[36] P. Zhang, S. Rajabzadeh, T. Istirokhatun, Q. Shen, Y. Jia, X. Yao, A. Venault, Y. Chang, H. Matsuyama, A novel method to immobilize zwitterionic copolymers onto PVDF hollow fiber membrane surface to obtain antifouling membranes, J. Membr. Sci., 656 (2022) 120592.

[37] C.M. Hansen, Hansen solubility parameters: a User's handbook, CRC Press, (2007).

[38] S. De Vito, F. Ciardelli, E. Benedetti, E. Bramanti, Thermal phase transitions of carbon monoxide-ethylene alternating copolymer: an FT/IR study, Polym. Adv. Technol., 8 (1997) 53-62.

[39] H. Roth, T. Luelf, A. Koppelmann, M. Abel, M. Wessling, Chemistry in a spinneret – Composite hollow fiber membranes in a single step process, J. Membr. Sci., 554 (2018) 48-58.

***Supporting information***

The solubility parameters of mixed diluents were calculated by Eqs. (S4-1)- (S4-3) [1].

$$\delta_{dM}=\varphi_1\delta_{d1}+\varphi_2\delta_{d2} \quad \text{(S4-1)}$$

$$\delta_{pM}=\varphi_1\delta_{p1}+\varphi_2\delta_{p2} \quad \text{(S4-2)}$$

$$\delta_{hM}=\varphi_1\delta_{h1}+\varphi_2\delta_{h2} \quad \text{(S4-3)}$$

where M, 1 and 2, represent the mixed diluent system, polyvinyl alcohol 300 (PEG300) and triethylene glycol (TEG), respectively. $\varphi_1$ and $\varphi_2$ are the volume fraction of PEG300 and TEG, respectively. $\delta_d$, $\delta_p$ and $\delta_h$ represent dispersion force, polar and hydrogen bond, respectively.

The *R*a value of two compositions was obtained by Eq. (S4-4) [1].

$$Ra=(4(\delta_{d1}-\delta_{d2})^2+\left(\delta_{p1}-\delta_{p2}\right)^2+(\delta_{h1}-\delta_{h2})^2)^{0.5} \quad \text{(S4-4)}$$

where 1 and 2, represent the composition 1 and composition 2, respectively. $\delta_d$, $\delta_p$ and $\delta_h$ represent dispersion force, polar and hydrogen bond, respectively.

The overall porosity $\phi$ of PK hollow fiber membrane is estimated by Eq. (S4-5).

$$\phi=\frac{\frac{W_{d1}}{D_{d1}}+\frac{W_{d2}}{D_{d2}}}{\frac{W_p}{D_p}+\frac{W_{d1}}{D_{d1}}+\frac{W_{d2}}{D_{d2}}}\times 100\% \quad \text{(S4-5)}$$

where W and D represents weight (g) and density (g $cm^{-3}$), respectively. The $p$, $d_1$ and $d_2$ represents the polymer (PK), diluent (PEG300) and diluent (TEG), respectively. The density of PK, PEG300 and TEG are 1.24 g $cm^{-3}$ [2], 1.13 g $cm^{-3}$ [3] and 1.13 g $cm^{-3}$ [4].

PK membrane with the highest water permeance (2430 L $m^{-2}h^{-1}bar^{-1}$) prepared by extruding solvent PC at the outermost layer of triple-orifice-spinneret (TOS) was selected, and the long-term pure water permeation for PK hollow fiber membrane was measured. In detail, the pure water was circled under a pressure of 0.5 bar using the outside-to-inside model. The pure water permeance retention (*PWPR*) of PK membrane was calculated by Eq. (S4-6).

$$PWPR=\frac{J_i}{J_c} \quad \text{(S4-6)}$$

where $J_i$ and $J_c$ are the initial water permeance (L $m^{-2}h^{-1}bar^{-1}$) and the water permeance under a constant filtration process (L $m^{-2}h^{-1}bar^{-1}$), respectively.

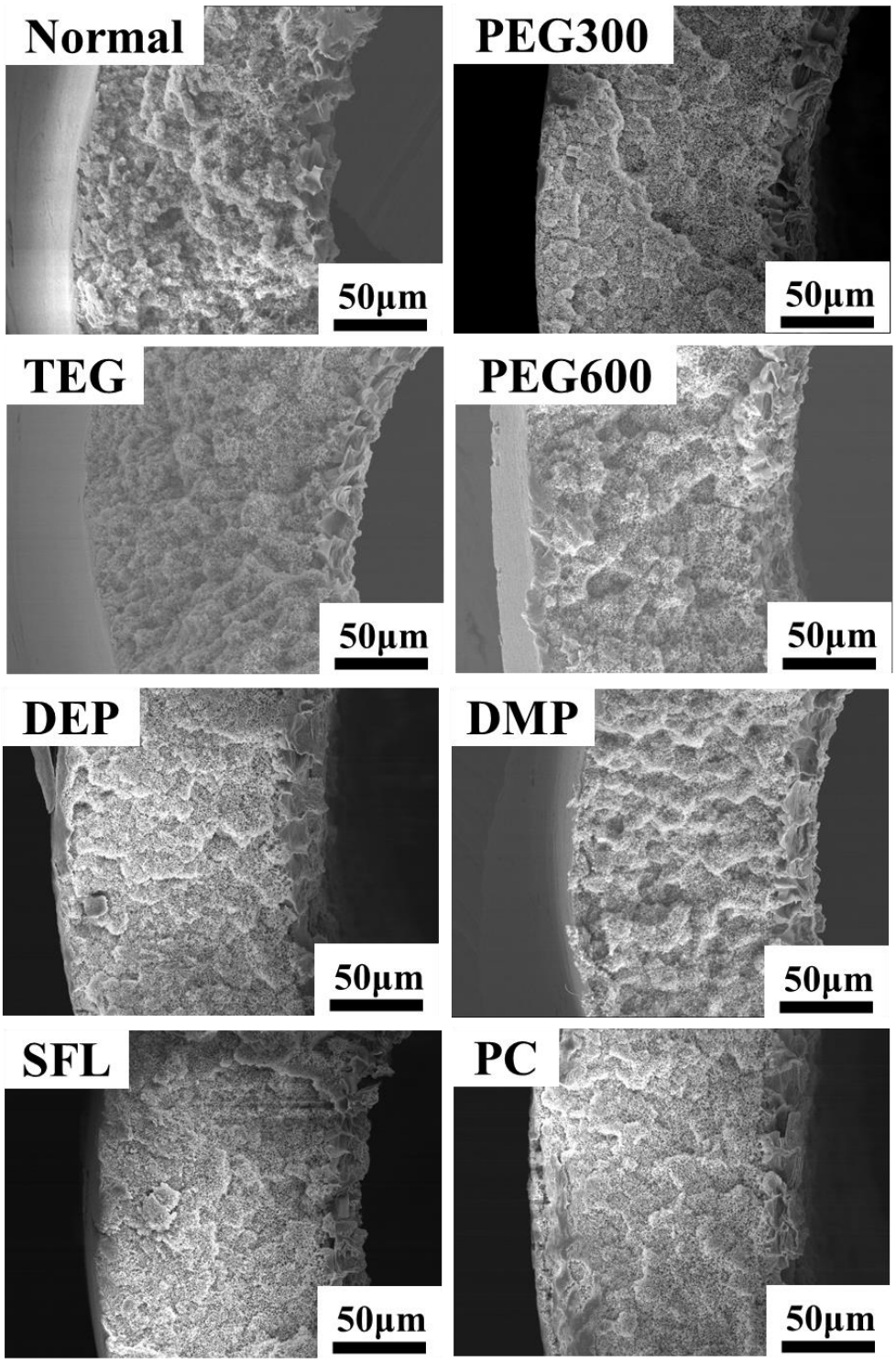


**Fig. S4-1** The whole cross-section structure of the prepared PK hollow fiber membrane using different kinds of extruded solvents. The air gap distance was fixed at 5 cm.

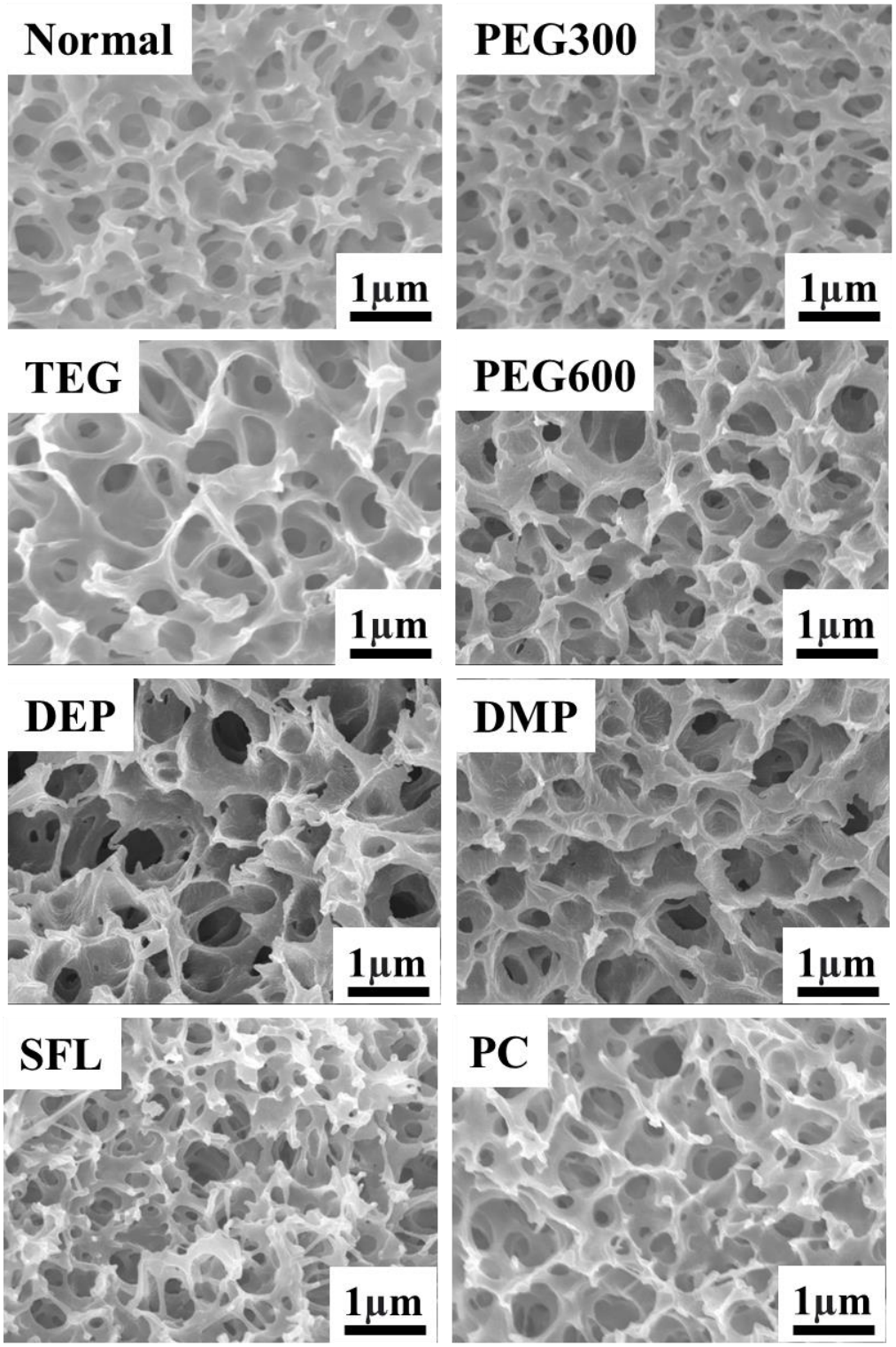


**Fig. S4-2** The cross-section structure of the prepared PK hollow fiber membrane using different kinds of extruded solvents. The air gap distance was fixed at 5 cm.

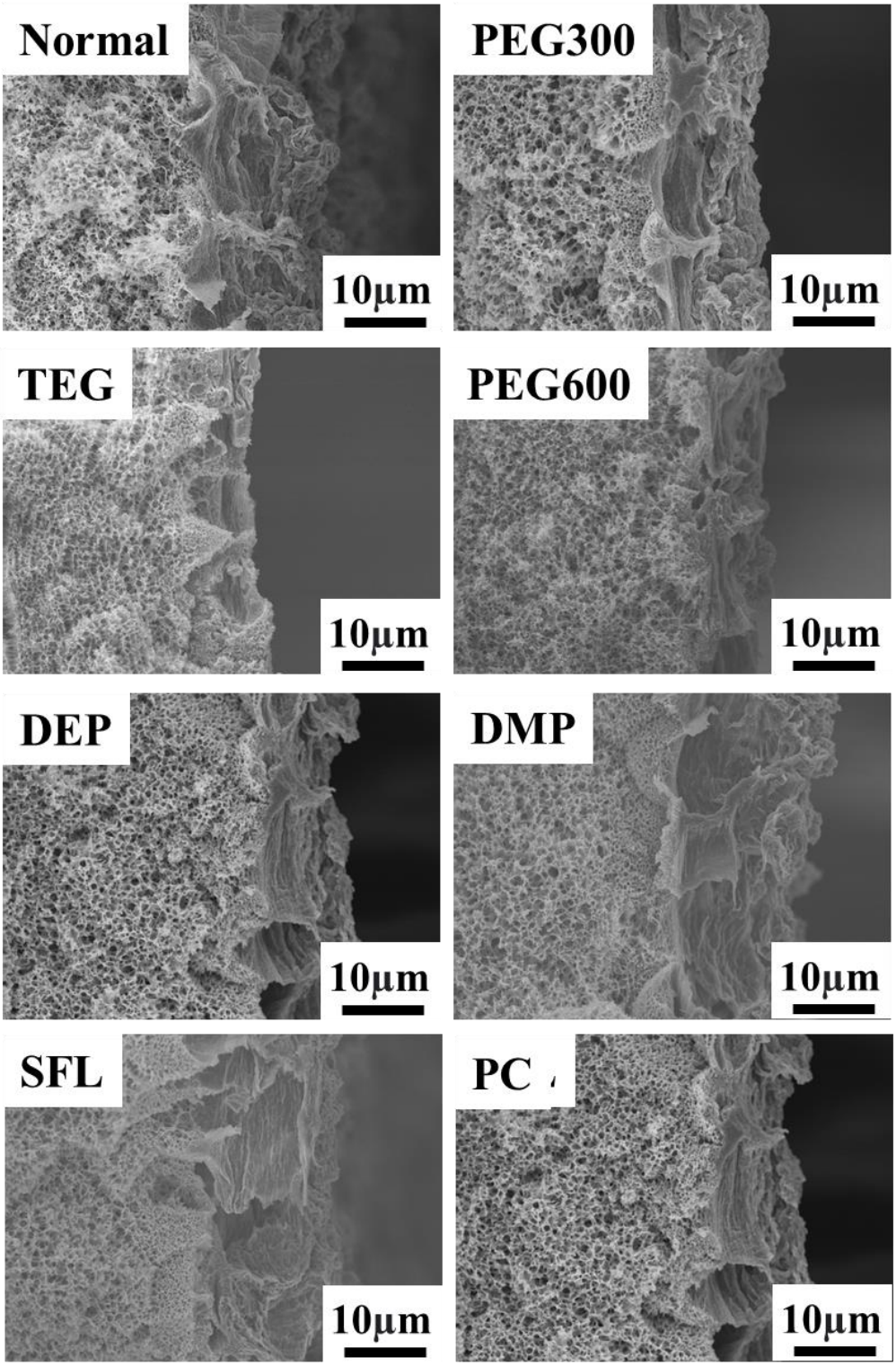


**Fig. S4-3** The cross-section near the inner surf

ace structure of the prepared PK hollow fiber membrane using different kinds of extruded solvents. The air gap distance was fixed at 5 cm.

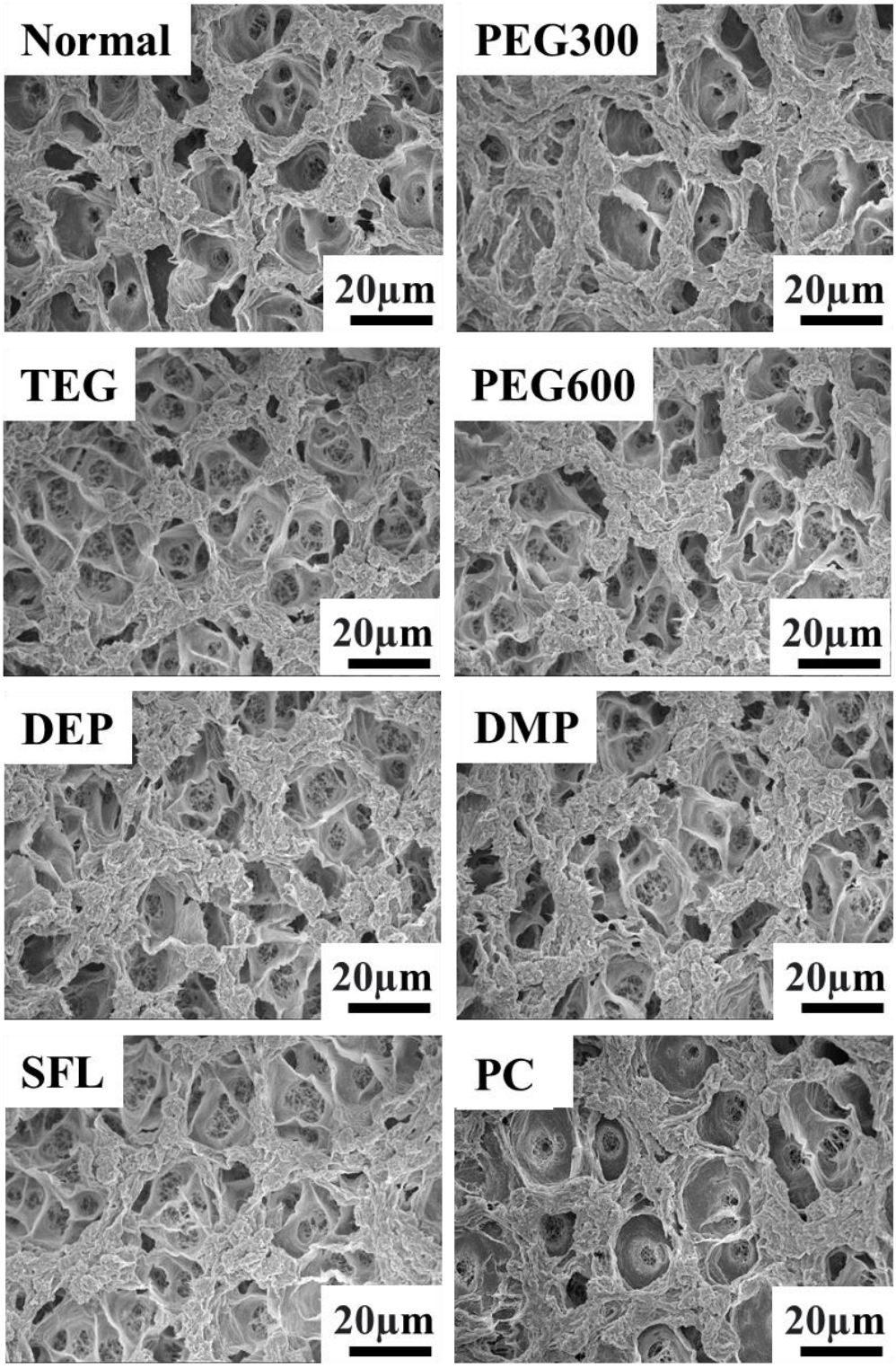


**Fig. S4-4** The inner surface structure of the prepared PK hollow fiber membrane using different kinds of extruded solvents. The air gap distance was fixed at 5 cm.

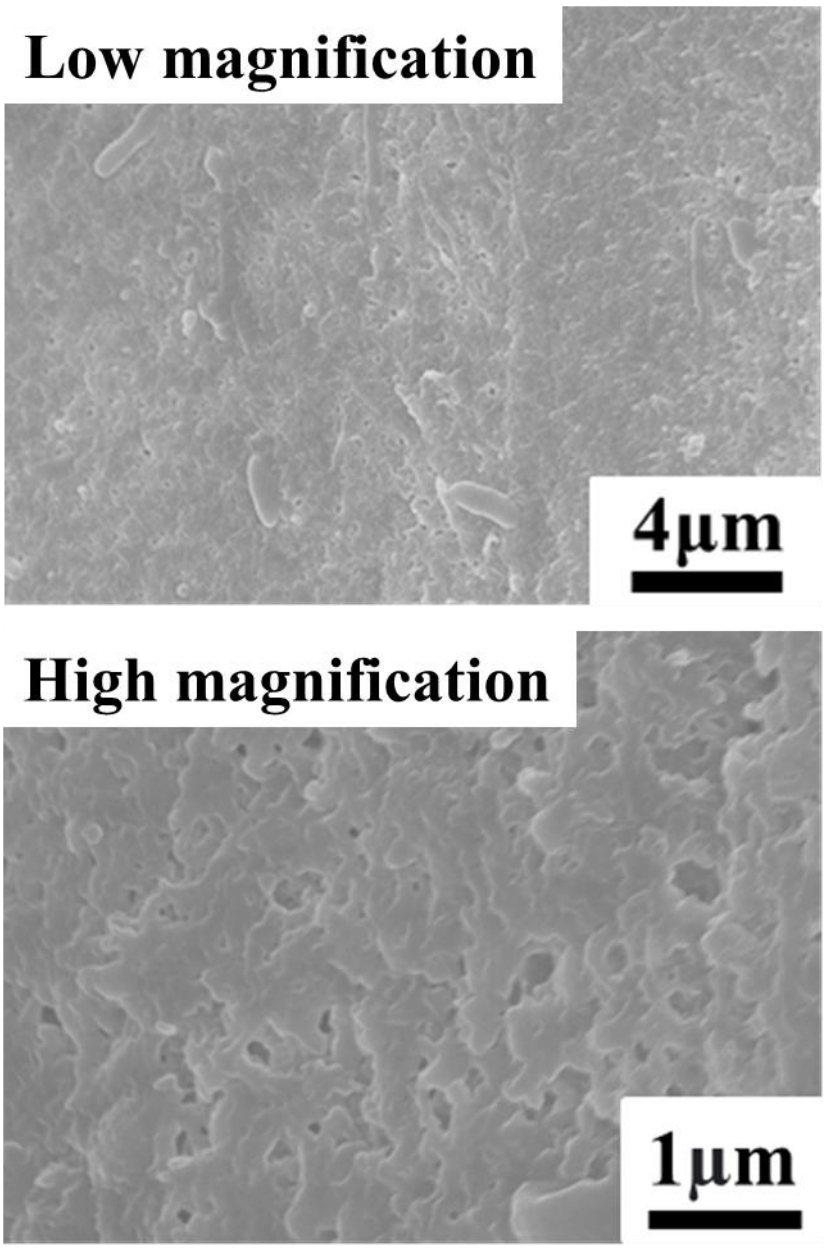


**Fig. S4-5** The outer surface structure of PK hollow fiber membrane with low magnification (X5000) and high magnification (X20000), respectively. TEG was used as the extruded solvent.

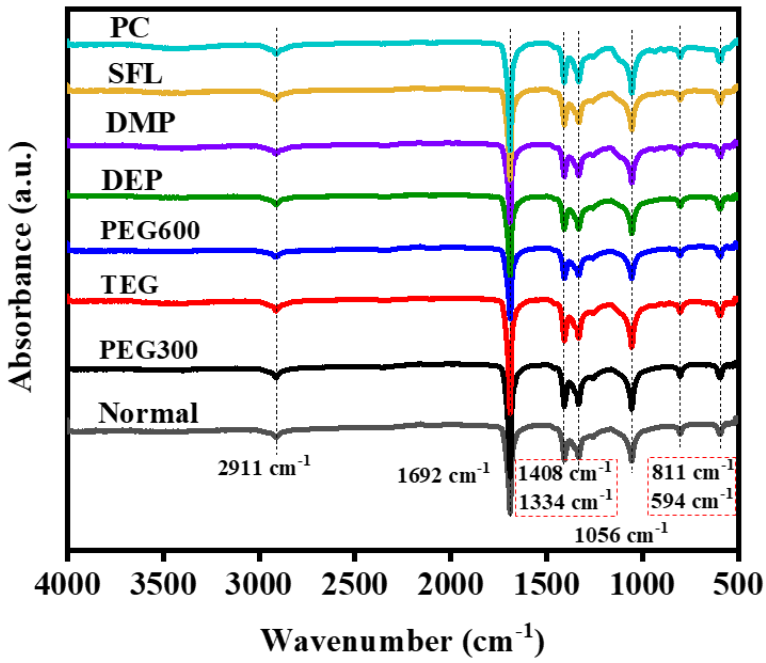


**Fig. S4-6** FTIR spectra of PK hollow fiber membranes.

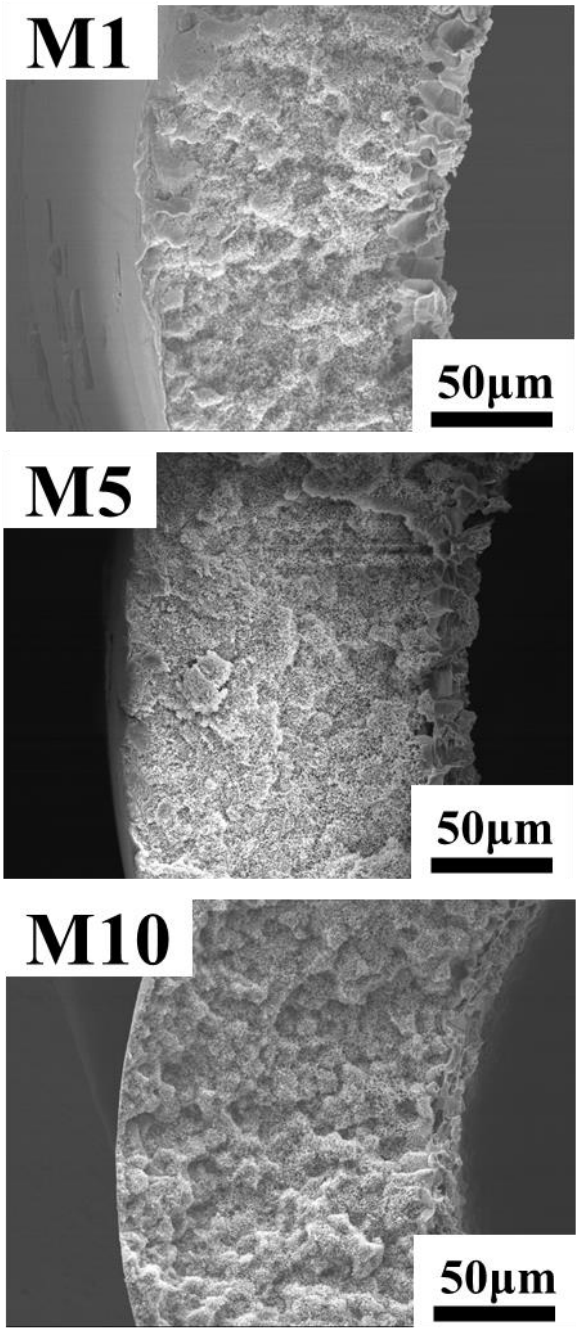


**Fig. S4-7** The whole cross-section structure of the prepared PK hollow fiber membrane with different air gap distances. M1, M5, and M10 represent 1, 5, and 10 cm of air gap distances, respectively. The extruded solvent was fixed at SFL.

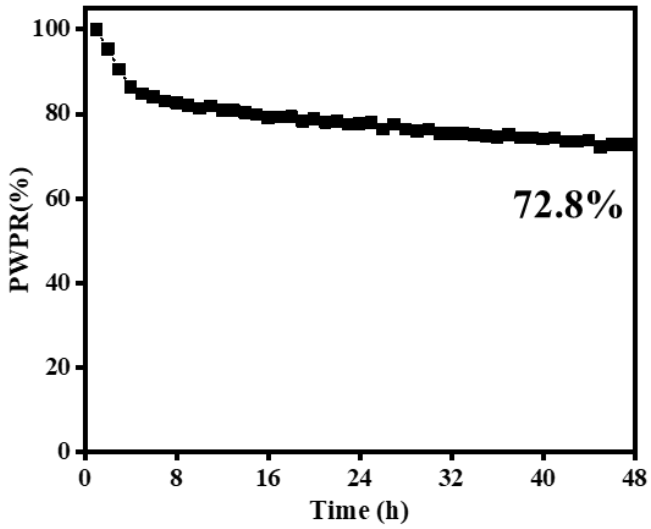


**Fig. S4-8** Pure water permeance retention of PK hollow fiber membrane prepared by extruding PC at the outmost layer.

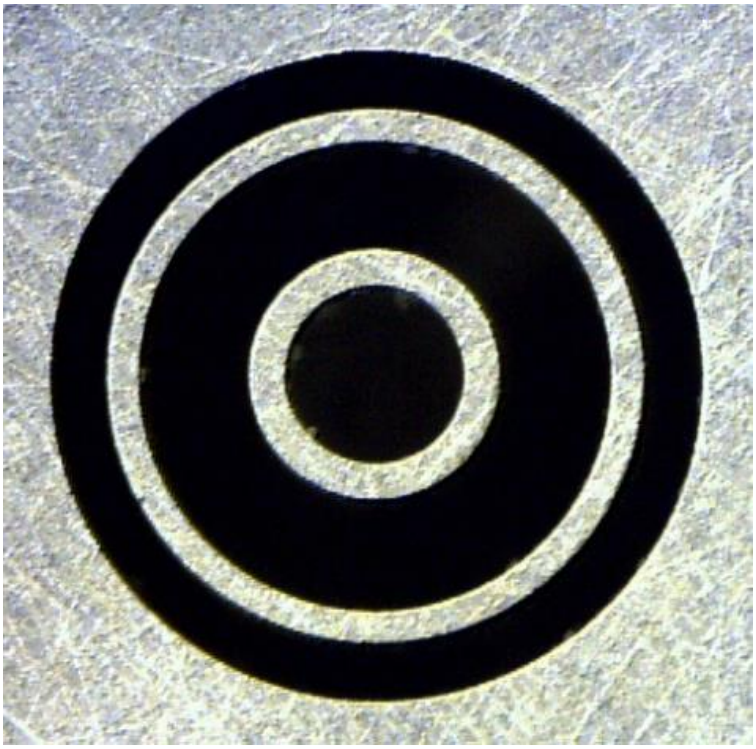

**Fig. S4-9** Diagram of the triple-orifice spinneret.

**Table S4-1** Some published papers concerning PK hollow fiber membranes via the TIPS method.

| Ref. | Polymer concentration (wt%) | Water permeance (L $m^{-2}h^{-1}bar^{-1}$) | Tensile strength (MPa) | Elongation at break (%) |
|---|---|---|---|---|
| This work | 20 | 1210-2430 | 1.82-2.5 | 42-92 |
| [5] | 26 | 15-250 | 6-8 | 20-35 |
| [6] | 20 | 122-820 | 2.4-3.3 | 48-125 |
| | 23 | 89 | 3.7 | 124 |
| | 27 | 43 | 6.6 | 118 |
| | 30 | 18 | 8.4 | 110 |

**Reference**

[1] C.M. Hansen, Hansen solubility parameters: a User's handbook, CRC Press, (2007).

[2] W.C.J. Zuiderduin, D.P.N. Vlasveld, J. Huétink, R.J. Gaymans, Mechanical properties of polyketone terpolymer/rubber blends, Polymer, 45 (2004) 3765-3779.

[3] J. Ai, F. Li, J. Zhang, Z. Wu, Density, viscosity, surface tension, and spectral analysis of polyethylene glycol 300 + 1,2-Propylenediaminebinary liquid mixture, J. Mol. Liq., 361 (2022) 119579.

[4] T. Sun, A.S. Teja, Density, viscosity and thermal conductivity of aqueous solutions of propylene glycol, dipropylene glycol, and tripropylene glycol between 290 K and 460 K, J. Chem. Eng. Data, 49 (2004) 1311-1317.

[5] Y. Park, W. Jang, J. Choi, Y. Woo, J. Hou, S. Jeon, H. Byun Fabrication of organic solvent resistant polyketone hollow fiber membranes, Membrane Journal 31 (2021) 363-370.

[6] S. Xiang, P. Zhang, R.R. Gonzales, R. Saeid, L. Deng, Y. Shi, W. Fu, Z. Li, K. Guan, H. Matsuyama, Lowering spinning temperature for polyketone (PK) hollow fiber membrane fabrication with low-toxic diluent system via thermally induced phase

separation, J. Membr. Sci., 689 (2023) 122176.

# Chapter 5

## Conclusions

In recent decades, the shortage of water resources is becoming a global risk, due to the rapid development of social industrialization and urbanization. Furthermore, the demand for freshwater was rapidly increased because of the increase in population and the water pollution resulting from the industrial activity accelerated the water shortage. Polymeric porous membrane, as the deep purification technique, has been widely used in water treatment, due to the simple fabrication process, low cost, and excellent performance.

Polyketone, as a crystalline polymer, possesses excellent hydrophilicity, mechanical properties, and chemical stability, demonstrating significant potential and cost-effectiveness in the field of polymer porous membranes. This is particularly due to its low-cost synthetic materials, including ethylene, carbon monoxide, and propylene. This dissertation aims to develop high-performance porous polyketone (PK) hollow fiber membranes using a thermally induced phase separation (TIPS) method. At present, the polyketone membrane was prepared via the NIPS process, and the prepared PK membrane exhibits excellent performance in oil-water separation or as a support layer for organic solvent nanofiltration and reverse osmosis processes, due to its outstanding solvent resistance. However, these PK membrane preparation techniques involve toxic solvents, as well as complicated and multistep membrane-forming processes using the nonsolvent induced phase separation (NIPS) method. Therefore, the development of a facile and environment-friendly method for PK membrane preparation is necessary.

Compared to the non-solvent induced phase separation (NIPS) method, the thermally induced phase separation (TIPS) method may be more suitable due to its simple membrane formation process and the potential use of low-toxic or non-toxic solvents. Therefore, in this dissertation, the high-water-permeance PK membrane was developed via the TIPS method. However, there is less reported on the preparation of PK membranes using the TIPS process. The solvents suitable for PK were screened to prepare PK membranes based on the TIPS process. Subsequently, based on the selected solvents, low-toxic or non-toxic solvent systems were chosen to develop porous PK fiber membranes and investigate the influence of membrane formation parameters on membrane structure and performance. During the experimental process, it was found that traditional spinning equipment (double orifice spinnerets) had difficulty effectively controlling the outer surface structure of PK hollow fiber membranes. Therefore, a triple orifice spinneret was used to extrude solvent on the outside of the polymer solution to control membrane structure and produce high-throughput PK hollow fiber membranes.

After the introduction in Chapter 1, polyketone (PK) porous membranes have attracted significant attention in separation technology owing to its high tolerance to organic solvents. However, its excellent solvent resistance complicates the PK membrane preparation procedure, requiring the use of toxic solvents in the conventional nonsolvent induced phase separation (NIPS) method. In this study, the thermally induced phase separation (TIPS) method was explored to prepare porous membranes with PK homopolymer and copolymer. By screening many diluents, we found potential diluents that could be applied to the TIPS method for PK membrane preparation. Two kinds of diluent (PEG300 and DPrP) for CPK and one kind of pure diluent (PEG200) for HPK were screened to induce L-L phase separation. In the membrane preparation by the liquid-liquid (L-L) phase separation system, the influence of the PK type, cooling conditions, and polymer concentration on the final membrane structure was investigated. Finally, the porous structure, water permeance, and mechanical properties

of the membranes prepared using the NIPS and TIPS methods were compared. Prepared CPK and HPK membrane with 25 wt% concentration by TIPS method showed high water permeability (400 and 480 L $m^{-2}h^{-1}bar^{-1}$) and tensile strength (4.6 and 4.9 MPa). This study will facilitate the development of high-performance PK membranes using the TIPS method, particularly in the selection of diluents.

In Chapter 3, we successfully and efficiently prepared PK hollow fiber membranes using the thermally induced phase separation (TIPS) method, capitalizing on a low-toxicity diluent system of polyethylene glycol 300 (PEG300) and triethylene glycol (TEG). Moreover, by simply adding TEG to the diluent, we achieved a reduction in the spinning temperature, resulting in membranes that display an interconnected structure formed through the liquid-liquid phase separation process. We systematically investigated the impact of the TEG ratio in the diluent, PK concentration, and propylene carbonate (PC) ratio in the bore liquid on the phase diagram, membrane morphology, and characteristics of PK membranes. Increasing the PC ratio in the bore liquid significantly improves the inner surface porosity due to PC penetration into the dope solution, leading to high water permeability. Additionally, the resulting PK membrane exhibits exceptional resistance to organic solvents. This work introduces a novel approach to lower the spinning temperature for PK membrane preparation in the TIPS process while preserving the membrane structure and properties.

In Chapter 4, co-extrusion technology is employed to fabricate high-water-permanence PK hollow fiber membranes by extruding another solvent at the outermost layer of the triple-orifice spinneret via the TIPS method. By extruding different kinds of solvents, the morphology, surface porosity, pore size, and water permeance of prepared PK membranes were systematically investigated. In addition to the solubility parameter between the extruded solvent, polymer, and diluent, the viscosity of the extruded outer layer solvent also plays an important role in the membrane surface structure during the co-extrusion process. When the solvent with low viscosity was extruded at the outermost layer of the triple-orifice spinneret, the penetration of the

outer solvent into the membrane surface region was highly effective in improving the membrane surface porosity by diluting the polymer concentration on the membrane surface. When PC was used as the outer layer solvent, the water permeance of the resultant PK membrane reached 2430 L $m^{-2}h^{-1}bar^{-1}$. It was also found that increasing the surface porosity of the membrane was a crucial factor in improving the membrane water flux without compromising the selectivity.

# Publication list

**Chapter 2**

**S. Xiang**, P. Zhang, S. Rajabzadeh, R.R. Gonzales, Z. Li, Y. Shi, S. Zhou, M. Hu, K. Guan, H. Matsuyama, Development of porous polyketone membrane via liquid–liquid thermally induced phase separation, Journal of Membrane Science, 677 (2023) 121639.

**Chapter 3**

**S. Xiang**, P. Zhang, R.R. Gonzales, R. Saeid, L. Deng, Y. Shi, W. Fu, Z. Li, K. Guan, H. Matsuyama, Lowering spinning temperature for polyketone (PK) hollow fiber membrane fabrication with low-toxic diluent system via thermally induced phase separation, Journal of Membrane Science., 689 (2023) 122176.

**Chapter 4**

**S. Xiang**, P. Zhang, R.R. Gonzales, B. Li, R. Saeid, Y. Shi, M. Hu, Z. Li, K. Guan, H. Matsuyama, Fabrication of high-permeance polyketone (PK) hollow fiber membrane using triple-orifice spinneret via TIPS method, Journal of Membrane Science, (Submitted).

Doctoral Dissertation, Kobe University

“Development of high-water-permeance polyketone (PK) membrane via thermally induced phase separation (熱誘起相分離法による高水透過性ポリケトン膜の開発)”, 168 pages

Submitted on January, 15, 2024

When published on the Kobe University institutional repository */Kernel/*, the publication date shall appear on the cover of the repository version.